Investigation of PINK1 cleavage and trafficking using novel PARL-targeted α-ketoamide-based inhibitors

Inaugural-Dissertation

zur
Erlangung des Doktorgrades
der Mathematisch-Naturwissenschaftlichen Fakultät
der Universität zu Köln

vorgelegt von
Elena Lara Heuten
aus Duisburg

angenommen in Köln, 2025

Erklärung zur Dissertation

gemäß der Promotionsordnung vom 12. März 2020
„Hiermit versichere ich an Eides statt, dass ich die vorliegende Dissertation selbstständig und ohne die Benutzung anderer als der angegebenen Hilfsmittel und Literatur angefertigt habe. Alle Stellen, die wörtlich oder sinngemäß aus veröffentlichten und nicht veröffentlichten Werken dem Wortlaut oder dem Sinn nach entnommen wurden, sind als solche kenntlich gemacht. Ich versichere an Eides statt, dass diese Dissertation noch keiner anderen Fakultät oder Universität zur Prüfung vorgelegen hat; dass sie - abgesehen von unten angegebenen Teilpublikationen und eingebundenen Artikeln und Manuskripten - noch nicht veröffentlicht worden ist sowie, dass ich eine Veröffentlichung der Dissertation vor Abschluss der Promotion nicht ohne Genehmigung des Promotionsausschusses vornehmen werde. Die Bestimmungen dieser Ordnung sind mir bekannt. Darüber hinaus erkläre ich hiermit, dass ich die Ordnung zur Sicherung guter wissenschaftlicher Praxis und zum Umgang mit wissenschaftlichem Fehlverhalten der Universität zu Köln gelesen und sie bei der Durchführung der Dissertation zugrundeliegenden Arbeiten und der schriftlich verfassten Dissertation beachtet habe und verpflichte mich hiermit, die dort genannten Vorgaben bei allen wissenschaftlichen Tätigkeiten zu beachten und umzusetzen. Ich versichere, dass die eingereichte elektronische Fassung der eingereichten Druckfassung vollständig entspricht."

Teilpublikation:

Poláchová, E.*, Bach, K.*, **Heuten, E.**, Stanchev, S., Tichá, A., Lampe, P., Majer, P., Langer, T., Lemberg, M. K., and Stříšovský, K. (2022). Chemical Blockage of the Mitochondrial Rhomboid Protease PARL by Novel Ketoamide Inhibitors Reveals Its Role in PINK1/Parkin-Dependent Mitophagy. Journal of Medicinal Chemistry.

11.01.2025, Elena Lara Heuten

Abstract

Mitochondrial quality control is a critical component of cellular homeostasis. The serine/threonine kinase PINK1 plays a pivotal role in maintaining a healthy pool of mitochondria. Under normal conditions, PINK1 is imported into intact polarized mitochondria, where it is cleaved by the inner mitochondrial rhomboid protease PARL and subsequently rapidly degraded via the proteasome. However, under circumstances such as depolarized mitochondria, uncleaved PINK1 accumulates at the outer mitochondrial membrane, initiating PINK1-Parkin-mediated mitophagy to remove the damaged organelle. Despite PINK1's importance, many aspects regarding the regulation of PARL activity, PINK1 cleavage and localization under physiological conditions remain unclear. A major challenge in investigating these processes is the reliance on depolarizing agents or time-consuming PARL knockdowns or knockouts, which bear the risk of masking other mitochondrial pathways and mechanisms. Specific PARL inhibitors, which would mitigate these problems, are so far lacking.

In this thesis, I establish a novel PARL-targeted group of α-ketoamide-based inhibitors by validating them using two PARL substrates, PGAM5 and PINK1, in human cell models. I demonstrate that these inhibitors exhibit high potency, do not disrupt the mitochondrial membrane potential, and are largely non-toxic at appropriate concentrations, making them well-suited for future research applications. Furthermore, I show that PARL inhibition results in alternative PINK1 cleavage fates and different submitochondrial localizations, leading also to PINK1 accumulation at the outer mitochondrial membrane and causing Parkin recruitment, a hallmark of mitophagy. Notably, I reveal PARL inhibition as a novel trigger for OMA1-mediated cleavage of PINK1 and uncover the interactions between PINK1 and the TOM and TIM23 import complexes upon PARL inhibition.

Taken together, these inhibitors open up new investigative strategies for advancing PARL research. My establishment and application of the novel PARL inhibitors has illuminated PINK1 processing and its downstream pathways, highlighting PARL as a dynamic regulator of mitochondrial homeostasis.

Zusammenfassung

Mitochondriale Qualitätskontrolle ist eine entscheidende Komponente der zellulären Homöostase. Die Serin/Threonin-Kinase PINK1 spielt eine zentrale Rolle bei der Aufrechterhaltung der angemessenen Anzahl gesunder Mitochondrien. Unter normalen Bedingungen wird PINK1 in polarisierte, intakte Mitochondrien importiert, wo es durch die innere mitochondriale Rhomboidprotease PARL gespalten und anschließend im Zytosol rasch durch das Proteasom abgebaut wird. Bei depolarisierten Mitochondrien hingegen akkumuliert ungespaltenes PINK1 an der äußeren Mitochondrienmembran und initiiert PINK1-Parkin-Mitophagie, um die beschädigten Organellen zu entfernen. Trotz der Bedeutung von PINK1 sind viele Aspekte der Regulation von PARL-Aktivität, PINK1-Spaltung und -Lokalisation unter physiologischen Bedingungen weiterhin unklar. Eine wesentliche Herausforderung bei der Untersuchung dieser Prozesse besteht in der Abhängigkeit von depolarisierenden Substanzen oder zeitaufwändigen PARL-Knockdowns oder -Knockouts, die das Risiko beinhalten, andere mitochondriale Signalwege und Mechanismen zu verdecken. Spezifische PARL-Inhibitoren, die diese Probleme beheben könnten, fehlen bisher.

In dieser Arbeit stelle ich eine neue Gruppe von PARL-spezifischen, auf α-Ketoamid basierenden Inhibitoren vor, die ich mithilfe zweier PARL-Substrate, PGAM5 und PINK1, in humanen Zellmodellen validiere. Ich weise nach, dass diese Inhibitoren eine hohe Wirksamkeit besitzen, dass sie das mitochondriale Membranpotential nicht zerstören und dass sie bei effektiven Konzentrationen größtenteils nicht toxisch für die Zellen sind, was sie für zukünftige Forschungsanwendungen ideal macht. Darüber hinaus zeige ich, dass die Inhibition von PARL zu alternativen PINK1 Spaltungswegen und unterschiedlichen submitochondrialen Lokalisationen führt, einschließlich der Akkumulation von PINK1 an der äußeren Mitochondrienmembran, was die Rekrutierung von Parkin – ein Kennzeichen der Mitophagie – auslöst. Insbesondere identifiziere ich die PARL-Inhibition als neuartigen Auslöser für die OMA1-vermittelte Proteolyse von PINK1 und decke Interaktionen zwischen PINK1 und den Importkomplexen TOM und TIM23 unter PARL-Inhibition auf.

Zusammenfassend eröffnen diese Inhibitoren neue Möglichkeiten für die PARL Forschung. Meine Etablierung und Anwendung der neuartigen PARL-Inhibitoren beleuchtet die Wege der PINK1-Prozessierung und deren nachgeschalteten Signalwege und hebt PARL als dynamischen Regulator der mitochondrialen Homöostase hervor.

Contents

List of Figures

List of Tables

List of Abbreviations

Abbreviation	Description
2D-PAGE	Two-dimensional polyacrylamide gel electrophoresis
$\Delta\Psi_m$	Mitochondrial membrane potential
ADP	Adenosine diphosphate
AFG3L2	Mitochondrial inner membrane m-AAA protease component AFG3L2
AIF	Apoptosis inducing factor mitochondria associated 1
APS	Ammonium peroxodisulfate
ATP	Adenosine triphosphate
B3GNT2	N-acetyllactosaminide beta-1,3-N-acetylglucosaminyltransferase 2
BN-PAGE	Blue Native polyacrylamide gel electrophoresis
BSA	Bovine serum albumin
CAA	Chloroacetamide
CCCP	Carbonyl cyanide 3-chlorophenylhydrazone
CLASP1	CLIP-associating protein 1
CLPB	Caseinolytic mitochondrial matrix peptidase chaperone subunit B family mitochondrial disaggregase
(Co)-IP	Co-Immunoprecipitation
CTE	C-terminal extension
CYCS	Cytochrome c
DAPI	4′,6-diamidino-2-phenylindole
DIABLO	Diablo IAP-binding mitochondrial protein
DMEM	Dulbecco's Modified Eagle Medium
DMSO	Dimethyl sulfoxide
DNA	Deoxyribonucleic acid
DRP1	Dynamin-related protein 1
DSP	Dithiobis[succinimidylpropionate]
DTT	Dithiothreitol
ECL	Enhanced chemiluminescence
EDTA	Ethylenediaminetetraacetic acid
EGTA	Ethylene glycol-bis (β-aminoethyl ether) - N,N,N′,N′-tetraacetic acid
ER	Endoplasmic reticulum
FACS	Fluorescence Activated Cell Sorting

FADH$_2$	Flavin adenine dinucleotide, fully reduced
FBS	Fetal bovine serum
GIGYF2	GRB10 interacting GYF protein 2
GO	Gene Ontology
GTP	Guanosine triphosphate
HEK	Human Embryonic Kidney
HeLa	Henrietta Lacks
HEPES	4-(2-Hydroxyethyl)-1-piperazineethanesulfonicacid
HSP70 / 90	Heat shock protein 70 / 90
IMM	Inner mitochondrial membrane
IMP	Inner membrane peptidase
IMS	Intermembrane space
ISR	Integrated stress response
KD	Knock-down
KO	Knock-out
LC3	Microtubule-associated proteins 1A/1B light chain 3
mAb	Monoclonal antibody
MAM	Mitochondria-associated ER membrane
MDV	Mitochondria-derived vesicle
MFN1	Mitofusin 1
MFN2	Mitofusin 2
MPP	Mitochondrial processing peptidase
MPTP	Mitochondrial permeability transition pore
mRNA	Messenger ribonucleic acid
mtDNA	Mitochondrial deoxyribonucleic acid
mtHSP70	Mitochondrial heat shock protein 70
MTS	Mitochondrial targeting signal
mtUPR	Mitochondrial unfolded protein response
NADH	Nicotinamide adenine dinucleotide, reduced
NBR1	Next to BRCA1 gene 1 protein
NDP52	Nuclear domain 10 protein 52
NTE	N-terminal extension
OMA1	Metalloendopeptidase OMA1
OMM	Outer mitochondrial membrane

OMS	Outer membrane localization signal
OPA1	Optic atrophy 1 mitochondrial dynamin-like GTPase
pAb	Polyclonal antibody
PAGE	Polyacrylamide gel electrophoresis
PAM	Presequence activated motor
PARL	Presenilin-associated rhomboid-like protein, mitochondrial or PINK1/PGAM5-associated rhomboid-like protease
PBS	Phosphate-buffered saline
PCA	Principal component analysis
PD	Parkinson's disease
PEI	25-kDa linear polyethylenimine
PGAM5	Phosphoglycerate mutase family member 5
PHB2	Prohibitin 2
PI	c0mplete, EDTA-free protease inhibitor cocktail
PINK1	PTEN-induced kinase 1
PMSF	Phenylmethylsulfonyl fluoride
PSD3	PH and SEC7 domain-containing protein 3
pUb	Phosphorylated ubiquitin
RAF1	RAF proto-oncogene serine/threonine-protein kinase
RNA	Ribonucleic acid
ROMO1	Reactive oxygen species modulator 1
SDS	Sodium dodecyl sulfate
SDS-PAGE	Sodium dodecyl sulfate polyacrylamide gel electrophoresis
SEM	Standard error of the mean
siRNA	Small interfering RNA
SLP2 / STOML2	Stomatin like 2
Smac / Diablo	Second mitochondria-derived activator of caspases / direct IAP-binding protein with low pI
SPY complex	SLP2, PARL, YME1L1 complex
STARD7	StAR-related lipid transfer protein 7, mitochondrial
TADA3	Transcriptional adapter 3
TANC2	Tetratricopeptide Repeat, Ankyrin Repeat And Coiled-Coil Containing 2
TAX1BP1	Tax1-binding protein 1
TBS	Tris-buffered saline

TCA	Trichloracetic acid
TEAB	Tetraethylammonium bromide
TEMED	Tetramethylethylenediamine
TIM	Translocase of inner mitochondrial membrane
TIPIN	TIMELESS-interacting protein
TIR	TOM70-interacting region
TMD	Transmembrane domain
TMRE	Tetramethylrhodamine ethyl ester perchlorate
TOM	Translocase of outer mitochondrial membrane
TTC19	Tetratricopeptide repeat domain 19
UPRmt	Mitochondrial unfolded protein response
VDAC	Voltage-dependent anion channel
YME1L1	ATP-dependent zinc metalloprotease YME1L1

1   Introduction

Colloquially, mitochondria are frequently referred to as the "powerhouses of the cell" due to their major contribution to the cell's energy metabolism. Of course, mitochondria are much more than simple energy production centers; for example, they also play a role in providing calcium for different cellular functions and are a major checkpoint in apoptosis. This makes mitochondrial functionality critical for cellular homeostasis, with defects in mitochondria-related processes being implicated in various human disorders. To ensure proper mitochondrial functionality, quality control mechanisms have evolved that act on both the protein level via proteases and on the organelle level via fission, fusion and degradation of the mitochondrion itself to different degrees.

1.1   Maintenance of mitochondrial function is a crucial aspect of cellular homeostasis

1.1.1   The complex mitochondrial architecture as the basis of mitochondrial functions

Mitochondria are unique among animal cell organelles due to their endosymbiontic origin from prokaryotes taken up into proto-eukaryotes (Sagan, 1967; Bonen et al., 1977; Yang et al., 1985) and the characteristics resulting from that origin. Mitochondria can be divided into several subcompartments. They have an outer and an inner mitochondrial membrane (OMM and IMM) which enclose the intermembrane space (IMS). Both OMM and IMM contain translocases, referred to as TOM (translocase of the outer mitochondrial membrane) and TIM (translocase of the inner mitochondrial membrane), respectively. The TOM and TIM complexes coordinate the protein import into mitochondria, as the vast majority of mitochondrial proteins are nuclear-encoded (**Section 1.2**). Further, the OMM contains the voltage-dependent anion channel (VDAC). As a porin, VDAC allows for passage of selective ions, including adenosine triphosphate (ATP) as the universal cellular energy source, over the OMM (Shoshan-Barmatz and Gincel, 2003). VDAC is also involved in interactions of mitochondria with the endoplasmic reticulum (ER) at contact sites known as the mitochondria-associated ER membranes (MAMs, **Section 1.1.3**).

 The IMM is folded into so-called cristae, which result in a surface area of the IMM several times that of the OMM. This internal structure is supported by the IMM lipid cardiolipin, which displays a high affinity for curved membranes and aids in cristae formation. This is facilitated by its higher intrinsic curvature originating from its four fatty acid chains instead of two as is the case in the other primary mitochondrial membrane lipids phosphatidylcholine and phos-

phatidylethanolamine (Huang et al., 2006; Khalifat et al., 2008; Falabella et al., 2021). The IMM, specifically the cristae, is the place where the proteins of the electron transport chain and oxidative phosphorylation are localized (**Section 1.1.2**). The IMM encases the matrix, the innermost mitochondrial compartment that contains the mitochondrial DNA (mtDNA) and mitochondrial ribosomes. These produce a limited set of proteins that are part of the respiratory chain complexes.

The division by the IMM and OMM into these subcompartments allows the mitochondrion to maintain an electrochemical proton gradient between IMS and matrix without influencing or being influenced by the cytosol. This gradient, hereafter referred to as the mitochondrial membrane potential ($\Delta\Psi_m$), is essential for the mitochondria's role in energy production.

1.1.2 Energy conversion within mitochondria

Mitochondria produce energy in the form of ATP, generated from adenosine diphosphate (ADP). Broadly speaking, the overall process known as cellular respiration involves oxidizing a glucose molecule with the use of oxygen as an electron acceptor to carbon dioxide and water which produces the equivalent of 30 ATP molecules per glucose molecule.

The citric acid cycle in the matrix produces one equivalent of ATP as well as further NADH and $FADH_2$ from the conversion of acetyl-CoA. Acetyl-CoA is converted from pyruvate, which itself is the product of cytosolic glycolysis, which also produces ATP and NADH. Further acetyl-CoA is produced from ketone bodies and via β-oxidation of fatty acids in the mitochondria, again producing NADH and $FADH_2$ in addition.

NADH as well as $FADH_2$ are then used as electron donors for oxidation in the electron transport chain at the cristae (**Figure 1**). The electrons first enter the electron transport chain at the IMM-anchored complex I or complex II, both of which pass the electrons to ubiquinone, a lipid-soluble electron carrier that can freely move within the membrane. Ubiquinone shuttles the electrons to complex III, which itself passes the electrons onto the water-soluble cytochrome c. Finally, the electrons are transferred to protons and oxygen which produces water molecules. This electron transfer along the protein complexes of the electron transport chain results in free energy which is used by the proton pumps (complex I, III and IV) to translocate protons from the matrix into the IMS. This allows the creation of $\Delta\Psi_m$. The electrochemical gradient drives the protons from the IMS back into the matrix through complex V, the F-ATP synthase, which generates further ATP via phosphorylation. Thus, the whole process at the IMM is known as oxidative phosphorylation.
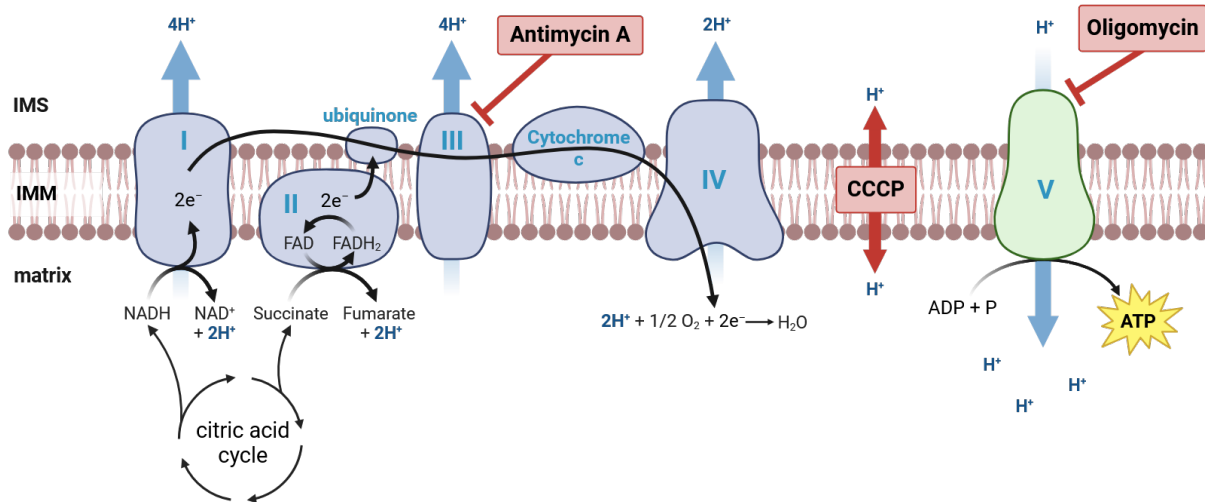
Figure 1: *Oxidative phosphorylation and selected inhibitors.* Schematic representation of the electron transport chain complexes involved in oxidative phosphorylation. Indicated in red are three inhibitors / uncouplers that are used within this study and their targets. For detailed explanation, see **Section 1.1.2**. Abbreviations: IMS = intermembrane space, IMM = inner mitochondrial membrane. Created using BioRender.

The process of oxidative phosphorylation is, however, not without downsides. The electron transfer risks generation of reactive oxygen species (ROS) when electrons prematurely reduce oxygen. ROS, when too abundant, cause oxidative stress to the cell: ROS are highly reactive with the potential to modify and damage nucleic acids (especially due to the close proximity to mtDNA in the matrix), proteins and lipids (Cadenas and Davies, 2000). Thus, this pathway is tightly regulated and has also been implicated in cell cycle functionality, as functional and heightened oxidative phosphorylation is linked to cellular proliferation (Zacksenhaus et al., 2017; Yao et al., 2019; Ghosh et al., 2020; Ren et al., 2023). Further, the folding of the IMM into multiple separated cristae is useful for maintaining different $\Delta\Psi_m$ sections, which may contribute to keeping a mitochondrion as a whole healthy when only specific cristae suffer defects in the electron transport chain (Wolf et al., 2019).

The oxidative phosphorylation can be modulated by inhibitors and so-called uncouplers (**Figure 1**, in red). These compounds interfere by uncoupling the electron transport chain from the F-ATP synthase by transporting protons through the IMM without involvement of the F-ATP synthase and thus dissipate the proton gradient which causes depolarization of the mitochondrion. A physiological uncoupler is the protein thermogenin which is expressed mostly in brown fat tissue in the IMM. This proton channel allows the reflux of protons to the matrix, thus producing heat instead of ATP (Fedorenko et al., 2012). A chemical uncoupler is carbonyl cyanide 3-chlorophenylhydrazone (CCCP), which as an ionophore can bind protons at the IMS side, transport them over the IMM and release the protons at the matrix side, dissipating the

electrochemical gradient (Hopfer et al., 1968; LeBlanc Jr., 1971). Two inhibitors of oxidative phosphorylation that will also be used in this study are Oligomycin and Antimycin A. Oligomycin inhibits complex V by interfering with its proton channel, thus stopping ATP production and exasperating $\Delta\Psi_m$ by limiting proton reflux (Penefsky, 1985; Devenish et al., 2000; Symersky et al., 2012). It has also been indicated to work as an uncoupler (Hearne et al., 2020). Antimycin A inhibits complex III, stopping progression of the electron transport and disrupting the formation of the proton gradient in the first place, causing ROS production and mitochondrial depolarization (Brandt, 1996; Han et al., 2001; Kalbáčová et al., 2003; Hytti et al., 2019).

1.1.3   Calcium storage and interaction with the endoplasmic reticulum

While the ER is the main cellular storage for calcium ions (Ca^{2+}), mitochondria serve as more transient storage as well. MAMs as the interface of ER and mitochondria are important for Ca^{2+} trafficking and signaling: The OMM at MAMs is enriched for VDAC and coupled with the ER channel inositol 1,4,5-trisphosphate receptor, which allow Ca^{2+} transfer from the ER to the mitochondria (Rapizzi et al., 2002; Szabadkai et al., 2006). The mitochondrial Ca^{2+} uniporter complex located at the IMM then permits Ca^{2+} entry into the matrix (Baughman et al., 2011; De Stefani et al., 2011). There, a sufficient supply of Ca^{2+} is necessary for the activation of several dehydrogenases involved in the citric acid cycle (Denton, 2009) and pronounces the essential role of mitochondrial Ca^{2+} for the cell's energy metabolism. On the other hand, too much Ca^{2+} uptake can trigger apoptosis (Rasola and Bernardi, 2011), which will be further addressed in **Section 1.1.5**.

1.1.4   Preservation of healthy mitochondria via fission and fusion

Fission and fusion account for a large part of the mitochondrial homeostasis processes to preserve a steady number of well-functioning mitochondria in the cell. Fission is involved in apoptosis by fragmenting the mitochondrial network, but also during cell division to ensure that the appropriate number of mitochondria is available to each daughter cell. Fusion permits the exchange of metabolites and genetic products between mitochondria and thus allows compensation for deficient mitochondria that have not yet accumulated too much damage (for review, see Youle and van der Bliek, 2012; Elgass et al., 2013; Adebayo et al., 2021).

The major actor in fission is the dynamin-related protein 1 (DRP1, Smirnova et al., 2001). It is recruited from the cytosol to mitochondria by the mitochondrial dynamics proteins MID49/51 (Palmer et al., 2011; Zhao et al., 2011), and mitochondrial fission factor (Gandre-Babbe and

van der Bliek, 2008; Otera et al., 2010). The recruitment of DRP1 often coincides with ER-mitochondria contact sites that narrow the mitochondrion to a smaller diameter already before arrival of DRP1 (Friedman et al., 2011). As the OMM is further constricted, the ER also releases Ca^{2+} into the mitochondrion, which results in the early division of the IMM before the OMM (Chakrabarti et al., 2018). The complete separation into two daughter mitochondria is then driven by DRP1 oligomerizing into a ring around the ER constriction site. Tightening of this ring upon guanosine triphosphate (GTP) hydrolysis (Smirnova et al., 2001), which is also stimulated by DRP1's interaction with cardiolipin (Bustillo-Zabalbeitia et al., 2014; Macdonald et al., 2014), finally severs the mitochondrion.

The essential protein players in fusion are GTPases mitofusin 1 and 2 (MFN1 and MFN2, Santel and Fuller, 2001; Rojo et al., 2002) and optic atrophy 1 mitochondrial dynamin-like GTPase (OPA1, Chen et al., 2005; Cipolat et al., 2006). The mitofusins are localized at the OMM, where they promote the docking of two mitochondria via oligomerization between opposite OMMs. At the IMM, fusion after docking is further mediated by OPA1 by its interaction with cardiolipin (Ban et al., 2017). OPA1 is cleaved by the IMM proteases OMA1 and by YME1L1 (see **Section 1.2.2**), resulting in multiple cleavage forms (Griparic et al., 2007; Song et al., 2007; Ehses et al., 2009; Head et al., 2009). The precise roles of the different cleavage forms in mitochondrial fusion are not yet fully elucidated; some publications favor a balance between short and long forms of OPA1 being necessary for fusion (Song et al., 2007; Ge et al., 2020), others emphasize the role of the long form (Ishihara et al., 2006; Anand et al., 2014). Nevertheless, it appears that stress-triggered OMA1 activity towards OPA1 is a key element in ensuring that depolarized mitochondria do not fully fuse with other healthier mitochondria (Meeusen et al., 2006; Head et al., 2009; Anand et al., 2014). Additionally, depolarized mitochondria can be prohibited from fusion via ubiquitination and proteasomal degradation of the mitofusins, which may help to prime the damaged mitochondria for mitophagy (Tanaka et al., 2010; Chen and Dorn, 2013), the selective autophagy of mitochondria which will be detailed in the next **Section 1.1.5**.

1.1.5 Damage control: mitophagy, mitochondrial-derived vesicles and apoptosis

There are several hiercharchically acting pathways to avoid mitochondrial toxicity to the cell besides fission and fusion. One of these is the mitochondrial unfolded protein response (UPRmt) in coordination with the the integrated stress response (ISR). Inner mitochondrial accumulation of unfolded proteins (e.g. caused by ROS) causes proteotoxic stress and decreases mitochondrial import. To help alleviate this stress, mitochondria can send signals to the nucleus to upregulate the transcription of proteases and chaperones. These then aid in removing the detrimental

proteins from the mitochondria or promote their proper folding. In ISR, global translation is decreased to prevent further protein accumulation, and like UPRmt upregulates the expression of specific proteins that help relieve the protein load (for review, see Ng et al., 2021).

When mitochondria accumulate enough damage to be deemed beyond saving, they are removed from the cellular pool via mitophagy. This is done to maintain the health of the cell as a whole: when damaged mitochondria are not removed in time, a consequence can be the accumulation of toxic ROS, resulting in apoptosis (Redza-Dutordoir and Averill-Bates, 2016). Mitophagy removes the mitochondria by enclosing them in the autophagosome and targeting them towards lysosomal degradation, which allows the cell to reuse their molecular components (Mizushima and Komatsu, 2011). To ensure that only specific mitochondria are removed, various mitophagy receptors are needed for targeting to the lysosome, and mitophagy can be divided into two pathways: receptor-mediated and PINK1-Parkin-mediated mitophagy.

Receptor-mediated mitophagy is involved in cellular maturation such as removal of mitochondria during erythrocyte development (Schweers et al., 2007), and in protection of heart tissue upon reperfusion injury (Zhang et al., 2016; Lampert et al., 2019). As the name implies, this mitophagy type is mediated by a subgroup of the so-called mitophagy receptors that reside constitutively at the OMM. Among those are BCL-2-like protein 13, FK506-binding protein 8, prohibitin 2 (PHB2), FUN14 domain-containing protein 1 (FUNDC1), NIP3-like protein X and BCL2 interacting protein 3. The receptors possess a microtubule-associated proteins 1A/1B light chain 3 (LC3)-interacting region (LIR), and thus can interact with ATG8 family proteins (LC3s and gamma-aminobutyric acid receptor-associated proteins; Novak et al., 2010; Hanna et al., 2012; Liu et al., 2012; Bhujabal et al., 2017). As ATG8 proteins are linked to the autophagosomal membrane via conjugation with phosphatidylethanolamine, receptor-mediated mitophagy is believed to function by recruitment of preexisting autophagosomal membranes. On the other hand, there is some evidence suggesting that it may also work by direct generation of new autophagosomal membranes (see Uoselis et al., 2023), similar to the process in PINK1-Parkin-mediated mitophagy, as detailed below.

PINK1-Parkin-mediated mitophagy mostly acts on impaired mitochondria (Narendra et al., 2008), the damaged sections of which are selected via DRP1-mediated fission (Burman et al., 2017). This mitophagy type depends on the serine/threonine PTEN-induced kinase 1 (PINK1) and its downstream target Parkin, an E3 ubiquitin ligase (Greene et al., 2003; Clark et al., 2006; Park et al., 2006; Narendra et al., 2008, **Figure 2**). Upon activation of this pathway, PINK1, which is usually imported into mitochondria, cleaved and then degraded, is stabilized on damaged mitochondria and undergoes activation of its kinase domain (see **Section 1.3.3**).

PINK1 then phosphorylates ubiquitin that is already present at OMM proteins of the affected mitochondria (Shiba-Fukushima et al., 2014; Okatsu et al., 2015). This causes recruitment of Parkin to the mitochondrion (Geisler et al., 2010a; Matsuda et al., 2010; Narendra et al., 2010b), where it interacts with the phosphorylated ubiquitin (pUb, Kane et al., 2014; Koyano et al., 2014; Kazlauskaite et al., 2014) and is then itself phosphorylated by PINK1 (Kondapalli et al., 2012; Shiba-Fukushima et al., 2012). This phosphorylation is necessary for activation of Parkin's E3 ubiquitin ligase activity; in concert with PINK1 phosphorylating ubiquitin, OMM proteins are decorated with pUb chains (Geisler et al., 2010a), which recruit further Parkin resulting in a feedforward loop. The pUb chains are recognized by various autophagy adapters which possess a ubiquitin-binding domain in addition to their LIR. The primary adapters in PINK1-Parkin-mediated mitophagy are Nuclear domain 10 protein 52 (NDP52, Lazarou et al., 2015) and optineurin (Wong and Holzbaur, 2014; Lazarou et al., 2015). Tax1-binding protein 1 (TAX1BP1, Lazarou et al., 2015) has only a minor role, while Next to BRCA1 gene 1 protein (NBR1, Kirkin et al., 2009; Chan et al., 2011) and sequestosome-1/p62 (Geisler et al., 2010a; Narendra et al., 2010a) are dispensable for mitophagy, as demonstrated by Lazarou et al. (2015). A regulator of autophagy adapters is the serine/threonine-protein kinase TBK1, which can phosphorylate NDP52, optineurin, sequestosome-1 and TAX1BP1. At least for optineurin, phosphorylation by TBK1 increases its binding to the pUb chains in PINK1-Parkin-mediated mitophagy (Richter et al., 2016). NDP52 recruits the protein kinase complex ULK1/2 (Vargas et al., 2019), and optineurin together with TBK1 recruits the lipid kinase complex PI3KC3 to the mitochondrion (Nguyen et al., 2023). In turn, this results in the recruitment of ATG9 vesicles, which facilitate the formation of autophagosomal membranes at the mitochondrion (Itakura et al., 2012; Yamano et al., 2020). The membrane-linked ATG8 family proteins amplify this process by recruiting more NDP52 and optineurin (Padman et al., 2019). Eventually, the organelle is engulfed by the autophagosome and fuses with the lysosome, for which ATG8 proteins are essential (Nguyen et al., 2016).

Mitochondria-derived vesicles (MDVs) are structures that section off parts of damaged mitochondria and target them to the lysosome for degradation (Soubannier et al., 2012a). Thereby, MDVs can be regarded as an attempt to keep the mitochondrial network healthy without degrading whole mitochondria. PINK1/Parkin contribute to a subtype of MDVs that appear under oxidative stress caused by e.g. Antimycin A treatment and are independent of the autophagy core machinery (Soubannier et al., 2012b; McLelland et al., 2014; Sugiura et al., 2014). The mechanism of MDV cargo selection, their creation and trafficking is still under investigation, especially with regards to when PINK1 and Parkin can be seen at MDVs, as they appear to only
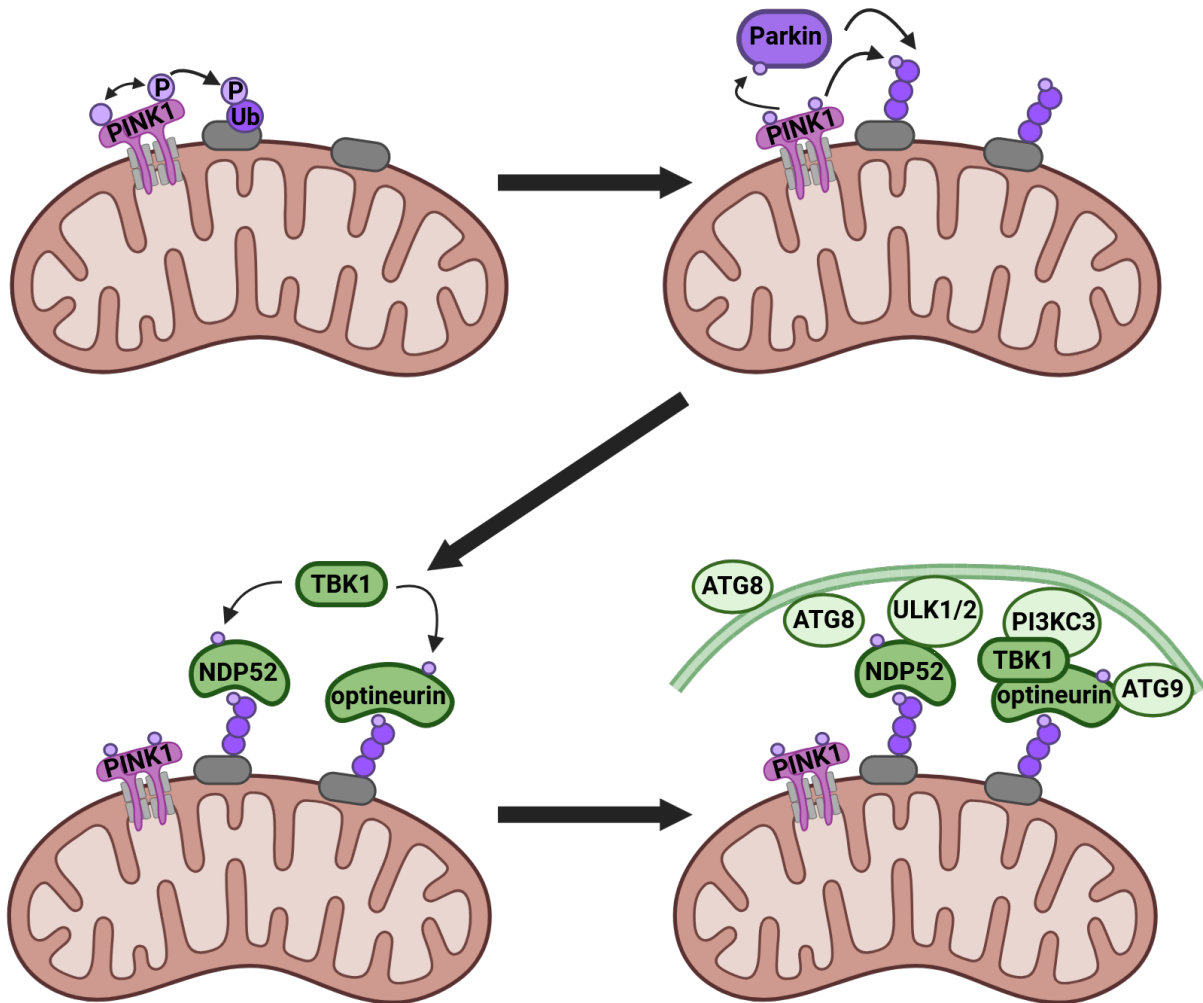
Figure 2: *PINK1-Parkin-mediated mitophagy.* PINK1 dimer stabilization at the outer mitochondrial membrane causes autophosphorylation and phosphorylation of other membrane proteins. This recruits Parkin for phosphorylation via PINK1 and establishment of phosphorylated polyubiquitin chains. Autophagy adapters NDP52 and optineurin are recruited and phosphorylated by TBK1. This recruits ULK1/2, PI3KC3 and ATG9 to the mitochondrion. Finally, the autophagosomal membrane encapsulates the mitochondrion via ATG8 family proteins and targets it for lysosomal degradation. Created using BioRender.

localize to a certain small subset of MDVs (McLelland et al., 2014; Ryan et al., 2020; König et al., 2021; Roberts et al., 2021).

Apoptosis is the very last consequence of cellular dysfunction. ROS as well as Ca^{2+} overload are two kinds of stressors that may trigger cell death (Fleury et al., 2002; Orrenius et al., 2015; Redza-Dutordoir and Averill-Bates, 2016). Mitochondria can contribute to apoptosis by releasing pro-apoptotic factors into the cytosol. The release through the IMM is governed by the mitochondrial permeability transition pore (MPTP). The composition of the MPTP is not yet clear, though current results point to the direct involvement of the adenine nucleotide translocase and complex V subunits at the IMM. Other proteins, like cyclophilin D at the IMM, VDAC at the OMM and the pro-apoptotic Bcl-2 family members Bak and Bax appear to module MPTP and passage of molecules over the OMM (see Bernardi et al., 2023). Mitochondrial outer membrane permeabilization and MPTP may work in concert, as the MPTP can result in swelling of mitochondria due to molecule influx into the matrix, and swelling can rupture the OMM. This causes the release of pro-apoptotic molecules, among them cytochrome c, apoptosis inducing factor mitochondria associated 1 (AIF), and second mitochondria-derived activator of caspases/direct IAP-binding protein with low pI (Smac/Diablo, Redza-Dutordoir and Averill-Bates, 2016).

1.2   Mitochondrial protein trafficking, import and cleavage are tightly regulated

The mtDNA encodes for only 13 mitochondrial proteins, all of which are IMM-integral proteins involved in oxidative phosphorylation (Anderson et al., 1981; Macreadie et al., 1983; Chomyn et al., 1985, 1986). The vast majority of mitochondrial proteins, including additional ones of the oxidative phosphorylation pathway, are nuclear-encoded and thus need to be imported into mitochondria. Due to the mitochondria's complex membrane architecture, this import is divided into several pathways and precursor processing steps, depending on the final localization of the imported precursor (**Figure 3**).

1.2.1   Mitochondrial import pathways

α-helical proteins and β-barrel proteins are imported into mitochondria for OMM insertion. The mechanism underlying the import of α-helical proteins is still under investigation: In yeast, the three α-helical subtypes signal-anchored, tail-anchored and polytopic proteins have all been shown to be involved with the mitochondrial import machinery complex at the OMM, sometimes in concert with the receptor TOM70 of the TOM import machinery (Becker et al., 2011; Papić et al., 2011; Doan et al., 2020). For β-barrel proteins, the first step of import is also mediated by

the TOM complex, where the protein's targeting signal is recognized and the protein is transported towards the IMS (Krimmer et al., 2001). It is there recognized by small TIM proteins, which aid in its shuttling towards the sorting and assembly machinery complex back at the OMM. There, the β-barrel is properly assembled and inserted into the membrane (Wiedemann et al., 2004; Qiu et al., 2013). The mitochondrial import machinery and the sorting and assembly machinery complexes also cooperate in the assembly of TOM complex subunits (Doan et al., 2020).

Cysteine-rich proteins destined for the IMS are imported first through TOM40, the import pore of the TOM complex (Milenkovic et al., 2009; Gornicka et al., 2014), and then recognized by the mitochondrial intermembrane space import and assembly machinery (Chacinska et al., 2004; Peleh et al., 2016). This machinery also facilitates the formation of disulfide bonds within the IMS protein, ensuring correct folding (Müller et al., 2008).

Carrier proteins are targeted towards the IMM. They contain internal targeting sequences and are delivered to the mitochondria by the cytosolic heat shock proteins HSP70/90 (Young et al., 2003). There they are recognized first by the TOM complex (Young et al., 2003) and then by the small TIM proteins in the IMS and the TIM22 complex at the IMM (Koehler et al., 1998; Sirrenberg et al., 1998; Endres et al., 1999). Also imported via this pathway are the TIM proteins TIM17 and TIM23 (Káldi et al., 1998).

Presequence proteins can have their final destination in the IMM/IMS or matrix. The term "presequence" refers to their positively charged N-terminal mitochondrial targeting signal (MTS) in the form of an amphipathic α-helix that is first recognized by the TOM complex, specifically by TOM20 and TOM22 (Bolliger et al., 1995). The protein is then handed over to the TIM23 complex. New structural studies of the TIM23 complex in yeast show that TIM17 together with the dynamically associated Mgr2, rather than TIM23 itself, mediate the actual protein translocation over the IMM, with TIM23 serving more of a scaffolding function (Fielden et al., 2023; Sim et al., 2023; Zhou et al., 2023; Maruszczak et al., 2024). TIM17 is also likely to bind the MTS via a negatively charged area that is accessible from the IMS side. On the matrix side, the TIM23 complex interacts with the presequence activated motor (PAM) machinery, which pulls the protein towards the matrix via mitochondrial HSP70 (mtHSP70), using ATP hydrolysis as the driving force (De Los Rios et al., 2006). In the matrix, the mitochondrial processing peptidase (MPP) removes the precursor's MTS (Hawlitschek et al., 1988; Ito, 1999; Taylor et al., 2001). Matrix-destined presequence proteins are imported completely by the PAM machinery. If the protein however contains an additional hydrophobic sorting signal known as stop-transfer sequence, such as a transmembrane domain (TMD), it can be released laterally from the TIM23 complex
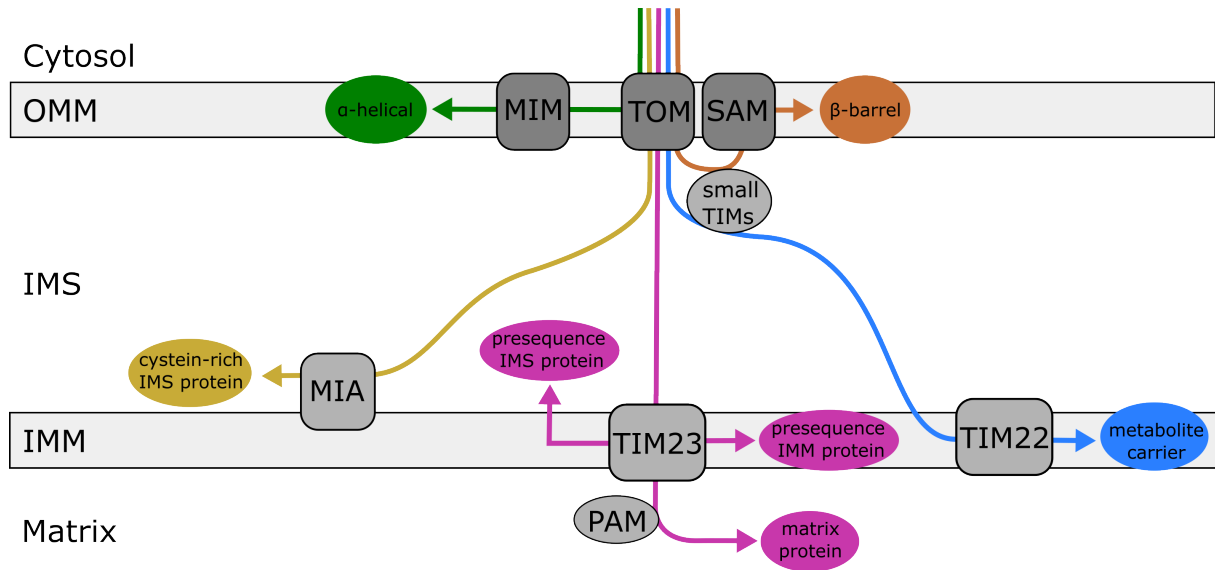
Figure 3: *Mitochondrial import pathways of cytosolic precursor proteins.* For detailed explanation, see **Section 1.2.1**. Abbreviations: OMM = outer mitochondrial membrane, IMS = intermembrane space, IMM = inner mitochondrial membrane, MIM = mitochondrial import machinery, TOM = translocase of outer mitochondrial membrane, SAM = sorting and assembly machinery, MIA = mitochondrial intermembrane space import and assembly machinery, TIM = translocase of inner mitochondrial membrane, PAM = presequence activated motor. Adapted from Wiedemann et al. (2009), Dudek et al. (2013) and Wiedemann and Pfanner (2017).

into the IMM. The switch between complete matrix release and IMM translocation appears to be mediated by association of TIM21 to and disassociation of the PAM machinery from the TIM23 complex (Chacinska et al., 2005). The lateral release into the IMM is regulated by Mgr2 in yeast; Mgr2 deletion promotes IMM integration of the imported protein and Mgr2 overexpression suppresses this integration (Ieva et al., 2014; Lee et al., 2020). The human orthologue reactive oxygen species modulator 1 (ROMO1) has further been implicated to play a role in ROS production, recruitment of TIM21 and import of the protease YME1L (Žárský and Doležal, 2016; Richter et al., 2019). If the presequence IMM protein contains multiple membrane-spanning sequences, its insertion into the IMM is further mediated by the oxidase assembly translocase (Bohnert et al., 2010). Finally, some stop-transfer signal proteins are destined for the IMS and are released from the IMM via cleavage by the inner membrane peptidase (IMP, Burri et al., 2005; Gomes et al., 2017).

Both import of the carrier proteins via the TIM22 complex (Sirrenberg et al., 1998; Endres et al., 1999) and of presequence proteins via the TIM23 complex needs an intact $\Delta\Psi_m$. For TIM23-complex-mediated import, this also drives the import of the positively charged MTS towards the negatively charged matrix (Martin et al., 1991).

1.2.2   Proteolysis of mitochondrial proteins

Mitochondria have 18 proteases that are exclusively active in mitochondria (Deshwal et al., 2020). Aside from the previously detailed presequence proteases MPP and IMP, I will here focus on seven other proteases and some of their functions. Four of these (LONP1, CLPXP, i-AAA and m-AAA) are ATP-dependent, which once again highlights the importance of properly functioning energy metabolism for mitochondrial protein homeostasis.

LONP1 is a serine protease complex component resident in the matrix. LONP1 associates with the TIM23 import complex and has a role as both a chaperone and protease of freshly imported, unfolded proteins (Bezawork-Geleta et al., 2015; Matsushima et al., 2021). Additionally, it is involved in maintaining mtDNA regulation by degrading a mitochondrial transcription factor (Matsushima et al., 2010). LONP1 serves as a checkpoint for both UPRmt and ISR activation. In the UPRmt pathway, LONP1 degrades the transcription factor ATFS-1 (mammalian homolog ATF5) upon its import; if it is not imported due to mitochondrial malfunctions and thus not degraded, it initiates UPRmt (Nargund et al., 2012; Fiorese et al., 2016). LONP1 prevents ISR activation by constitutively cleaving DELE1 upon its import (Sekine et al., 2023).

The CLPXP protease complex, consisting of CLPP and CLPX subunits, is also localized in the matrix and there degrades aberrant proteins. The degradation fragments are then involved in the translocation of transcription factors to the nucleus, where they launch the UPRmt response (Haynes et al., 2007, 2010).

YME1L1 is a component of the IMM localized i-AAA complex which has its catalytic domains residing in the IMS. There, it acts as a chaperone and protease for unfolded IMS(-facing) proteins (Leonhard et al., 1999). It has been shown to have a reciprocal relationship with the TIM23 complex component ROMO1, being reliant on ROMO1 for its import, but also cleaving ROMO1 (Richter et al., 2019). YME1L1 is also involved in fusion, as it constitutively cleaves OPA1 (Griparic et al., 2007; Song et al., 2007).

AFG3L2 is one of two proteins that constitute the IMM localized m-AAA complex, with its catalytic domains reaching into the matrix. The complex associates with Prohibitin-1/-2, which negatively regulate its cleavage activity (Steglich et al., 1999). The proteolysis is aimed at various matrix(-facing) proteins, amongst them a regulator of Ca^{2+} import. Thus, AFG3L2 plays a role in modulating MPTP opening and cell death (König et al., 2016).

The IMM protease OMA1 has its catalytically active site directed towards the IMS (Head et al., 2009; Baker et al., 2014). It is hyper-activated under various stressors, though the exact mechanism of activation regulation is being debated between auto-cleavage (Baker et al., 2014; Zhang et al., 2014) or reciprocal degradation via YME1L1 (Rainbolt et al., 2016). Furthermore,

OMA1-mediated cleavage of OPA1 is negatively regulated by AFG3L2 (Ehses et al., 2009; Head et al., 2009). OMA1 plays a role in ISR signaling by cleaving DELE1, though contrary to processing by LONP1, this cleaved form actively contributes to triggering ISR (Guo et al., 2020; Fessler et al., 2020).

The IMS-localized protease HTRA2 is also involved in DELE1 processing; this cleavage has been linked to Parkinson's disease (Bi et al., 2024). Additionally, HTRA2 can contribute to apoptosis (for review, see Vande Walle et al., 2008).

Last but not least, there is the IMM rhomboid protease PARL, which will be further introduced in the next **Section 1.3**.

1.3 Intramembrane proteolysis

1.3.1 Structure and functions of rhomboid proteases

Rhomboid (serine) proteases are a subclass of intramembrane proteases. Study of the bacterial rhomboid GlpG is the foundation of the vast majority of knowledge about rhomboid proteases' structures and proteolysis mechanism. Like all intramembrane proteases, rhomboids have an aqueous active site. This is composed of a serine-histidine catalytic dyad that is localized within the lipid bilayer of a membrane and opens towards the luminal space contained by this membrane, in the case of GlpG with the N- and C-termini oriented towards the cytosol (Wang et al., 2006; Tichá et al., 2018, **Figure 4**). Rhomboids cleave TMDs of their substrates, which thus need to move into this membrane-embedded active site and in some cases partially unfold to be accessible for the nucleophilic attack by the serine (for more detail on the molecular cleavage mechanism, see Strisovsky, 2017). Access to the active site is proposed to be blocked by a lateral gate; involvement of the luminal loops L1 and L5 between the TMDs has been implied (Wang et al., 2006; Zoll et al., 2014) as well as displacement of the TMD before L5 (Wu et al., 2006; Baker et al., 2007; Bohg et al., 2023). Loop L1 also plays a role in binding of the substrate via a tryptophan-arginine motif (Zoll et al., 2014). Substrate access to and cleavage at the active site may happen following the substrate docking to an exosite of the protease (Strisovsky et al., 2009; Dickey et al., 2013; Tichá et al., 2018; Lysyk et al., 2020b).

In mammals, five active rhomboids are described. Four of them are rhomboid-like protein 1 to 4 (RHBDL1-4). RHBDL1 is located at the Golgi apparatus, though so far, no substrates have been found and its functions remain unknown (Kühnle et al., 2019). RHBDL2 resides within the plasma membrane and RHBDL3 in late endosomes, thus being likely responsible for molecule secretion into the extracellular space (Kühnle et al., 2019). For RHBDL2, a wide range of sub-
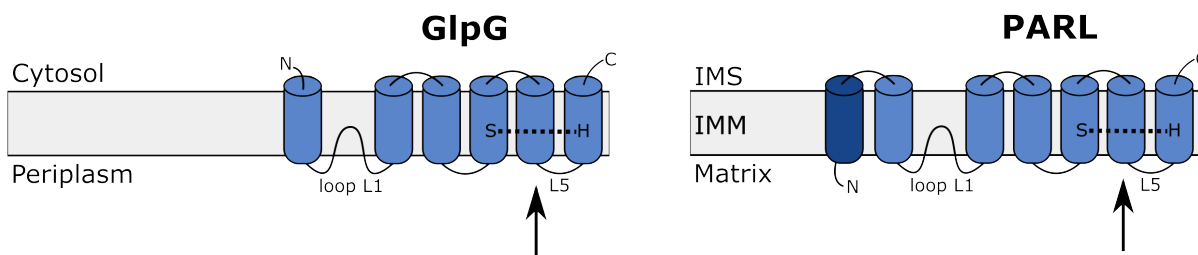
Figure 4: *Scheme of GlpG's and PARL's topology.* The catalytic dyad between the serine (S) and the histidine (H) is indicated, as well as loops L1 and L5 between the transmembrane domains. The arrow indicates from where the active site is likely accessible. Scheme adapted from Tichá et al. (2018).

strates has been identified, including the receptor for interleukin-6 and the epidermal growth factor (Lohi et al., 2004; Pascall and Brown, 2004; Adrain et al., 2011; Noy et al., 2016; Johnson et al., 2017); meanwhile, no substrates or cellular functions could be assigned to RHBDL3 so far. RHBDL4 is located at the ER and targets proteins towards the ER-associated degradation pathway (Fleig et al., 2012; Knopf et al., 2020; Bock et al., 2022). It has also been tied to protein secretion such as alternative amyloid precursor protein processing (Paschkowsky et al., 2016), promoted trafficking of transforming growth factor-α to the golgi apparatus (Wunderle et al., 2016) and immunity regulation via toll-like receptor 4 (Knopf et al., 2024).

The fifth mammalian rhomboid protease is PARL, localized at the IMM. PARL was originally named presenilin-associated rhomboid-like protein, as it was identified in a yeast two-hybrid system using presenilin-1/-2 as bait (Pellegrini et al., 2001). As functional interaction of PARL with the presenilins could not be shown, PARL is also more aptly referred to as PINK1/PGAM5-associated rhomboid-like protease after two of its substrates. PARL contains seven TMDs; compared to GlpG, it has an additional N-terminal TMD with an MTS. This added TMD likely positions PARL with its N-terminus reaching into the matrix and the C-terminus into the IMS (Jeyaraju et al., 2006, **Figure 4**). As the catalytic dyad is located between TMD five and seven, this would position it to be accessible from the matrix. PARL has been reported to undergo several cleavage events: α-cleavage of the MTS to generate the mature protein (Sík et al., 2004; Jeyaraju et al., 2006); β-cleavage further upstream but before the first TMD (Sík et al., 2004; Jeyaraju et al., 2006; Shi and McQuibban, 2017); and γ-cleavage after the first TMD, reducing PARL to just six TMDs (Jeyaraju et al., 2011). However, the physiological consequences and regulation of these various cleavage events are still a matter of debate (see Lysyk et al., 2020b).

1.3.2   The mitochondrial rhomboid protease PARL and its substrates

PARL itself is a part of a larger protein complex residing in the IMM, named SPY complex after its three components: stomatin-like protein 2 (SLP2), PARL and the i-AAA protease YME1L1. It could be shown that while PARL is associated with the SPY complex, it is regulated by SLP2, which also regulates OMA1 (Wai et al., 2016). So far, there are six PARL substrates known.

Smac/Diablo is released into the cytosol upon PARL cleavage where it binds a caspase inhibitor, signaling apoptosis (Saita et al., 2017). PARL cleavage of tetratricopeptide repeat domain 19 (TTC19), a subunit complex III of the electron transport chain, ensures proper TTC19 presence and thus correct function of complex III (Ghezzi et al., 2011; Spinazzi et al., 2019). StAR-related lipid transfer protein 7, mitochondrial (STARD7) is cleaved by PARL during its import, producing cytosolic and IMS protein pools. When localized within the mitochondria, STARD7 is involved in phosphatidylcholine accumulation in the IMM (Saita et al., 2018) and ubiquinone synthesis, whereas cytosolic STARD7 mediates ubiquinone transport to the cell membrane (Deshwal et al., 2023). The activity of the mitochondrial disaggregase CLPB is enhanced by PARL cleavage of an autoinhibitory sequence (Cupo and Shorter, 2020), and has been implied in SPY complex regulation (Baker et al., 2024). Phosphoglycerate mutase family member 5 (PGAM5), an IMM resident phosphatase, is targeted by PARL when $\Delta\Psi_m$ is disrupted. PGAM5's phosphatase activity is important for FUNDC1-receptor-mediated mitophagy (Chen et al., 2014), DRP1-mediated fission (Yu et al., 2020), MFN2-mediated fusion (Nag et al., 2023) and has been implicated also in PINK1-Parkin-mediated mitophagy (Lu et al., 2014; Park et al., 2018) together with prohibitin-2 (Yan et al., 2019). PINK1, best known for its involvement in mitophagy as already detailed in **Section 1.1.5**, is cleaved upon mitochondrial import by MPP and PARL (Jin et al., 2010; Deas et al., 2011; Meissner et al., 2011; Greene et al., 2012). The shortened PINK1-55 is, comparable to Smac/Diablo and STARD7, retrotranslocated to the cytosol and recognized at its N-terminal phenylalanine for rapid degradation via the N-end rule ubiquitin ligase Ubr1/2/4 and the proteasome (Yamano and Youle, 2013).

1.3.3   PARL, PINK1 and PGAM5 in differentially energized mitochondria

PGAM5 and PINK1 are cleaved in an inversely correlated manner, depending on the state of $\Delta\Psi_m$ and the association of PARL in the SPY complex (Sekine et al., 2012; Wai et al., 2016).

In healthy mitochondria (**Figure 5**, left), PINK1 is imported into mitochondria via the TOM and TIM23 complexes. This process is supported by PINK1's MTS (**Figure 6**), the function of which is dependent on $\Delta\Psi_m$ (Jin et al., 2010). Deletion of this classical MTS however does
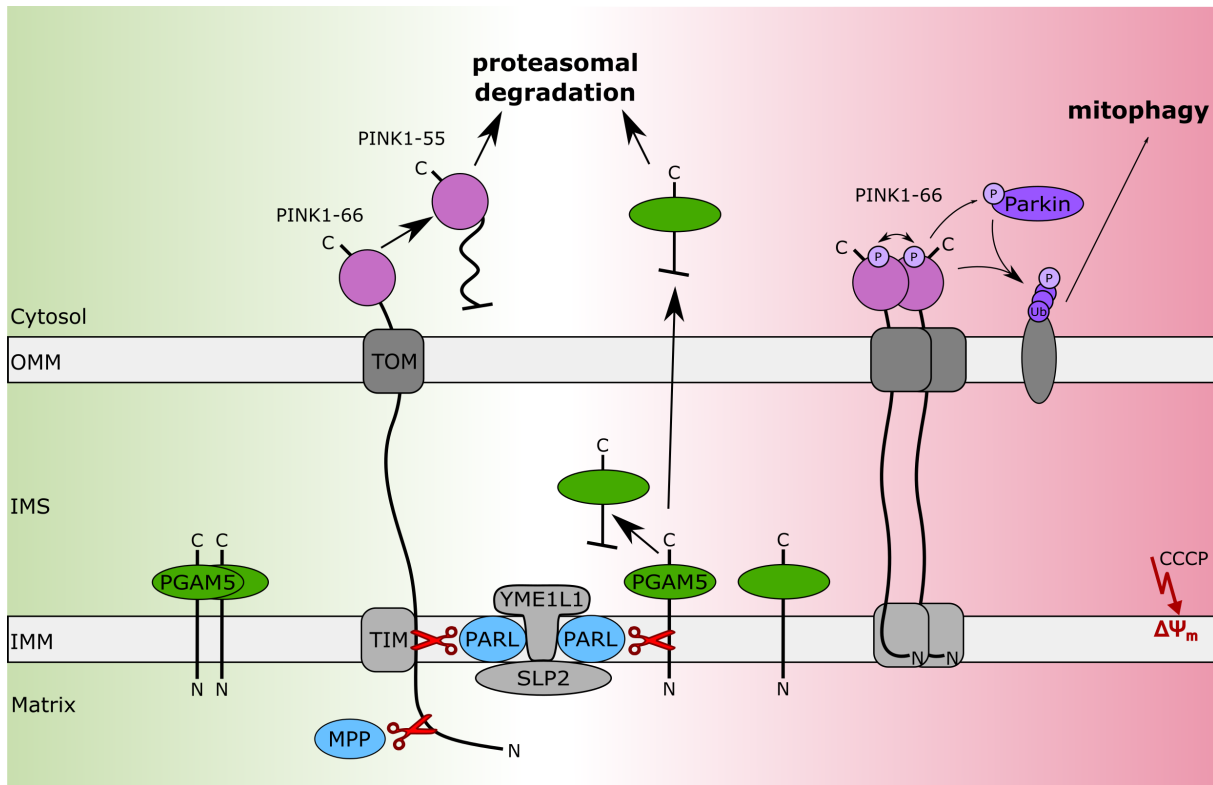
Figure 5: *Scheme of PINK1 and PGAM5 processing via PARL.* PGAM5 and PINK1 are cleaved in an inversely correlated manner by PARL. In healthy mitochondria (**left half**), PINK1 is cleaved by MPP and PARL. The shortened PINK1 is targeted towards proteasomal degradation. In damaged mitochondria (**right half**, i.e. $\Delta\Psi_m$ disruption by CCCP), PGAM5 is preferentially cleaved by PARL. Full-length PINK1 accumulates at the OMM, autophosphorylates and can then phosphorylate ubiquitin on ubiquitinated proteins. This causes Parkin to relocalize from the cytosol to mitochondria where it is phosphorylated and activated by PINK1, further ubiquitinating OMM proteins. The poly-ubiquitin chains at mitochondria then can trigger mitophagy. Scheme adapted from Siebert et al. (2022).

not prevent PINK1 from localizing to the mitochondria, which is additionally conferred by the sequence downstream of the classical MTS: it has been identified to contain an internal MTS (Bayne et al., 2023) and a OMM localization signal (OMS) which is dependent on the TOM machinery (Okatsu et al., 2015; Sekine et al., 2019; Raimi et al., 2024). Further, the N-terminal extension (NTE) upstream of the kinase domain has been shown to engage with the complex subunits TOM7 (Sekine et al., 2019) and TOM20 (Eldeeb et al., 2024; Raimi et al., 2024). While the stop-transfer sequence of its TMD prevents full translocation over the IMM (Becker et al., 2012; Okatsu et al., 2015), the MTS reaching into the matrix is cleaved off by MPP (Greene et al., 2012; Okatsu et al., 2015). A few amino acids downstream, PARL cleaves PINK1 in its TMD between A103 and F104 (Jin et al., 2010; Deas et al., 2011; Meissner et al., 2011), resulting in its proteasomal degradation via the N-end rule pathway.

Despite recent progress in the understanding of the molecular mechanisms of PINK1 regulation, there are various key open questions in this pathway. Whether PINK1 is completely imported into the mitochondria, or if the majority of the kinase domain remains in the cytosol is

still a matter of debate (see Trempe and Gehring, 2023; Narendra and Youle, 2024). Similarly, the precise hierarchy of the opposing forces of the MTS and the OMS, specifically in polarized mitochondria, is unclear. A role in PINK1 import has also been demonstrated for three negatively charged amino acid residues located just C-terminally of the TMD (E112/113/117); their mutation stabilizes PINK1 at the OMM already in polarized mitochondria and upon disruption of $\Delta\Psi_m$, this PINK1 is then degraded by OMA1 (Sekine et al., 2019). How exactly these residues may confer PINK1 import or OMM stabilization in intact mitochondria is not known. Lastly, to which degree the TIM23 complex is involved in PINK1 import is questioned by ambiguous reports (Filipuzzi et al., 2017; Hoshino et al., 2019; Sekine et al., 2019).

In damaged mitochondria (**Figure 5**, right) for example when $\Delta\Psi_m$ is disrupted by the uncoupler CCCP, PINK1's MTS is unable to pass through the TIM23 complex at the IMM and uncleaved PINK1 accumulates (Jin et al., 2010; Greene et al., 2012). As mentioned, PARL's cleavage activity instead shifts to PGAM5 accompanied by PGAM5's dissociation from its multimeric state (Sekine et al., 2012; Siebert et al., 2022). Full-length PINK1 stabilizes with the TOM and TIM23 complex into a membrane-spanning supercomplex (Lazarou et al., 2012; Okatsu et al., 2013; Fallaize et al., 2015; Akabane et al., 2023; Eldeeb et al., 2024). Whether PINK1 undergoes transfer, lateral or otherwise, out of the TOM40 pore or remains associated is still being debated (Maruszczak et al., 2022; Rasool et al., 2022). The arrest at the TOM complex is mediated by the three previously mentioned glutamic acid residues C-terminal of PINK1's TMD interacting with the TOM complex subunit TOM7, and the following activation of PINK1 kinase activity needs and is promoted by TOM7 as well as the internal MTS/OMS domain (Hasson et al., 2013; Sekine et al., 2019). Folding of the PINK1 kinase and interaction with the TOM complex is further conferred by PINK1's NTE and C-terminal extension (CTE) (Eldeeb et al., 2024; Raimi et al., 2024). Upon dimerization, PINK1 trans-autophosphorylates at S228 and subsequently the dimer is destabilized; the phosphorylated PINK1 monomer can then phosphorylate ubiquitin and start the mitophagic pathway as described in **Section 1.1.5** (Okatsu et al., 2012; Koyano et al., 2014; Gan et al., 2022; Rasool et al., 2022).
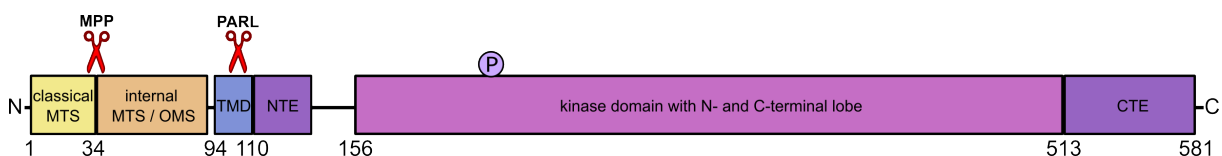
Figure 6: *Scheme of PINK1's structure and domains.* PINK1 starts N-terminally with a classical mitochondrial targeting signal (MTS) which is cleaved by MPP. It is followed by an internal MTS combined with an outer membrane localization signal (OMS). The transmembrane domain (TMD) is cleaved by PARL. The kinase domain containing the autophosphorylation site S228 ("P") is flanked by an N-terminal and a C-terminal extension (NTE and CTE).

Though it is widely accepted that PINK1 is stabilized and activated at the OMM upon $\Delta\Psi_m$ disruption, research on PINK1 substrates other than Parkin has further opened up the discussion on whether active PINK1 may also be located elsewhere within the mitochondria. Multiple studies have shown that PINK1 appears to phosphorylate inner membrane proteins such as Mic60 (related to cristae remodelling, Tsai et al., 2018) and NdufA10 (a subunit of complex I important for the electron transport chain, Morais et al., 2014). How exactly it is possible for PINK1 to phosphorylate targets at the IMM if its kinase domain is only present at the OMM, and how this interacts with PARL cleavage, remains an open question.

1.4 Consequences of PARL and PINK1 dysregulation

1.4.1 Phenotypes of PARL dysregulation

Aside from downstream defects caused by PARL cleavage regulation on its substrates, also the consequences of PARL deficiency itself has been investigated. PARL knockout (KO) mice develop normally in utero, but after birth soon show atrophy, male infertility and encephalomyelopathy resulting in premature death (Cipolat et al., 2006; Spinazzi et al., 2019; Radaelli et al., 2023). Their mitochondria show dysregulated OPA1 cleavage and trafficking (Cipolat et al., 2006), as well as problems in complex III activity and ubiquinone synthesis (Spinazzi et al., 2019; Radaelli et al., 2023). They also present faster reactions to apoptotic stimuli, such as cristae remodeling and release of cytochrome c (Cipolat et al., 2006).

PARL has also been speculated to be directly involved in Parkinson's disease (PD), as a mutation at its N-terminus which blocks β-cleavage had been identified in two patients, one with familial PD and one without family history of PD (Shi et al., 2011). However, this mutation, or other PARL mutations for that matter, is exceedingly rare and has not been found in other PD patient data sets (Heinitz et al., 2011; Wüst et al., 2016).

1.4.2 Role of PINK1 in Parkinson's disease

PD is a neurodegenerative disorder that is characterized by degeneration of dopaminergic neurons in the substantia nigra. Patients present with symptoms such as tremors, dementia, postural instability and behavioral changes. While the vast majority of PD cases are sporadic ones, there are also subtypes, such as recessive early-onset PD, which are hereditary. PINK1 and Parkin mutations have been linked to this subtype; Parkin was the first gene to be linked to familial PD (Kitada et al., 1998; Valente et al., 2004; Park et al., 2006).

Mutations in PINK1's kinase domain (such as H271Q, G309D, L347P) often correlate with

destabilization of PINK1 as a whole and a reduced kinase activity, which then causes dysregulation of mitophagy and accumulation of cellular damage due to a lack of removal of malfunctioning mitochondria (Valente et al., 2004; Beilina et al., 2005; Weihofen et al., 2008). It has been shown that some PD-related PINK1 mutations that are located C-terminally of the TMD (C125G, Q126P) cause PINK1 to not accumulate in its full-length form at the OMM under CCCP treatment and do not cause Parkin recruitment (Geisler et al., 2010b; Sekine et al., 2019). Those mutants are however cleaved by OMA1 and OMA1 suppression results in accumulation of full-length PINK1 at the OMM (Sekine et al., 2019). Still, not all of these mutations (Q126P) are then also able to successfully recruit Parkin to the mitochondria (Geisler et al., 2010b; Sekine et al., 2019); the exact mechanisms remain to be elucidated.

Two mutations (R98W, I111S) at the TMD have been shown to be mostly resistant to PARL processing while still being targeted to the IMM. For R98W, Parkin recruitment is present even in absence of mitochondrial depolarization via CCCP, and it has been shown that this PINK1 mutant still interacts with PARL without being cleaved (Meissner et al., 2015). For I111S, there seems to be a slight reduction of the normally CCCP-induced accumulation of full-length PINK1 and Parkin recruitment; an effect that is rescued with OMA1 knockout (Meissner et al., 2011, 2015; Sekine et al., 2019).

All in all, the effects that the over 60 PD-associated mutations of PINK1 (Vizziello et al., 2021) have on its trafficking, processing and signaling are manifold and still under heavy investigation.

1.5 Thesis objectives

In investigating PARL, its substrates and its regulation in a native environment, a great obstacle results from the use of PARL KO and knockdown (KD). As any KO, PARL KO risks displaying adaptive mechanisms that may mask the more subtle regulations, and PARL KD is experimentally suboptimal due to PARL's long half-life that necessitates a KD of around five days, making it a very time-consuming set-up. The ideal solution thus would be to have potent, specific PARL inhibitors available that do not cause secondary issues like effects on cellular health or mitochondrial membrane potential. Such inhibitors could even have therapeutic value if they are successful in stabilizing and activating PINK1 at the OMM. As some PD-related PINK1 variants present with reduced kinase activity, this artificial accumulation of PINK1 at the mitochondria could lower the threshold of additionally required active PINK1 needed by the cells to initiate mitophagy (Waters et al., 2023), resulting in a healthier mitochondrial population. In this work, I showcase the successful development and validation of such inhibitors. Following their establishment, I use them to investigate non-PARL proteolysis and the resulting trafficking fates of alternative PINK1 cleavage, including the influence on interaction with the TOM-TIM23 supercomplex in differentially energized mitochondria and on PINK1-Parkin-mediated mitophagy.

2   Results

2.1   Development, establishment and potency determination of novel α-ketoamide-based PARL inhibitors

In order to develop and establish potent PARL inhibitors, I collaborated with the group of Kvido Stříšovský from the Institute of Organic Chemistry and Biochemistry, Prague, resulting in a publication (Poláchová et al., 2022). The Stříšovský group has previously shown that peptidyl α-ketoamides can be modified to specifically bind to the catalytically active serine of rhomboid proteases in a covalent, reversible and non-competitive manner, as formation of a substrate-protease complex is still possible likely due to the substrate then only interacting with the protease exosite (Tichá et al., 2017).

To design inhibitors specific for PARL, we fused the P5 to P1 sequence of its substrate PINK1 (AVFLA, Deas et al., 2011) C-terminally to the acetyl group, followed by the warhead α-ketoamide portion and the hydrophobic substituent (tail) phenylbutyl. The tail is presumed to extend into the protease's active site and the catalytic serine covalently binds to the ketone carbonyl group of the α-ketoamide portion (Tichá et al., 2017, 2018). The resulting inhibitor was termed compound 5 (for molecular structure, see **Figure 7**A). With the intention of increasing solubility, we generated another inhibitor, termed compound 6, with two arginines N-terminally of the consensus sequence (**Figure 7**B). Additionally, two more inhibitors were designed to include branching of the hydrophobic tail, which was theorized to increase the compounds' binding capability to PARL, thus increasing their potency (inhibitors 1258 and 1343, **Figure 7**C and D). The Stříšovský group also tested inhibitor compounds 5 and 6 in their own assays (for details, see Poláchová et al., 2022).

2.1.1   Novel first-generation α-ketoamide-based PARL inhibitors show high potency on PGAM5 processing in HEK293T cells

I tested these four first-generation inhibitor compounds in the HEK293T cell-based system. I opted for determining cleavage efficiency on PGAM5, since PGAM5 cleavage is easy to analyze via its presence as either full-length protein or its singular cleavage product. I used CCCP as a trigger to induce PGAM5 cleavage by PARL which would then be inhibited by the compounds.

The resulting western blots and IC_{50} curves for all four first-generation PARL inhibitors are shown in **Figure 7**. While all compounds exhibit a reducing effect on CCCP-induced PGAM5 cleavage after three hours of treatment, compound 5 (**Figure 7**A) has the best resulting IC_{50} value of 0.18 ± 0.06 µM, while compound 6 is the worst 3.57 ± 2.24 µM (**Figure 7**B). Comparing
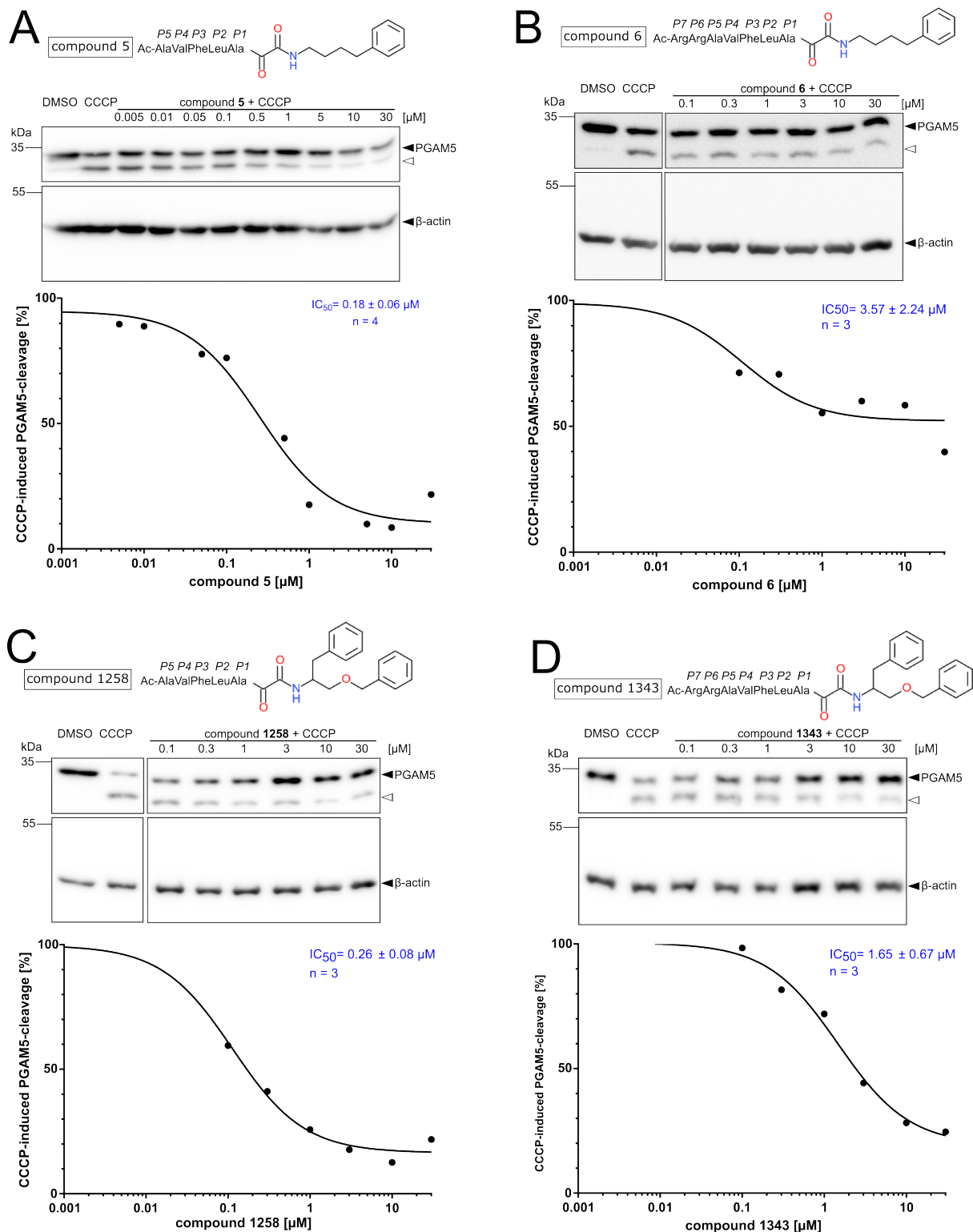
Figure 7: *First-generation α-ketoamide based PARL inhibitors show high potency on PGAM5 processing.* **A-D)** At the top, molecular structures of the inhibitor compounds are shown. HEK293T cells were transfected with PGAM5-FLAG and treated for 3 h with DMSO, 10 µM CCCP or 10 µM CCCP + indicated inhibitor. β-actin was used as loading control. For quantification, PARL-cleaved PGAM5 (white triangle) was measured as the percentage of total PGAM5 and normalized to the DMSO condition as zero cleavage and to the CCCP condition as complete cleavage. The resulting IC_{50} curve of the blot is shown as well as the mean IC_{50} value ± SEM from three or four independent experiments.

these results to the obtained values by the Střísovský group via their suppression of PGAM5 cleavage by overexpressed PARL in HEK293 T-REx cells (Poláchová et al., 2022) reveals that the IC_{50} value of compound 5 is decreased by factor 2.3 while the IC_{50} values of compound 6 are nearly identical. This difference is likely due to the employed endogenous PARL levels in my setup. It appears like the N-terminal addition of the arginines did not improve inhibitor potency, as compound 5 is more potent than compound 6, and 1258 is also more potent than 1343. The novel compound 5 is thus the most potent inhibitor of the first-generation inhibitors and can be used to further investigate proteolysis mechanisms of PARL.

2.1.2   Improvements to second-generation α-ketoamide-based PARL inhibitors show increased potency on PGAM5 processing in HEK293T as well as HeLa cells

After the successful proof-of-concept for these first-generation α-ketoamide-based PARL inhibitors, the molecular designs were altered to hopefully further improve PARL inhibition of the two resulting compounds. The first compound, called 1866, is identical to compound 5 except for an altered peptide tail, where acetyl-alanine-valine are replaced by isovaleryl which mimics the side chain of the valine in P4 (**Figure 8**A). The isovaleryl replacement should minimize the compound size and its polarity while maintaining its binding region specificity for PARL, so that the compound's membrane permeability and therefore its potency are increased. The second compound, called 1868, has the same altered peptide tail as compound 1866, but the phenylbutyl tail is the same branched tail that also compound 1258 and 1343 possess (**Figure 8**B).

These compounds were again tested in the previously described PGAM5 cleavage assay. Compound 1866 has an IC_{50} value of 0.031 ± 0.012 μM (**Figure 8**A) which is 5.8 times more potent than compound 5. Compound 1868 shows an even higher PARL inhibition with an IC_{50} value of 0.008 ± 0.002 μM (**Figure 8**B), a potency increase over compound 5 by factor 22.5. Compound 1868's efficiency thus demonstrates that both the shortening of the peptide chain and the branching of the hydrophobic tail have succeeded in improving the compound inhibition capabilities.

After compound 1868 has been shown to be the most potent PARL inhibitor of the six tested compounds, I checked how its capability to inhibit PARL is influenced by the used cell type and turned to HeLa cells as another commonly used human cell model. HeLa cells with knocked-out PARL (PARL-KO) transfected with PGAM5 were, as expected, lacking any PGAM5 cleavage even under CCCP treatment (**Figure 8**C). Wildtype HeLa cells do present with PGAM5 cleavage pronounced by CCCP treatment that is prevented by compound 1868. Calculation of the remaining PGAM5 cleavage with 0.5 μM 1868 reveals a mean cleavage value of 30.2 ± 7.1 %.

In comparison, the same inhibitor concentration in HEK293T cells yields a mean cleavage value of 40.2 ± 2.9 %, based on the calculated IC_{50} curve fits from three experiments. Thus, the inhibitor is even more potent in HeLa cells than in HEK293T cells regarding CCCP-induced PGAM5 cleavage.
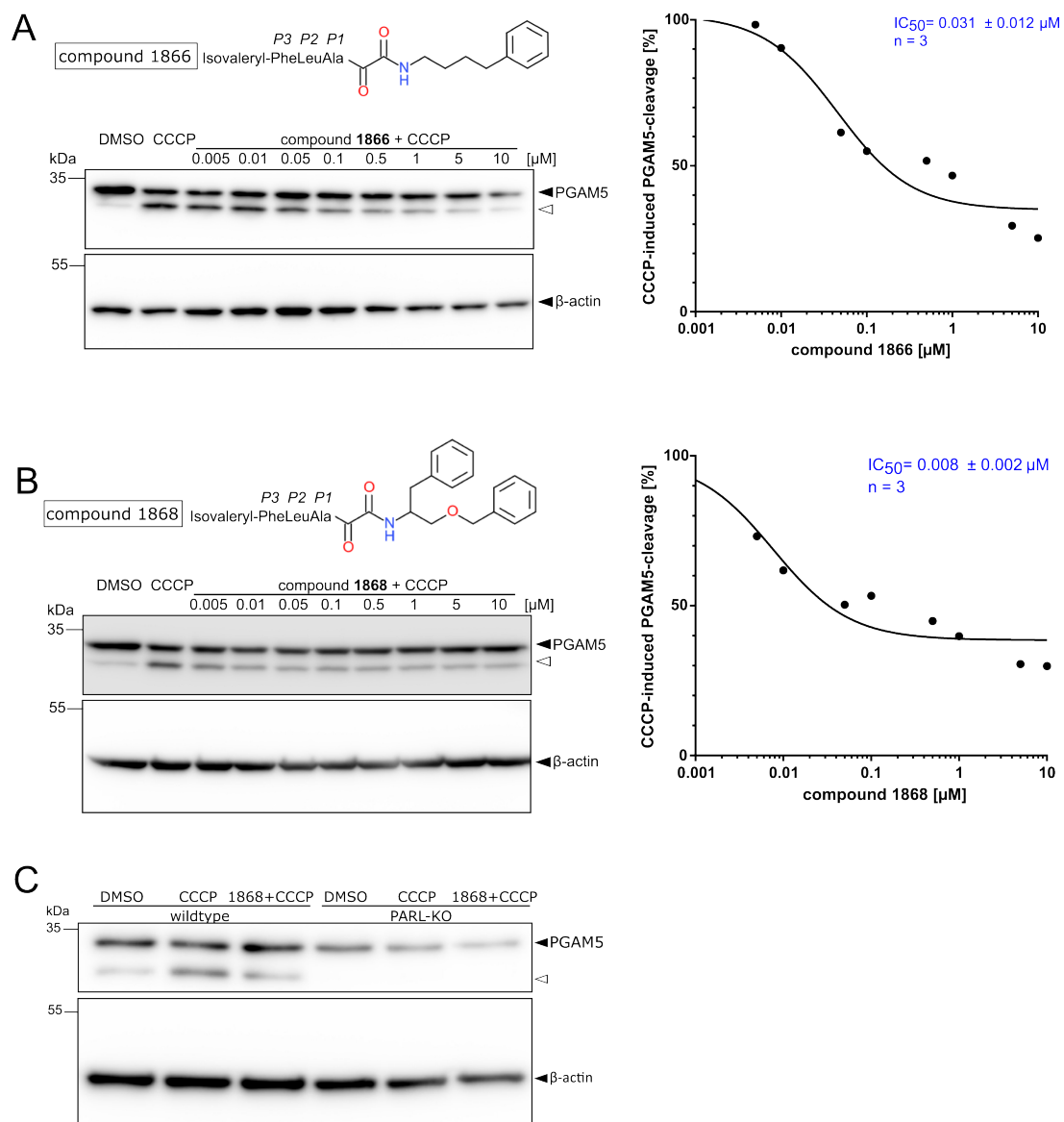
Figure 8: *Second-generation α-ketoamide based PARL inhibitors show improved potency on PGAM5 processing.* **A, B)** Molecular structures of the improved inhibitors are shown. HEK293T cells were transfected with PGAM5-FLAG and treated for 3 h with DMSO, 10 µM CCCP or 10 µM CCCP + indicated inhibitor. β-actin was used as loading control. For quantification, PARL-cleaved PGAM5 (white triangle) was measured as the percentage of total PGAM5 and normalized to the DMSO condition as zero cleavage and to the CCCP condition as complete cleavage. The resulting IC_{50} curve of the blot is shown as well as the mean IC_{50} value ± SEM from three independent experiments. **C)** HeLa wildtype or PARL-KO cells were transfected with PGAM5-FLAG and treated for 3 h with DMSO, 10 µM CCCP or 10 µM CCCP + 0.5 µM compound 1868. β-actin was used as loading control. A representative blot of three independent experiments is shown.

2.1.3   PARL inhibitors cause potent ablation of PARL-associated PINK1 cleavage and reveal alternative PINK1 cleavage fates

After establishing the potency range of the inhibitor compounds via PGAM5, I switched my focus to PINK1 as another PARL substrate. Here the advantage is that PINK1 is constitutively cleaved by PARL, so no artificial trigger like CCCP treatment is necessary. However, since endogenous PINK1 has a relatively low expression level (Waters et al., 2023) and is therefore difficult to detect on an immunoblot level, I predominantly used an inducible PINK1 overexpression cell line in HEK293 T-REx cells rather than wildtype HEK293T cells like before.

First, I wanted to verify if the inhibitor compounds show a clear dose response on PINK1 cleavage like they did on PGAM5 (**Figure 9**). Cells treated with DMSO as vehicle control show full-length PINK1 (PINK1-66) and a lower but visible level of PARL-cleaved PINK1 (PINK1-55). Upon disruption of $\Delta\Psi_m$ by CCCP, PINK1-55 levels are reduced and PINK1-66 is stabilized, accompanied by a slight molecular weight shift upwards indicative of its phosphorylation. All PARL inhibitors, both the four first-generation (**Figure 9**A) and the two second-generation compounds (**Figure 9**B) show a clear stabilization of PINK1, most prominently of PINK1-66, and of various cleavage fragments. In line with a concentration dependency, this stabilization increases with higher inhibitor dosage, verifying that the PARL inhibitors are efficient on both PGAM5 and PINK1. Of the PINK1 cleavage fragments that are observed with the inhibitors, one is caused by cleavage of the MTS by MPP (Greene et al., 2012) and is here termed PINK1-62. The origin of the additional cleavage fragment visible below PARL-cleaved PINK1-55, here termed PINK-53, will be explored in **Section 2.3.2**. There also appears to be a fainter band that runs slightly above PINK1-55 following PARL inhibition (mostly appreciable in **Figure 9**B, left panel), but unlike PINK1-53 and PINK1-62, it is not stabilized in a concentration-dependent manner. As phosphorylation is a known PINK1 post-translational modification resulting in a slight upwards shift on western blot level, this band could possibly represent a phosphorylated version of PINK1-53. This additional fragment is not further highlighted in the PINK1 blots since it is currently unclear what this PINK1 fragment is the result of and its band was difficult to properly resolve, and thus investigate, in certain experimental approaches.
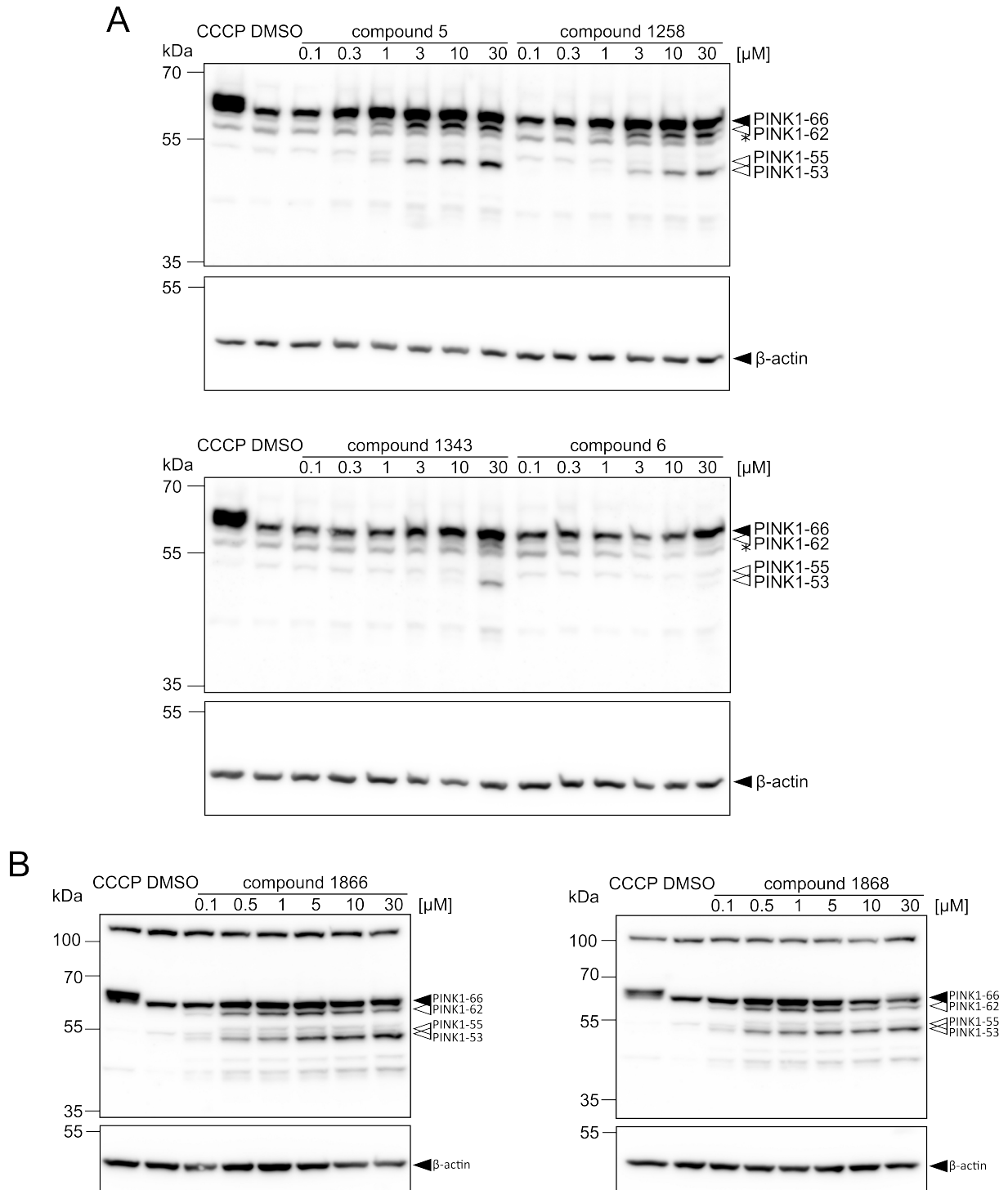
Figure 9: *PARL inhibition results in accumulation of unprocessed PINK1 and reveals alternative cleavage events.* **A)** HEK293 T-REx cells overexpressing PINK1 were treated for 3 h with 10 µM CCCP or 8 h with DMSO or first-generation inhibitors as indicated. β-actin was used as a loading control. A representative blot of three independent experiments is shown for compound 5. **B)** HEK293 T-REx cells overexpressing PINK1 were treated for 3 h with 10 µM CCCP or 8 h with DMSO or second-generation inhibitors as indicated. β-actin was used as a loading control. A representative blot of two independent experiments is shown.

2.2   Physiological characterization of novel α-ketoamide-based PARL inhibitors

2.2.1   PARL inhibitors do not affect the mitochondrial membrane potential

Following the successful establishment of the PARL inhibitors in terms of PGAM5 and PINK1 cleavage, a major concern left to be addressed was whether the inhibitors influence $\Delta\Psi_m$.

The JC-1 dye is a commonly used method to detect changes in $\Delta\Psi_m$. In this assay, the positively charged JC-1 dye is added to live cells where it accumulates within healthy mitochondria and forms red fluorescent aggregates. Upon disruption of $\Delta\Psi_m$, the aggregates disperse as monomers into the cytoplasm and fluorescent green (see **Figure 10**A). Therefore, the ratio of red to green fluorescence can be used to measure changes in $\Delta\Psi_m$ (Reers et al., 1991). Analysis of the PARL inhibitors on HEK293T cells via JC-1 assay shows that compound 5 does not cause a significant change in $\Delta\Psi_m$, which is in clear contrast to CCCP as a depolarizing agent (**Figure 10**B). As an additional positive control, Antimycin A was employed. Antimycin A shows a high variance in this assay, potentially caused by even minor differences in treatment times between experimental replicates, rendering it a less useful control than CCCP here. The three other first-generation inhibitors were analyzed in duplicates only, as it was at this point clear that they were inferior to compound 5 in terms of potency. Their preliminary data trends towards a slight depolarization effect, which reinforced the focus on compound 5 from the first-generation inhibitors.

When the second-generation inhibitors were tested, I opted to check the influence on $\Delta\Psi_m$ with a more straight-forward and high-throughput fluorescence-activated cell sorting (FACS) assay using tetramethylrhodamine ethyl ester (TMRE) dye. TMRE accumulates only within healthy mitochondria with a red fluorescence. As a proof-of-principle that TMRE signal reflects intact $\Delta\Psi_m$, live cell imaging of PINK1 overexpressing HEK293 T-REx cells stained with Hoechst and TMRE shows clear mitochondrial signal under DMSO or compound 5 treatment, but no TMRE signal in CCCP treated cells (**Figure 10**C). I thus moved forwards with the FACS analysis and tested compound 1868 as well. Indeed, TMRE signal in cells treated with compound 5 or the newer compound 1868 does not differ significantly from signal under DMSO treatment, but does so from signal under CCCP treatment (**Figure 10**D).

In conclusion, the PARL inhibitors do not affect $\Delta\Psi_m$ under the treatment times of three hours and concentrations of 10 µM (compound 5) or 0.5 µM (compound 1868) usually used during this study, regardless of PINK1 expression levels, and therefore are well-suited to investigate the consequences of PARL inhibition in healthy polarized mitochondria.
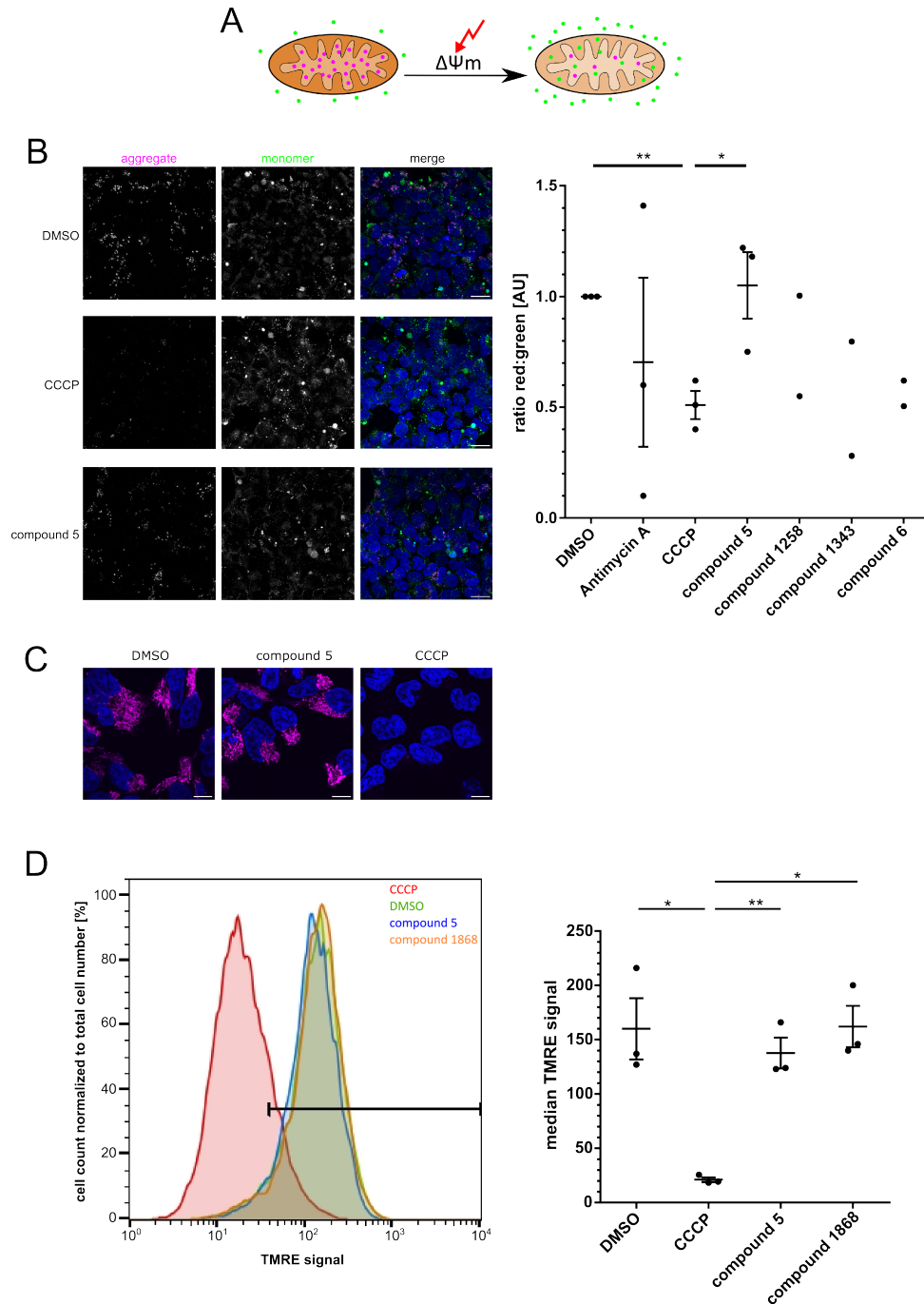
Figure 10: *Evaluation of mitochondrial membrane potential reveals no effect of PARL inhibitors.* **A)** Schematic depiction of JC-1 assay. **B)** HEK293T cells were stained with Hoechst (blue), treated for 3 h with DMSO, 10 μM CCCP, 30 μM Antimycin A or 5 μM of the inhibitors and then stained with JC-1 and taken for live-cell imaging. Left side displays exemplary microscopy images as maximum intensity z-stack projections for DMSO, CCCP and compound 5 (scale bars 20 μm). Right side shows the quantification of signal intensity ratios (*p ≤ 0.05, **p ≤ 0.01, unpaired t-test; means ± SEM, n = 3 for N(DMSO) = 1584, N(Antimycin A) = 1385, N(CCCP) = 1500, N(compound 5) = 1358; n=2 for N(compound 6) = 997, N(1343) = 957, N(1345) = 996). **C)** HEK293 T-REx cells overexpressing PINK1 were treated for 2 h with DMSO, 10 μM CCCP or 10 μM compound 5, stained with Hoechst (blue) and TMRE (magenta) and taken for live-cell imaging (scale bars 10 μm). **D)** HEK293 T-REx cells overexpressing PINK1 were treated for 3 h with DMSO, 10 μM CCCP, 10 μM compound 5 or 0.5 μM compound 1868 before being stained with DAPI and TMRE and taken for FACS analysis. Left side shows a representative FACS result with the black bar indicating the area of live TMRE-positive cells based on internal controls. The right graph shows the quantification of median TMRE signals (*p ≤ 0.05, **p ≤ 0.01, unpaired t-test; means ± SEM, n = 3).

2.2.2 PARL inhibitors are largely non-toxic at potent concentrations

With the inhibitors' non-influence on $\Delta\Psi_m$ proven, I investigated whether the two best inhibitors, compound 5 and compound 1868, show toxicity by measuring cell proliferation upon longer treatment times than the usual three to eight hours employed in previous experiments.

In wildtype HEK293T cells (**Figure 11**A), compound 5 does not affect cell proliferation much even at higher concentrations of 30 µM over five days of treatment, and the same is true for lower concentrations of compound 1868 (0.5 µM and 2.5 µM). However, compound 1868 has a detrimental effect on the cells at 10 µM, with delayed attainment of full cellular confluency at 102 hours instead of 79 hours compared to DMSO treatment, and increasing its concentration to 30 µM enhances this effect even further. In T-REx cells overexpressing PINK1 (**Figure 11**B) the toxicity effect is more pronounced: compound 5 at 10 µM and 30 µM here slows down the proliferation rate to a similar degree as 0.5 µM and 2.5 µM of compound 1868 do, but the cells still manage to reach 100 % confluency at 102 hours. 10 µM of compound 1868 however keep the cells from reaching full confluency over the course of the measured five days, and 30 µM of compound 1868 even result in complete arrest of cell proliferation from the beginning, comparable to CCCP treatment. As seen from the western blots in **Figure 9**, the overexpression of PINK1 combined with PARL inhibition causes a massive PINK1 stabilization. Upon prolonged treatment like in this proliferation assay, the accumulation of PINK1 could result in enhanced rates of mitophagy and the removal of otherwise healthy mitochondria, which would negatively influence cellular health and therefore proliferation. Wildtype HEK293T cells would likely be more resistant to this effect, since their level of PINK1 expression is much lower and levels of mitophagy would presumably be so as well.

To verify whether the toxic effect is due to PARL inhibition itself or rather due to a different off-target effect of the inhibitors, I repeated the proliferation assay comparing HeLa wildtype and PARL-KO cells. It appears that HeLa cells (**Figure 11**C) are in general more sensitive to the inhibitors influencing proliferation compared to HEK293(T) cells; even low concentrations of compound 5 negatively impact proliferation, and this is enhanced at higher concentrations and with compound 1868. As I have seen before that compound 1868 shows a higher potency on HeLa as compared to HEK293T cells (see **Figure 8**C), also the negative effects could be stronger in HeLa cells if they are due to PARL inhibition. Curiously, HeLa PARL-KO cells (**Figure 11**D) seem to exhibit fewer of the detrimental proliferation effects of the inhibitors at lower concentrations than wildtype HeLa cells while still showing complete proliferation arrest at the higher inhibitor concentrations. A better cell proliferation in the PARL-KO cells indicates that the adverse effect of the inhibitor compounds is indeed due to their PARL inhibition, which

would be in line with heightened cell toxicity observed in PINK1 overexpressing T-REx cells (see **Figure 11**B). However, the persisting toxicity at higher inhibitor concentrations, especially for compound 1868, even in PARL-KO cells doesn't quite fit into the picture, so it is probable that additional off-target effects of the PARL inhibitors influence cell proliferation independent of their PARL interaction.

It thus appears that optimization of the compound 5 structure that results in the higher potency of compound 1868 also comes at the cost of having a more pronounced cell toxic effect. To mitigate adverse cellular effects, I therefore kept to largely non-toxic yet potent inhibitor concentrations (10 µM for compound 5 and 0.5 µM for compound 1868) for the experiments shown in this study.
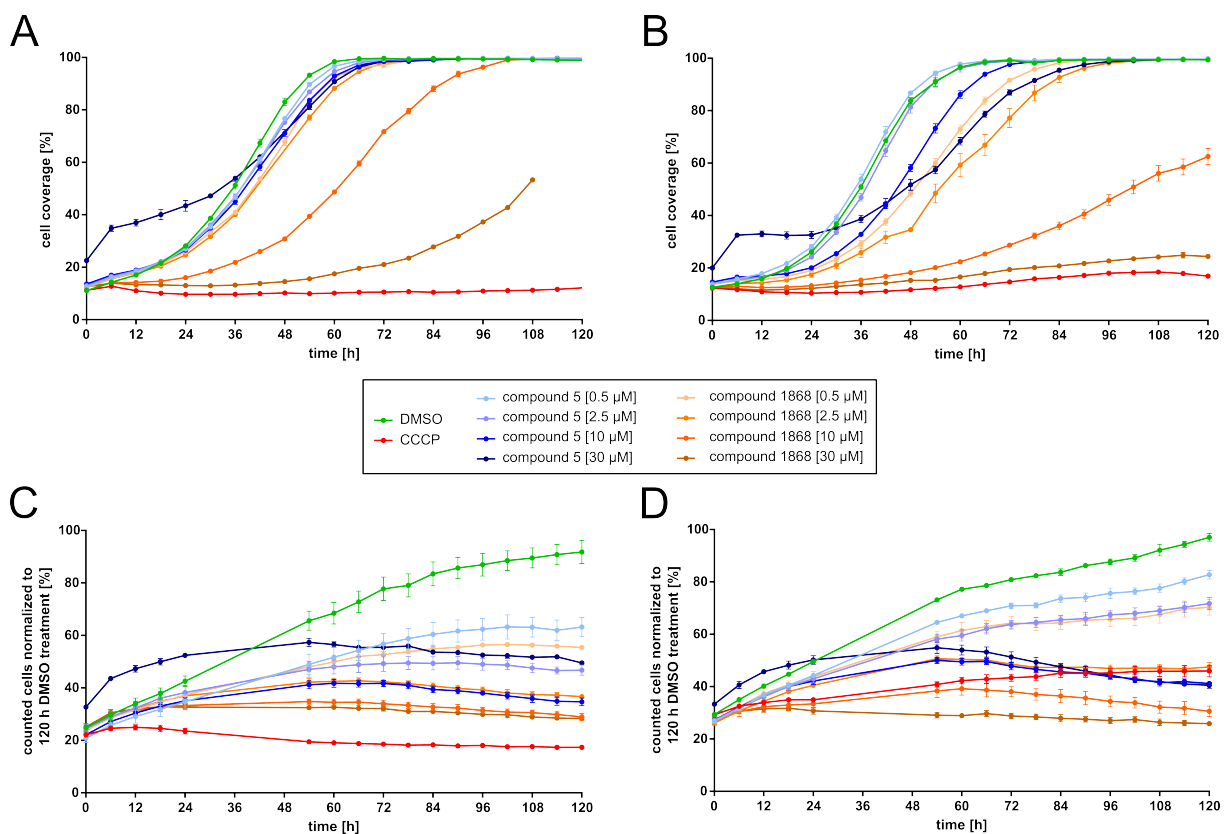
Figure 11: *PARL inhibitors show cell toxicity in the higher µM-ranges.* **A)** HEK293T cells or **B)** HEK293 T-REx cells overexpressing PINK1 were treated with DMSO, 10 µM CCCP or the indicated amounts of compound 5 or 1868 and imaged with the Axion BioSystems Omni in 6 h intervals for five days. **C)** HeLa wildtype cells or **D)** HeLa PARL KO cells were treated with DMSO, 10 µM CCCP or the indicated amounts of compound 5 or 1868 and imaged with the Incucyte S3 (Sartorius) in 6 h intervals for five days. Dots represent the mean of 1-3 imaged wells ± SEM; missing values are due to condensation interfering with imaging.

2.3 Characterization of PARL inhibition on PINK1 cleavage, trafficking and downstream pathways

As I observed multiple cleavage fragments of PINK1 under PARL inhibition (see **Figure 9**) whose submitochondrial localizations were unclear, I now turned to take a closer look at where these PINK1 species are trafficked to and what causes the cleavage fragment annotated as PINK1-53.

2.3.1 PARL inhibitors result in PINK1 cleavage fragments being localized in specific mitochondrial subcompartments

I started my investigation in HEK293T cells since there the inhibitors showed the least cell toxicity (see **Section 2.2.2**) and since their endogenous expression system is closer to the normal physiological state than the PINK1 overexpression system. Due to endogenous PINK1 being difficult to detect, I performed a sodium carbonate extraction of mitochondrial membranes (**Figure 12**A). The stabilized full-length PINK1-66 is present in all first-generation inhibitors, but most pronounced and significantly increased in compound 5. Also visible is the PINK1-62 form (cleaved by MPP), mostly appreciable in compound 5 and compound 6. The lower PINK1 fragments observed in **Figure 9** could not be detected in this approach.

After obtaining a new PINK1 antibody that is able to detect endogenous PINK1 with an increased sensitivity, I applied another approach in HEK239T cells using a subcellular fractionation, which leaves the mitochondrial subcompartments intact (**Figure 12**B). Here, the detectable endogenous PINK1 fragments mimic those previously observed in whole cell lysates of PINK1-overexpressing T-REx cells (see **Figure 9**). DMSO treatment results in PINK1-66 and PINK1-55 (PARL-cleaved PINK1) forms being present mostly in the cytosol, as PINK1 isn't stabilized at the mitochondria here. Still, a faint band of PINK1-62 is present in the mitochondrial fraction, indicative of PINK1 being imported and cleaved by MPP but not yet cleaved by PARL and retrotranslocated into the cytosol. With CCCP treatment, a great stabilization of PINK1-66 (full-length and phosphorylated form based on the upwards shift) is present, mostly in the mitochondrial fraction where it localizes to the OMM. Under inhibitor treatment, a stabilization of PINK1-62 can be observed in the mitochondrial fraction, and for PINK1-66 also to a lesser degree in the cytosol, accompanied by a similar stabilization of the yet-to-be-defined PINK1-53 fragment. A very similar image to this is revealed under inducible overexpression of PINK1 (**Figure 12**C). This similarity between endogenous and overexpressed PINK1 confirms that the overexpression system can be used for further exploration of the inhibitor effects on PINK1.

Following these results of the different PINK1 species mostly localizing to the mitochondria under PARL inhibition, the question arised where each species is located within the mitochondria. To answer this, I used a proteinase K assay on the isolated mitochondrial fraction (**Figure 12**D). Since proteinase K digests any peptide sequence accessible to it and the PINK1 antibody used here binds to the residues 175-250 within PINK1's kinase domain, PINK1 localized with its kinase domain towards the cytosol shows a lessened signal with more proteinase K applied (CCCP lanes). With compound 5 treatment, proteinase K completely degrades PINK1-66 as well as PINK1-55/-53, generating smaller cleavage fragments of 50/40/20 kDa. This proteinase K accessibility shows that these PINK1 species are indeed localized at the OMM. PINK1-62 is partially protected from proteinase K, showing only a slight signal reduction. There are two possible explanations for this: PINK1-62 may exist as two pools, one protected at the inside of the mitochondria below the OMM, and one located at the OMM, accessible to proteinase K. Alternatively, and as an artifact of this experimental setup, proteinase K treatment may slightly disrupt the OMM such that the IMS-localized AIF and some fraction of PINK1-62 (localized purely within the mitochondria) are also partially digested by proteinase K.

Notable in **Figure 12**B-D is the higher quantity of PINK1-62 over PINK1-66, whereas in the whole lysate samples in **Figure 9**, there is clearly more of PINK1-66 than of PINK1-62. This circumstance is indicative of PINK1 being present as a flexible import-intermediate form, spanning all mitochondrial compartments and can be explained by residual protease activity (namely MPP) targeting PINK1-66 over the duration of the fractionation protocol. This can be seen in the gradual decrease of PINK1-66 and increase of PINK1-62 in the steps between whole cell lysate, obtaining the mitochondrial fraction and subjecting the same fraction to the proteinase K assay (**Figure 12**E).

Taken together, these results demonstrate that PINK1 import and submitochondrial trafficking under PARL inhibition is a highly dynamic process. Especially interesting is the potential dual-targeting of PINK1-62 at the OMM and within mitochondria, which will be further discussed in **Section 3.1**.
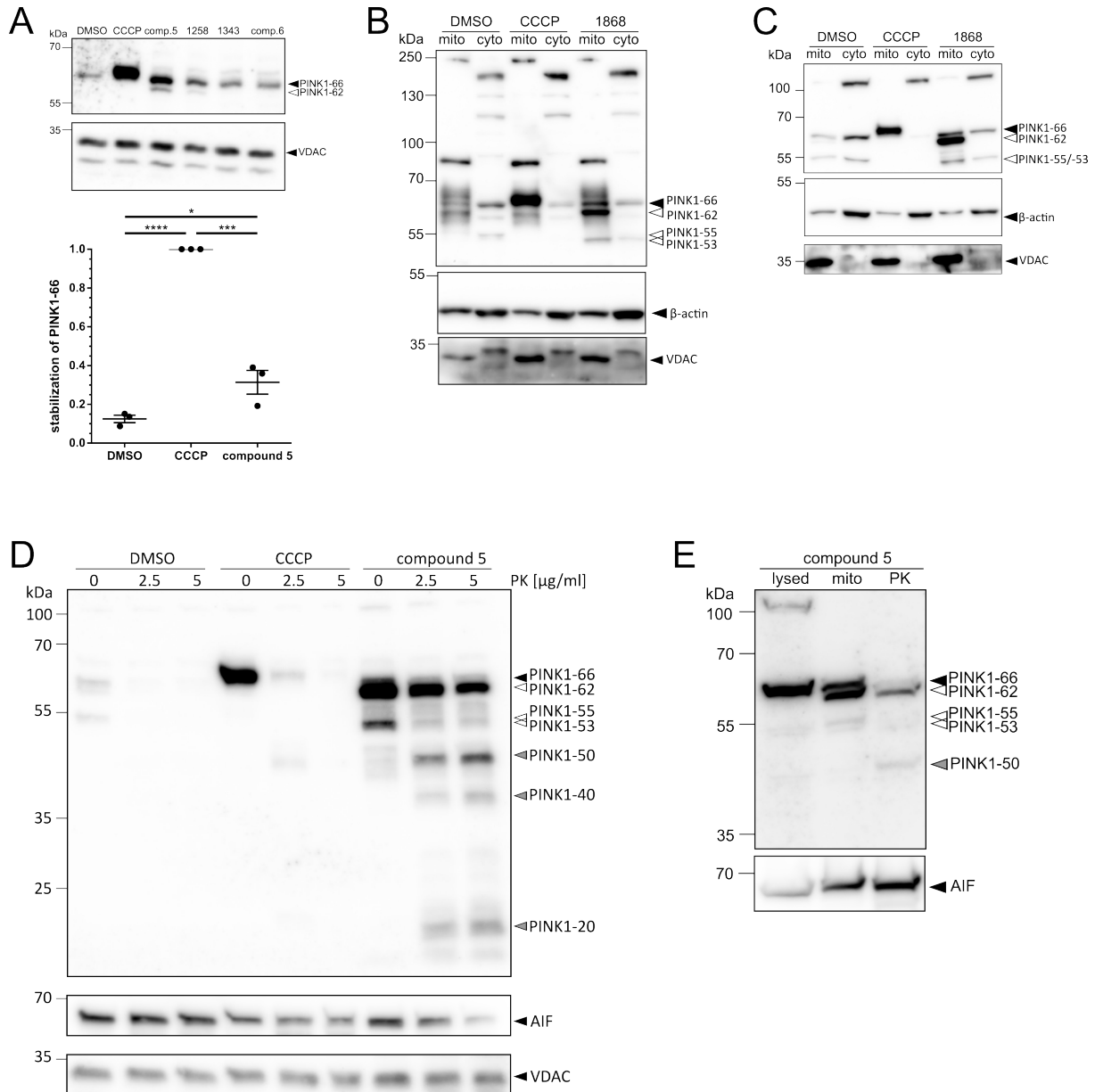
Figure 12: *Different PINK1 cleavage fragments generated by PARL inhibition are localized to specific cellular and mitochondrial subcompartments.* **A)** HEK293T cells were treated for 8 h with DMSO, 10 µM CCCP or 5 µM of the inhibitors before being subjected to a sodium carbonate fractionation. VDAC was used as fractionation control. The mitochondrial membrane fraction samples are shown. The quantification below shows the relative PINK1-66 stabilization, compared to PINK1-66 levels in the CCCP condition, in DMSO, CCCP and compound 5 samples (*p ≤ 0.05, ***p ≤ 0.001, ****p ≤ 0.0001, unpaired t-test; means ± SEM, n = 3). **B)** HEK293T cells were treated for 3 h with DMSO, 10 µM CCCP or 0.5 µM 1868 before being subjected to a subcellular fractionation into mitochondrial (mito) and cytosolic (cyto) fractions. β-actin and VDAC were used as fractionation controls. A representative blot of two independent experiments is shown. **C)** HEK293 T-REx cells overexpressing PINK1 were treated for 3 h with DMSO, 10 µM CCCP or 5 µM compound 5 before being subjected to a subcellular fractionation into mitochondrial (mito) and cytosolic (cyto) fractions. β-actin and VDAC were used as fractionation controls. A representative blot of two independent experiments is shown. Samples were prepared by Master student Simon Feldkamp. **D)** HEK293 T-REx cells overexpressing PINK1 were treated for 3 h with DMSO, 10 µM CCCP or 5 µM compound 5 before being subjected to a proteinase K (PK) protection assay for 1 h. AIF and VDAC were used as fractionation controls. A representative blot of three independent experiments is shown. **E)** HEK293 T-REx cells overexpressing PINK1 were treated for 6 h with 5 µM compound 5 before being either lysed directly (lysed), subjected to a subcellular fractionation to isolate mitochondria (mito), or subjected to a PK protection assay for 30 min. AIF was used as fractionation control. A representative blot of three independent experiments is shown.

2.3.2 The cleavage activity of the mitochondrial protease OMA1 is targeted specifically towards PINK1 under PARL inhibition

To investigate which protease is responsible for the cleavage fragment PINK1-53 under PARL inhibition, I tested the effect of siRNA-mediated knockdown of the PINK1-cleaving protease OMA1 (Sekine et al., 2019; Akabane et al., 2023). As shown in **Figure 13**A, the knockdown of OMA1 results in a reduction of PINK1-53 and an increase of PINK1-62, indicating that OMA1 targets PINK1 under PARL inhibition. This finding is intriguing as thus far, there have only been cases described where OMA1 cleaves PINK1 in depolarized mitochondria, upon certain PINK1 mutations and/or when TIM23 is downregulated (Sekine et al., 2019; Akabane et al., 2023), none of which is true in this study. It would therefore suggest that PARL inhibition is a novel trigger for OMA1 cleavage activity directed towards PINK1. To check whether OMA1 cleavage is specifically directed towards PINK1 here, I looked at OPA1 cleavage as an established OMA1 substrate (Ehses et al., 2009) under PARL inhibition (**Figure 13**B). Thus, it is clear that while CCCP treatment causes OPA1 cleavage, OPA1 is not cleaved under PARL inhibition with either inhibitor compounds, so OMA1 cleavage activity appears to be specific towards PINK1 under these circumstances.
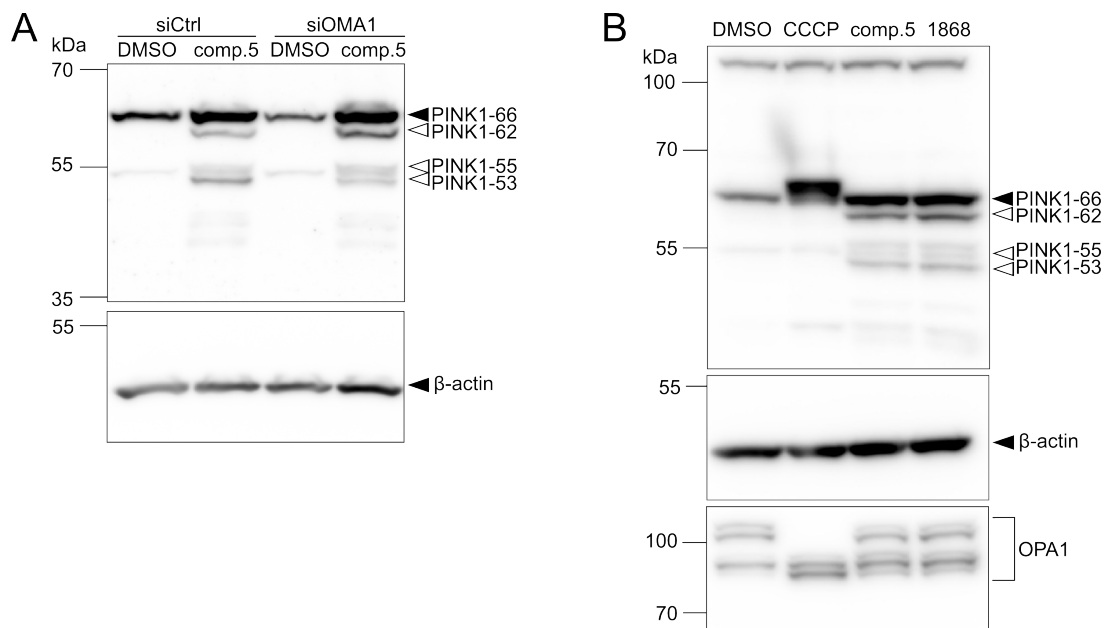
Figure 13: *The mitochondrial protease OMA1 cleaves specifically PINK1 under PARL inhibition, rather than another of its substrates, OPA1.* **A)** HEK293 T-REx cells overexpressing PINK1 were transfected with control siRNA (siCtrl) or siRNA directed against OMA1 (siOMA1). Cells were treated for 8 h with DMSO or 10 µM compound 5. β-actin was used as a loading control. A representative blot of four independent experiments is shown. **B)** HEK293 T-REx cells overexpressing PINK1 were treated for 3 h with DMSO, 10 µM CCCP, 10 µM compound 5 or 0.5 µM 1868. β-actin was used as a loading control. A representative blot of two independent experiments is shown.

2.3.3   PARL inhibition stabilizes different PINK1 forms within the PINK1-TOM-TIM23 supercomplex

Following the discovery of the multiple differently cleaved and submitochondrially targeted PINK1 forms (for a summarized scheme, see **Figure 18** in **Section 3.1**), I was then interested in the processes of PINK1 stabilization. Typically under CCCP treatment, PINK1 stabilizes at the TOM complex while maintaining interaction with the TIM23 complex (Akabane et al., 2023; Eldeeb et al., 2024). I asked whether PARL inhibition results in the same PINK1-TOM-TIM23 super-complex and if yes, which of the PINK1 species participate in the interaction.

To this end, I used a FLAG-immunoprecipitation approach on HEK293 T-REx cells inducibly overexpressing PINK1 with a FLAG tag. **Figure 14**A and **Figure 14**C show that treatment with both inhibitors (compound 5 and compound 1868) results in co-immunoprecipitation of PINK1 with TOM20 and TOM22, two TOM complex proteins. In order to judge the actual complex interaction of PINK1 with the TOM complex, I applied the PINK1-FLAG immunoprecipitation samples to a Blue Native PAGE (BN-PAGE) (**Figure 14**B and D). This corroborated that indeed, PINK1, TOM20 and TOM22 reside in one complex at ~750 kDa in both CCCP and PARL inhibitor treated cells. While the interaction of PINK1 with the TOM proteins is not as strong with PARL inhibition as under CCCP treatment, it is much stronger than under DMSO control treatment. This difference between CCCP and inhibitor treatment could be explained by not all PINK1 in inhibitor-treated cells residing at the mitochondria in the first place, in contrast to CCCP-treated cells where essentially all PINK1 localizes to mitochondria (see **Figure 12**C). In addition, even the PINK1 fraction that does localize to the mitochondria exists as different species that may not all interact stably with the TOM complex under PARL inhibition, such as the mostly inner mitochondrially localized portion of PINK1-62 (see **Figure 12**D).

To address the question of which PINK1 species are present in the PINK1-TOM complex, I used the BN-PAGE gel for a subsequent 2D-PAGE (**Figure 14**E). Interestingly, this shows that under PARL inhibition, all previously observed PINK1 fragments can be found within the PINK1-TOM complex band, even PINK1-62. However, it appears that PINK1-66 and PINK1-62 are the most prominent forms within the PINK1-TOM complex. PINK1-55 and PINK1-53, while present, are less pronounced in the complex as compared to the total PINK1 protein loaded on the left side of the gel.

Lastly, I asked if the PINK1 species under PARL inhibition also interact with TIM23 complex proteins via another PINK1-FLAG immunoprecipitation. **Figure 15**A demonstrates that PINK1 co-immunoprecipitates with the TIM23 complex members TIM17A, TIM23 and TIM50 under PARL inhibition. This interaction, again, is weaker than under dissipation of $\Delta\Psi_m$, here caused
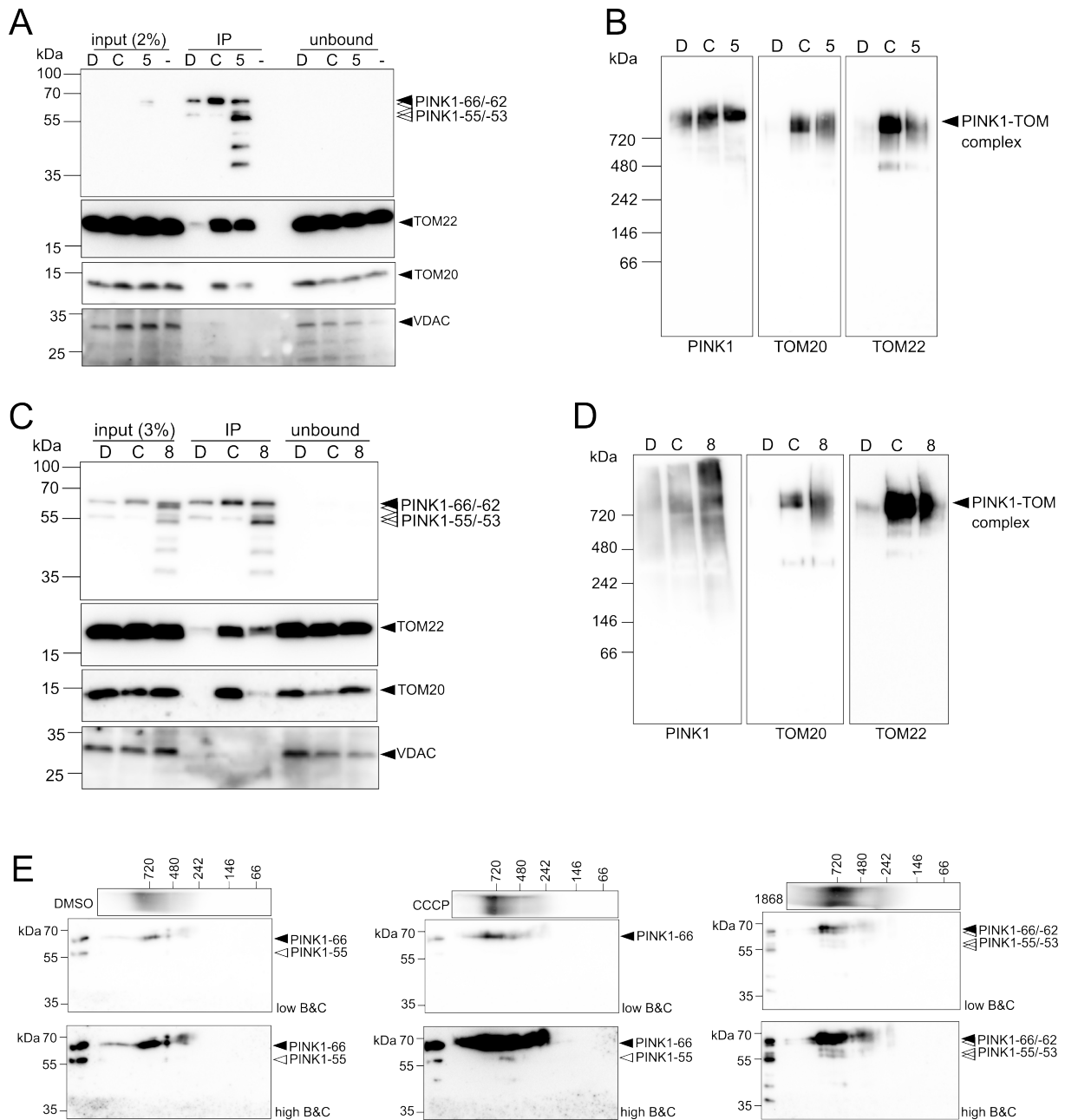
Figure 14: *PARL inhibition results in stabilization of all PINK1 forms at the the PINK1-TOM supercomplex.*
HEK293 T-REx cells overexpressing PINK1-FLAG were treated for 3 h with DMSO ("D"), 10 µM CCCP ("C"), 10 µM
compound 5 ("5") or 0.5 µM 1868 ("8") and subjected to a FLAG immunoprecipitation. **A/C)** SDS-PAGE showing
all immunoprecipitation fractions. VDAC was used as non-binding control. "-" indicates non-induced cells. In A),
the PINK1 blot exhibited sensitivity issues when imaging the input samples only. **B/D)** BN-PAGEs of the bound
immunoprecipitation fractions shown in A) and C) as "IP". A) and B) show representative blots of two independent
experiments, C) and D) show representative blots of three independent experiments. **E)** The horizontally tilted tops
represent the BN-PAGE of the bound immunoprecipitation fraction that was loaded as a duplicate to the 2D SDS-
PAGE below. The 2D SDS-PAGEs are all adjusted for low and high brightness/contrast ("B&C") individually to best
show the present PINK1 forms.

by the combined treatment of Oligomycin and Antimycin A. There was no co-immunoprecipitation of mtHSP70, an associated protein of the TIM23 complex, fitting to what has been published (Akabane et al., 2023). The pulldown of TOM22 mimics the results from **Figure 14**C; in addition, it was possible to show association of PINK1 with another TOM complex protein, TOM40. Seeing how the co-immunoprecipitation of the TIM23 complex proteins appeared weaker than that of the TOM complex, crosslinking was applied prior to the co-immunoprecipitation procedure **Figure 15**B). This greatly increased pulldown of TIM17A, TIM23 and TIM50 in inhibitor-treated cells, indicating that the interaction of PINK1 with the TIM23 complex might be of a more transient nature as compared to interaction with the TOM complex.

Altogether, these results indicate that PARL inhibition results in various PINK1 species interacting with and stabilizing at components of the TOM and TIM23 complex.
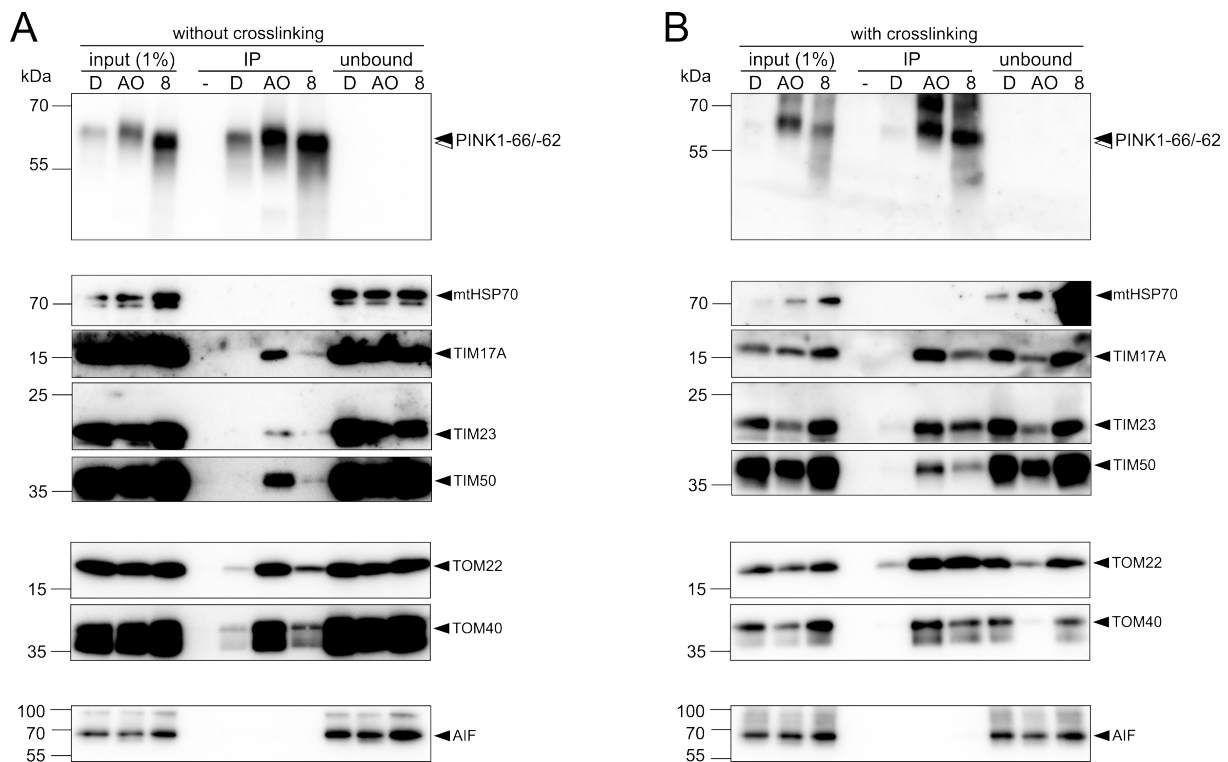
Figure 15: *PARL inhibition results in stabilization of PINK1 forms within the PINK1-TOM-TIM23 supercomplex.* HEK293 T-REx cells overexpressing PINK1-FLAG were treated for 3 h with DMSO ("D"), 10 µM Oligomycin and Antimycin A ("AO"), or 0.5 µM 1868 ("8") and subjected to a FLAG immunoprecipitation. "-" indicates use of non-induced cells. AIF was used as non-binding control. **A)** SDS-PAGE showing all immunoprecipitation fractions. Representative blots of two independent experiments are shown. **B)** SDS-PAGE showing all immunoprecipitation fractions, with crosslinking applied prior to co-immunoprecipitation. Representative blots of two independent experiments are shown. Experiments were conducted by Master student Simon Feldkamp.

2.3.4 Exploration of downstream effects of PARL inhibition via (phospho-) proteomics

I could show that PARL inhibition results in stabilized PINK1 at the TOM-TIM23-supercomplex similar to what can be observed under $\Delta\Psi_m$ dissipation, which is the first step in PINK1 auto-phosphorylation and activating its kinase function. Therefore, I was interested to see whether PARL inhibition would allow screening for PINK1 kinase substrates or enrichment of proteins involved in mitophagy overall. For this, I turned to a proteomics approach, including measurements of the whole proteome and phosphoproteome in the mitochondrial fraction of wildtype HEK293T cells, comparing DMSO treatment to inhibitor compound 1868.

In the whole proteome, even though my mitochondrial fraction samples were rather impure with only 16 % of all recognized proteins being mitochondrially localized, I achieved a good coverage of known mitochondrial proteins with 77 % (**Figure 16**A). As a consequence, very few of the detected phosphoproteomic peptides were localized to mitochondria (3 %, **Figure 16**B). This contamination of the mitochondrial fraction with non-mitochondrial proteins is likely due to remaining association of the ER with the mitochondria via the MAMs. For future proteomics approaches, the applied subcellular fractionation protocol should therefore be further improved, for example with additional washing steps and differential centrifugation to separate MAMs from purified mitochondria.

Due to the high amount of protein load that is required for phosphoproteomics, I pooled technical replicates and included two biological replicates in a single proteomics run for a total of four samples per condition. As a result of the drastic replicate pooling, variance within and between the condition groups was a concern. Taking a look at the principal component analyses of whole proteome (**Figure S.1**A) and phosphoproteome (**Figure S.1**B) confirms this concern. In the whole proteome data set, the DMSO control values (blue) are quite spread-out when compared to the inhibitor values (orange). Same can be said from the phosphoproteome data set, where the DMSO control values show an even bigger spread (mind the different axis ranges between **Figure S.1**A and B), while three of the inhibitor values cluster nicely. From the phosphoproteomics data, two samples could be considered as outliers ("PP_03" in the control group and "PP_05" in the inhibitor group). However, due to the overall large variance also in the whole proteome set, it was decided to include all samples in the analysis so as to not introduce subjective biases by excluding samples that present as clear outliers in the phosphoproteome data set but not in the whole proteome data set.

Analysis of the whole proteome (**Figure 16**C, for curated results table see **Table S.1**) yielded three significant hits that are downregulated in the inhibitor condition. Of greatest interest is NBR1, one of the ubiquitin-binding autophagy adapters (Kirkin et al., 2009; Chan et al., 2011).

However, NBR1 is dispensable in PINK1-Parkin-mediated mitophagy (Lazarou et al., 2015). From the three adapters involved in PINK1-Parkin-mediated mitophagy (NDP52, optineurin and TAX1BP1), only TAX1BP1 was detected and is downregulated in the inhibitor condition (p-value = 0.12). The regulator TBK1 was also downregulated upon inhibitor treatment (p-value = 0.21). Also noteworthy is the detection of STARD7 which did not reach the significance cut-off q-value but is enriched in the inhibitor condition. STARD7's enrichment as another PARL substrate corroborates the mechanism of PARL inhibition. Lastly, cytochrome c (CYCS), which is localized in the IMS and is released into the cytosol in apoptosis, was downregulated under inhibitor treatment but barely did not reach the significance cut-off q-value ≤ 0.05.

The phosphoproteomics approach (**Figure 16**D, for curated results table see **Table S.2**) resulted in each three significantly up- and downregulated hits upon inhibitor treatment. The potentially most relevant one is the proto-oncogene serine/threonine-protein kinase RAF1, as it can translocate to mitochondria to protect against apoptosis (Wang et al., 1996; Jin et al., 2005). RAF1 is more phosphorylated at site S619 in the inhibitor condition.

Taken together, the lesser abundance of autophagy-involved proteins NBR1 and specifically TAX1BP1 and TBK1 may indicate that PARL inhibition results in mitophagy and that the employed 16 hours of compound 1868 treatment are enough to measure their decreased protein levels due to autolysosomal degradation.

Furthermore, the downregulation of cytochrome c in the inhibitor condition implies that release of cytochrome c into the cytosol has been triggered, as the cytosol has largely been eliminated from the used mitochondrial sample fraction. This would then point towards the beginning of apoptosis after 16 hours of PARL inhibition. PARL has been implicated in apoptosis regulation, either as pro-apoptotic via Smac/Diablo processing (Saita et al., 2017) or as anti-apoptotic via cytochrome c release dependent on cristae remodelling by OPA1 (Cipolat et al., 2006). Both studies have however observed increased or faster cytosolic release of cytochrome c upon apoptotic stimuli in PARL KO systems, which could relate to my observed reduction of mitochondrial cytochrome c upon prolonged PARL inhibition.

Contrary to this, the detected enhanced phosphorylation of RAF1 under PARL inhibition may relate to anti-apoptotic regulations. When activated, RAF1 can relocate to mitochondria and exert its anti-apoptotic function via Bcl-2 (Wang et al., 1996). This mechanism has been associated with phosphorylation at S338/339 (Jin et al., 2005), whereas the detected phosphorylation site here is S619. Not much is known about this site, other than that it does activate RAF1's kinase function and is caused by protein kinase C (Carroll and May, 1994).

All in all, further investigations are needed to verify whether RAF1 may be directly or in-

directly phosphorylated by PINK1 under PARL inhibition, and how regulation of apoptosis and mitophagy are affected by the PARL inhibitor. To further substantiate my claim that PARL inhibition can lead to mitophagy, I lastly turned to direct investigation of Parkin recruitment.
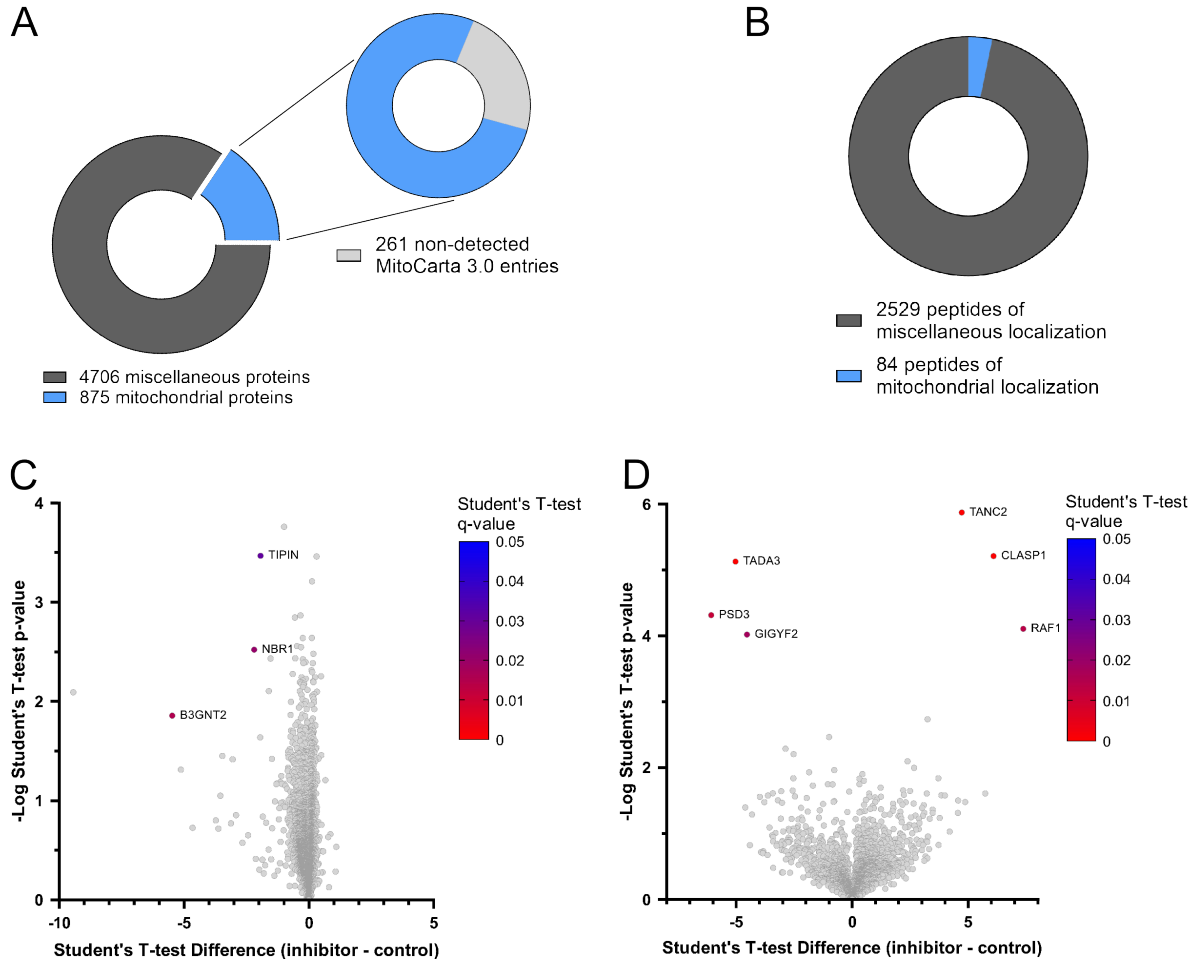
Figure 16: *Analysis of whole proteome and phosphoproteins following PARL inhibition.* **A)** Breakdown of detected proteins in whole proteomics approach on the mitochondrial fraction of HEK293T cells treated for 16 h with either DMSO or 0.5 µM inhibitor 1868. **B)** Breakdown of detected peptides in phosphoproteomics approach on the mitochondrial fraction of HEK293T cells treated for 16 h with either DMSO or 0.5 µM inhibitor 1868. **C)** Volcano plot for whole proteomics approach. **D)** Volcano plot for phosphoproteomics approach.

2.3.5   Inhibition of PARL results in Parkin recruitment

The proteomics data sets did not include detection of the PINK1 target Parkin, the E3 ubiquitin ligase that is recruited to the mitochondria, activated by PINK1 and that is responsible for attaching ubiquitin chains to OMM proteins, targeting mitochondria towards mitophagy. However, Parkin recruitment to the mitochondria is expected upon the PINK1 stabilization at the TOM-TIM23 supercomplex upon $\Delta\Psi_m$ dissipation, which is mimicked by PARL inhibition as shown in **Figure 14** and **Figure 15**. I thus decided to investigate possible Parkin recruitment to the

mitochondria upon PARL inhibition by two more targeted assays.

I first tested for Parkin recruitment via its presence in the mitochondrial or the cytosolic fraction after a subcellular fractionation (**Figure 17**A). The recruitment of Parkin to the mitochondrial fraction is observable especially in compound 5 and compound 1258. Included here as an additional positive control is again Antimycin A, which also results in Parkin recruitment. While quantification shows a much less drastic Parkin recruitment in response to PARL inhibition compared to Antimycin A or CCCP treatment, the difference between compound 5 treatment and DMSO condition is still significant.

As an additional assay, I evaluated Parkin recruitment to mito-mCherry marked mitochondria via confocal microscopy and quantified the number of cells that showed more than three Parkin recruitment events to mitochondria (**Figure 17**B-D). In this assay, compound 5 yielded a similar Parkin recruitment efficiency as Antimycin A and was again significantly different from recruitment in the DMSO control condition.

Overall, PARL inhibition results in mild but evident Parkin recruitment to mitochondria, which can be postulated as the next step towards mitophagy following PINK1 stabilization. The reduced level of Parkin recruitment compared to the CCCP condition is also in line with the slightly less prominent interaction of PINK1 with the TOM complex as observed in **Figure 14**A-D): a lower amount of TOM-stabilized PINK1 under PARL inhibition would result in less autophosphorylated PINK1 and therefore reduced levels of Parkin recruitment following PINK1 kinase activity.
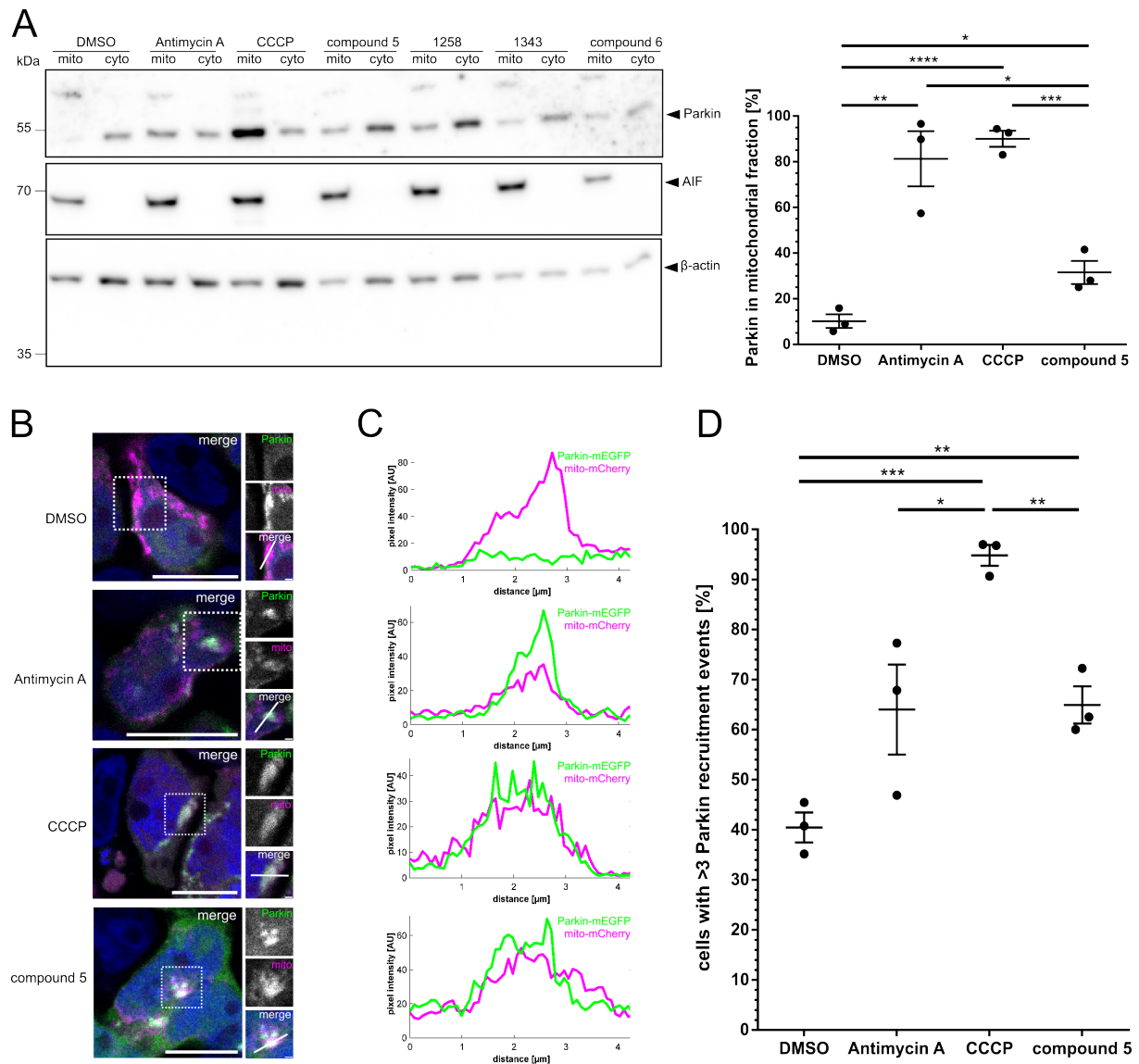
Figure 17: *Parkin recruitment occurs as a result of PARL inhibition.* **A)** HEK293 T-REx cells overexpressing PINK1 were transfected with HA-Parkin-IRES-GFP and treated for 22 h with 5 µM inhibitors or DMSO or 3 h 30 µM Antimycin A or 10 µM CCCP before being subjected to a subcellular fractionation (mito = mitochondrial fraction, cyto = cytosolic fraction). The right side shows the quantification of Parkin recruited to the mitochondrial fraction as a percentage of total detected Parkin in DMSO, Antimycin A, CCCP and compound 5 samples (*p ≤ 0.05, **p ≤ 0.01, ***p ≤ 0.001, ****p ≤ 0.0001, unpaired t-test; means ± SEM, n = 3). AIF and β-actin were used as fractionation controls. **B)** HEK293 T-REx cells overexpressing PINK1 were transfected with mito-mCherry and Parkin-mEGFP and treated for 3 h with DMSO, 30 µM Antimycin A, 10 µM CCCP or 5 µM compound 5 before being stained with Hoechst (blue) and fixed. Representative fluorescence microscopy images are shown (scale bars 10 µm, insets scale bars 1 µm). **C)** Corresponding pixel intensity plots for the white line in the merge inset image of B), showing Parkin recruitment to the fluorescent mitochondria via overlaps in channel intensity values. **D)** Quantification of cells from B) that show more than three Parkin recruitment events (*p ≤ 0.05, **p ≤ 0.01, ***p ≤ 0.001, unpaired t-test; means ± SEM, n = 3, N(DMSO) = 86, N(Antimycin A) = 82, N(CCCP) = 96, N(compound 5) = 80).

3 Discussion

In this work, I established a group of novel α-ketoamide-based PARL inhibitors and showed their rapid effect on two PARL substrates, PGAM5 and PINK1. Recently, the Stříšovský group has also been able to show that compound 5's inhibitor capacity is specific towards PARL, and not other rhomboid proteases like GlpG or RHBDL2 (Bach et al., 2024). I showed in tissue culture cells that these inhibitor compounds are effective at concentrations and treatment durations that do not cause cell toxicity, and that they do not disrupt the mitochondrial membrane potential under the employed conditions. This proved the inhibitor compounds to be excellent tools to investigate non-PARL governed PINK1 proteolysis and the resulting trafficking fates of PINK1. Under PARL inhibition, PINK1 exhibits pronounced stabilization as a full-length protein at the mitochondria, as well as cleavage by the proteases MPP and OMA1. Interestingly, MPP-cleaved PINK1 can localize fully within the mitochondria, where it may phosphorylate proposed putative PINK1 substrates. While OMA1-mediated proteolysis of PINK1 is not unheard of, I herein show that this cleavage is specific towards PINK1 and not OPA1, another OMA1 substrate, and happens in non-depolarized mitochondria, which is unprecedented. In addition, the various PINK1 forms all interact with the TOM-TIM23 import supercomplex, resulting in Parkin recruitment to the mitochondria, indicating mitophagy. I propose a model in which PARL inhibition promotes a PINK1 import intermediate that transiently interacts with the mitochondrial import complexes and can be cleaved alternatively by OMA1, resulting in a more moderate activation of mitophagy than is the case in depolarized mitochondria. PARL inhibition may thus even open up therapeutic avenues for directing mitochondria affected by PD-related activity-reduced PINK1 mutants towards a reduced threshold for mitophagic induction and thus aid in maintaining an appropriate level of mitophagy.

3.1 PARL inhibition causes different PINK1 forms and mitochondrial localizations

In intact $\Delta\Psi_m$ conditions, human cells usually show both full-length PINK1 and an additional PARL-cleaved PINK1 form, the latter of which is rapidly degraded via the N-end rule pathway. As PINK1 is first partially imported into mitochondria, there processed by MPP and PARL, and then retrotranslocated into the cytosol again for proteasomal degradation, PINK1 is present in both the cytosol and the mitochondria. When $\Delta\Psi_m$ is disrupted in damaged mitochondria, full-length PINK1 stabilizes as a mitochondrial membrane spanner and recruits Parkin. Upon PARL inhibition, I observe that multiple PINK1 forms are present, summarized in **Figure 18**. Most

prominent is the stabilization of full-length PINK1-66, mostly at the mitochondrial surface (**Figure 12**). In addition, I showed that OMA1 is responsible for cleaving longer PINK1 forms to generate PINK1-53 (**Figure 13**), which is readily accessible to proteinase K with its kinase domain reaching into the cytosol and is also localized in a smaller quantity in the cytosol. Also clearly visible is the MPP-cleaved form PINK1-62, which presence is emphasized when performing a subcellular fractionation to enrich mitochondria. Intriguingly, I found that this PINK1-62 form is mostly located within the mitochondria and not oriented with its C-terminal kinase towards the cytosol, though a certain fraction of this PINK1-62 pool also exists within the PINK1-TOM-TIM23 supercomplex (**Figure 14**E). Using sodium carbonate extraction for isolating mitochondrial membranes, I detected endogenous PINK1-62, in addition to PINK1-66 (**Figure 12**A); thus it appears that at least these two PINK1 forms are stably bound to mitochondrial membranes as integral membrane proteins.

A surprising finding was the mostly inner-mitochondrially localized pool of PINK1-62. However, PINK1 being present within the mitochondria isn't without precedence. Previous work from our laboratory and others showed PINK1-55 being partially protected within polarized mitochondria (Jin et al., 2010; Meissner et al., 2011); additionally, Pridgeon et al. (2007) and Fallaize et al. (2015) detected PINK1 presence at the IMM and IMS of intact mitochondria, whereas Jin et al. (2010) found PINK1 only at the IMM. Of note are various reported accounts of PINK1 potentially phosphorylating IMM or IMS proteins such as the cristae related protein Mic60 (Tsai et al., 2018), the complex I subunit NdufA10 (Morais et al., 2014), the calcium and potassium exchanger LETM1 (Huang et al., 2017), the HSP90-paralog TRAP1 (Pridgeon et al., 2007; Fallaize et al., 2015) and the serine protease HTRA2 (Plun-Favreau et al., 2007).

How PINK1, which canonically has only been postulated as being autophosphorylated and thus possessing its kinase activity after forming a supercomplex with the TOM complex at the OMM (Hasson et al., 2013; Okatsu et al., 2015; Sekine et al., 2019; Maruszczak et al., 2022; Rasool et al., 2022; Eldeeb et al., 2024; Raimi et al., 2024), would phosphorylate proteins that are localized at the IMM/IMS has not been elucidated for any of those potential substrates. However, the current PINK1-TOM-TIM23 stabilization models are primarily based on data acquired from depolarized mitochondria where the TIM23 import machinery is impaired. In my study conducted in mitochondria with intact $\Delta\Psi_m$, the stabilized PINK1-62 is mostly localized within mitochondria, including its kinase domain, and would thus be in the right place to potentially phosphorylate IMM/IMS targets. However, it is still undetermined whether the kinase of this particular PINK1 form is actually active, how this PINK1 form is finally targeted to its inner mitochondrial localization, and where exactly it is located (matrix, IMS or IMM).
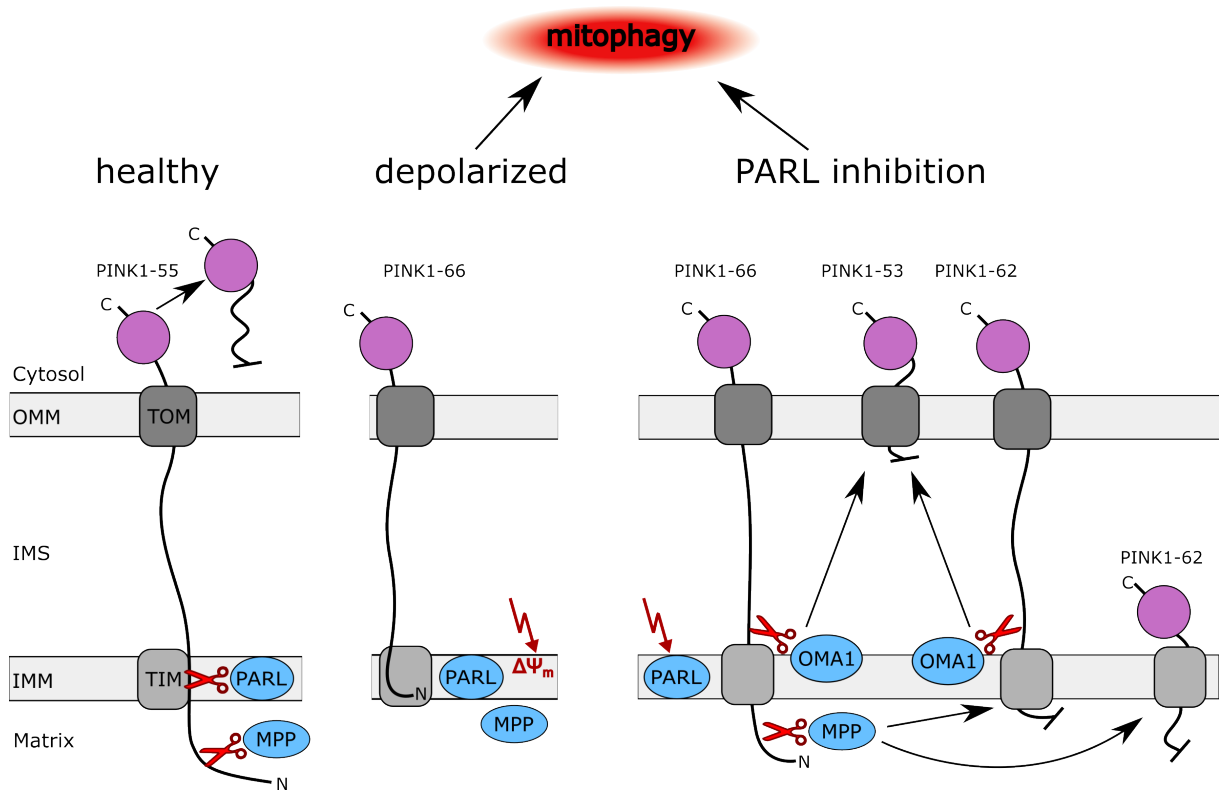
Figure 18: *Model of PINK1 cleavage events and submitochondrial trafficking in healthy or depolarized mitochondria or under PARL inhibition.* In healthy, polarized mitochondria (**left panel**), PINK1 is partially imported into the mitochondria via the TOM-TIM23 complex and is cleaved by MPP after its MTS and by PARL in its TMD. The shortened PINK1-55 fragment is released into the cytosol and is degraded by the proteasome. In depolarized mitochondria (such as via CCCP, **middle panel**), PINK1 cannot be fully imported into the mitochondria and remains bound to the TOM-TIM23 complex, presumably without being accessible to PARL or MPP. The stabilized PINK1-66 autophosphorylates and initiates mitophagy. Under PARL inhibition (**right panel**), PINK1 can also be stabilized at the TOM-TIM23 complex in various forms, causing mitophagy. PINK1-66 remains present in its full-length form, although to a lesser degree than what is seen under CCCP treatment. It however also exists as an import intermediate which can be cleaved by MPP to form PINK1-62. PINK1-62 is divided between two mitochondrial pools, one fraction also with its kinase domain reaching towards the cytosol like PINK1-66, the other larger fraction located fully within the mitochondria, possibly localized at the IMM bound to the TIM23 complex. Lastly, PINK1-66 and PINK1-62 can be cleaved by OMA1 within the IMS, resulting in PINK1-53 present with its kinase domain towards the cytosol. Both depolarization of mitochondria and inhibition of PARL thus result in PINK1 being stabilized at the TOM complex, which is the first step towards mitophagy.

3.2 PINK1 as a flexible import intermediate

As mentioned, PINK1 and its cleavage forms have been shown to localize to various mitochondrial subcompartments. I here observed low amounts of loosely OMM-attached PINK1-66 and PINK1-55 in untreated mitochondria, OMM-stabilized and phosphorylated PINK1-66 upon dissipation of $\Delta\Psi_m$, and finally OMM-stabilized PINK1-66, PINK1-62 that localizes to both the OMM and within mitochondria, and OMM-stabilized PINK1-53 upon PARL inhibition. How does PINK1 exist in these distinct forms that are even differently localized within the mitochondria? Based on previous publications on the fate of PINK1 import upon PARL KD (Meissner et al., 2011, 2015) and my findings presented herein, I corroborate and extend a model of PINK1 existing as a flexible import-intermediate form, which spans both mitochondrial membranes until it is properly processed by the various mitochondrial proteases and localizes to its final destinations (**Figure 18**), assisted by interaction with the HSP90/CDC37 chaperone complex. This import intermediate appears to be more stable upon PARL inhibition as indicated by first, the concurrent presence of full-length PINK1-66 and MPP-cleaved PINK1-62 at mitochondria (**Figure 12**B-E), and second, the transient interaction with and existence of PINK1 in the TOM-TIM23 supercomplex upon PARL inhibition (**Figure 14** and **Figure 15**).

Precedent for this import-intermediate state has previously been postulated, for example by Lin and Kang (2010) and Meissner et al. (2011, 2015). More recently, PINK1 being able to span the IMS, however without being imported towards the matrix in any capacity, has been shown in Akabane et al. (2023) and Eldeeb et al. (2024). They showed that PINK1, stabilized at the OMM due to depolarization, is still in contact with not only the TOM complex but also the inner mitochondrial TIM23 complex. However, no actual import through the TIM23 complex is taking place in the depolarization condition. Additionally, it has been shown that upon mitochondrial repolarization, PINK1 is rapidly being imported to the matrix and processed within the mitochondria again in a span of only 2.5 minutes (Lazarou et al., 2012). Also, PINK1 relocation from an IMM/matrix localization to the OMM/IMM does not depend on synthesis of new PINK1 (Fallaize et al., 2015). For both fast reimport and relocation an import-competent form that is already bridging the IMS is highly convenient.

An import-intermediate form of PINK1 with its kinase domain remaining largely in the cytosol while its N-terminal segments are processed by various inner mitochondrial proteases is also supported by the findings of Gaume et al. (1998). Their study found that bridging of the two mitochondrial membranes and access to matrix proteins during mitochondrial import of presequence-containing proteins is possible already by 52, possibly less, amino acids. This would be enough to allow PINK1's kinase domain to remain in the cytosol even as it undergoes the N-terminal

cleavages (compare **Figure 6**). Moreover, while the MTS is cleaved in the matrix, PINK1's TMD may be released laterally from the TIM17-Mgr2(ROMO1) translocation channel into the IMM via its hydrophobic stop-transfer signal, allowing cleavage of already this import intermediate by PARL. PINK1 accessing PARL's active site from the matrix side would position the NTE domain as the IMS-bridging sequence. Conveniently, this would keep the NTE domain away from interacting with the CTE domain located in the cytosol, preventing both correct folding of the kinase and stabilization at the TOM complex for PINK1 activation (Sekine et al., 2019; Rasool et al., 2022; Eldeeb et al., 2024; Raimi et al., 2024), as suggested also by (Trempe and Gehring, 2023). That would help to ensure that there is no premature activation of the kinase domain while PINK1 is still interacting with PARL. Why would prevention of kinase domain activation be needed, if PINK1 will be cleaved by PARL anyway and then degraded via the proteasome? Rhomboid proteases exhibit a very slow substrate turnover rate compared to other proteases; PARL processes only about a single substrate molecule per minute (Lysyk et al., 2020a), while for example MPP is six times faster (Arretz et al., 1994). Therefore, delaying PINK1's kinase domain folding so that PARL has enough time to actually process PINK1 is a fitting mechanism to prevent premature mitophagy induction on healthy mitochondria.

By inhibiting PARL, the PINK1 import-intermediate form is more stable. I also do observe Parkin recruitment, which is indicative of PINK1's kinase domain actually folding and being active under this circumstance. I suggest that this is possible by PINK1 only transiently interacting with PARL at its exosite for substrate docking (Dickey et al., 2013). Under normal conditions, PINK1's TMD would then unfold to reach into PARL's active site for cleavage (see Tichá et al., 2018). However, because PARL's active site is already occupied by the inhibitor, PINK1 eventually dissociates from PARL again. This frees up the NTE domain for cytosolic interaction with the CTE domain and subsequently, activation of the kinase domain can take place.

How is this import-intermediate form facilitated? Various publications have provided puzzle pieces that point to the cytosolic chaperone complex HSP90/CDC37 as a critical component in PINK1's stability, mitochondrial localization and therefore activity.

HSP90/CDC37 interaction is not strictly required for PINK1 import into mitochondria and proteolytic processing by PARL (Lin and Kang, 2010; Ando et al., 2017). However, abolishing HSP90/CDC37 interaction (by replacing PINK1's kinase domain with GFP) removes all cytosolic PINK1, instead targeting it all to the mitochondria, either to the inside (protected from proteinase K treatment) or tethered to the OMM (Lin and Kang, 2010). This mitochondrial dual-localization is likely due to a "tug of war" between the OMS, NTE and TMD conferring OMM localization and import stop past the IMM, while the MTS draws PINK1 towards the matrix. This

model is supported by the observation that deletion of just the OMS, NTE and TMD does retain a cytosolic PINK1 pool, but all mitochondrial PINK1 is targeted to within the mitochondria (Lin and Kang, 2010; Okatsu et al., 2015). HSP90/CDC37 interaction via PINK1's kinase thus maintains the cytosolic PINK1 pool. More specifically, Lin and Kang (2010) and Meissner et al. (2015) have suggested that HSP90/CDC37 may act as a cytosolic anchor for PINK1 during mitochondrial import, therefore contributing to PINK1's import-intermediate state. Removing the three N-terminal domains, namely the OMS, TMD and NTE, combined with inhibiting HSP90 interaction with the kinase domain then consequently targets all cellular PINK1 to an inner mitochondrial localization (Lin and Kang, 2010). It thus appears that HSP90/CDC37 in concert with PINK1's N-terminal domains act to maintain a cytosolic PINK1 pool and also tether a PINK1 import intermediate at the cytosolic side of the mitochondria. This prevents PINK1's full mitochondrial import and also allows for its release after inner mitochondrial cleavage events.

Interaction of PINK1 with HSP90/CDC37 protects PINK1 from premature degradation via the proteasome (Lin and Kang, 2008; Moriwaki et al., 2008; Weihofen et al., 2008). That ensures that PINK1 is readily available for signaling mitophagy upon mitochondrial depolarization, which is abolished in certain Parkinson's disease mutations that lack HSP90/CDC37 interaction (for example I368N, Ando et al., 2017). The proteasome-protective effect of HSP90/CDC37 on PINK1 and yet the known proteasomal degradation of PARL-cleaved PINK1-55 necessitates that at some stage of PINK1's life cycle, HSP90/CDC37 has to dissociate from PINK1.

An attractive model for this removal of HSP90 from PINK1 is via the import force that is exerted upon PINK1 under all conditions, including depolarization. Meissner et al. (2015) have demonstrated that the import of PINK1 is an important factor for PINK1 activation: A fusion construct of PINK1's kinase domain to TOM20, thus lacking any way to access the normal PINK1 import route, did show PINK1 activation, though less pronounced than with wildtype PINK1 under CCCP treatment. Meissner et al. (2015) therefore postulated that by PINK1 inserting into the TOM40 channel as an import intermediate, HSP90 is stripped off, which allows optimal activation of PINK1. A possibly involved TOM protein in this removal may be TOM70. TOM70, a receptor subunit of the TOM complex, has been identified as the TOM complex protein responsible for HSP90 interaction (Young et al., 2003). TOM70 mostly recognizes internal targeting sequences, whereas the canonical N-terminal MTS is commonly recognized by TOM20 and TOM22 (Söllner et al., 1989, 1990; Brix et al., 1997), though TOM20 and TOM70 share some overlap in their recognized substrates (Ramage et al., 1993). Interestingly, PINK1 has been shown to be imported into mitochondria as well as activated on depolarized mitochondria also in the absence of its canonical MTS (Okatsu et al., 2015; Sekine et al., 2019). Maruszczak

et al. (2022) have found that TOM70 binds to PINK1 even when PINK1 is lacking the MTS, that TOM70 is also capable of binding to its N-terminal regions such as the MTS, OMS and TMD, and that TOM70 KD has a more pronounced decreasing effect on PINK1 import than TOM20 KD. Recently, Raimi et al. (2024) have found an internal sequence in the OMS including three conserved arginines (R83/R88/R98, labeled TOM70-interacting region or TIR) which are important for the interaction between PINK1 and TOM70. They also described that TOM70, in addition to TOM20, is necessary for PINK1's mitochondrial import as well as an optimal stabilization and activation of PINK1 at the OMM. Thus, TOM70's pronounced engagement with PINK1 and HSP90 would play well into a suggested role of eventually removing HSP90 from PINK1, priming PINK1 for either proteasomal degradation or stabilization and activation at the OMM. Whether PINK1's interaction with HSP90 is changed in the more pronounced presence of the import-intermediate form upon PARL inhibition and if HSP90 is present at the various observed PINK1 species remains to be seen by future studies.

3.3 Influence of PARL inhibition on PINK1 cleavage events

In the context of protein quality control, it is not uncommon that one substrate is processed by multiple different, even unrelated proteases. Reasons for that can be differing functional forms produced by separate cleavages, or purposeful redundancy to safeguard the organism against malfunctioning of one of the responsible proteases. In this thesis, I perceived two distinct PINK1 cleavage forms upon PARL inhibition and was able to show that they are caused by MPP, producing PINK1-62 (see Greene et al., 2012), and by OMA1, which cleaves both PINK1-66 and PINK1-62 to PINK1-53 (**Figure 13**).

When comparing my data on PARL inhibition with what is known about PINK1 cleavage in PARL KO or PARL KD conditions, some similarities emerge. PARL KD and KO result in stabilization of full-length PINK1 (Jin et al., 2010; Deas et al., 2011; Meissner et al., 2011; Greene et al., 2012) as well as MPP-mediated cleavage (Jin et al., 2010; Deas et al., 2011; Greene et al., 2012) into the slightly smaller form PINK1-62. Greene et al. (2012) also observed a cleavage form appearing just below the PARL-mediated PINK1 fragment upon PARL KD. Similarly, Deas et al. (2011) noted that in PARL KO cells, the PARL-cleaved form is replaced by two bands, one of slightly higher and one of slightly lower molecular mass, similar to what I have observed (compare **Figure 9**). Sekine et al. (2019) have demonstrated that OMA1 produces a proteasome-degradable PINK1 cleavage fragment of around that size under conditions of TOM7 KO or in a PINK1 mutant of E112/113/117, both only under CCCP treatment. However, they could not distinguish the specific band size. In my data, the OMA1-mediated PINK1-53 form

corresponds to the smaller form published by Deas et al. (2011). A direct proof by comparing PINK1 forms under PARL KD, KO and inhibition with and without OMA1 KD and depolarization is, however, still needed. A combination of these factors is likely necessary to delineate the precise circumstances under which OMA1 targets PINK1, as no stabilization of PINK1 has been observed by simple KD of OMA1 in otherwise normal cells with polarized mitochondria (Greene et al., 2012).

Akabane et al. (2023) concluded that OMA1 and AFG3L2 can target PINK1 in depolarized mitochondria, as a KD of either stabilizes full-length PINK1. They also demonstrated that this cleavage is enhanced upon TIM23 KD, indicating that TIM23 protects against OMA1 and AFG3L2 cleavage, likely facilitated by PINK1's interaction with the TIM23 complex under depolarization. Further, OMA1 and AFG3L2 can act in concert via an unknown mechanism to cleave PINK1 also in polarized mitochondria; a KD of both proteins at the same time is necessary to stabilize uncleaved PINK1. In my work, I could now showcase an additional condition - that of PARL inhibition - in which KD of OMA1 alone is sufficient to stabilize PINK1-66 and PINK1-62 in polarized cells.

Even though OMA1's cleavage site of PINK1 is not known, it stands to reason that, due to OMA1's predicted catalytic site pointing towards the IMS (Head et al., 2009; Baker et al., 2014), PINK1 is cleaved such that it no longer has any connection with the TIM23 complex at the IMM. PINK1 would thus be localized at the TOM complex or general OMM with its kinase reaching into the cytosol as found in **Figure 12**D. Intriguingly though, **Figure 14**E implies that also this PINK1 form is present within the TOM-TIM23 supercomplex; an issue that remains to be investigated. Based on the molecular mass of OMA1-generated PINK1-53, which runs slightly below PINK1-55 generated by PARL, it is likely that OMA1 acts in the vicinity of PARL's cleavage site. Assuming an actual difference of 2 kDa between PARL- and OMA1-cleaved PINK1, this corresponds to approximately 18 amino acid residues and places the putative OMA1 cleavage site at around residue V122. Consequently, I predict that PINK1 processing by OMA1 removes its N-terminal domains MTS, OMS, TMD and parts of the NTE (see **Figure 6**). This would prime the remaining C-terminal kinase for eventual proteasomal degradation after its retrotranslocation to the cytosol, similar to the fate of PARL-cleaved PINK1-55.

Altogether, this further expands the view of how PINK1 can be cleaved by OMA1. As OMA1 has already been known to process PGAM5 in depolarized mitochondria, though more marginally than PARL does (Sekine et al., 2012; Wai et al., 2016), this positions OMA1's function even closer to PARL. One could envision OMA1 acting as a fail-safe system in case of PARL processing defects, such as PARL inhibition. Precisely how OMA1 is regulated under PARL

inhibition remains to be seen; especially interesting is the demonstrated lack of activity towards its substrate OPA1, which implies that further regulators are at play to restrain OMA1 activity to PINK1 specifically.

3.4   Interaction of PINK1 with the TOM-TIM23 supercomplex under PARL inhibition

My work establishes that under PARL inhibition, PINK1 interacts with the TOM complex proteins TOM20, TOM22 and TOM40 (**Figure 14**), as well as with the TIM23 complex proteins TIM17A, TIM23 and TIM50 (**Figure 15**). These findings are summarized in **Figure 19** and mimic the state in the membrane depolarization condition, though with an overall reduced co-precipitated amount of TOM-TIM23 complex proteins. The interaction of PINK1 with the TIM23 complex proteins appears to be more transient than that with the TOM complex proteins, as evidenced by improved protein pulldown upon crosslinking. Further, I demonstrated via BN- and 2D-PAGE that all PINK1 forms present under PARL inhibition exist in this TOM-TIM23 supercomplex.

The presence of the various PINK1 forms in the TOM-TIM23 supercomplex again strengthens the previously detailed hypothesis that MPP-cleaved PINK1-62 can exist as two pools, one tethered at the OMM and another residing completely within the mitochondria, as evidenced by protection from proteinase K proteolysis (**Figure 12**D). Nevertheless, additional immuno-precipitations of TOM-TIM23 supercomplex proteins would be necessary to elucidate complex associations and precise submitochondrial localizations of the individual PINK1 forms. With those approaches it will also be possible to clarify the positioning of OMA1-cleaved PINK1-53.

Moreover, I showed that under PARL inhibition, PINK1 stabilization at the TOM-TIM23 supercomplex is sufficient to recruit Parkin to the mitochondria, albeit again at lower levels than under membrane depolarization (**Figure 17**). Similarly, Meissner et al. (2015) showed that a PARL KD also causes slightly reduced Parkin recruitment and autophagosome formation compared to CCCP treatment. The reason appears to be twofold. For one, as mentioned in **Section 3.2**, the chaperone complex HSP90/CDC37 may support the flexible PINK1 import intermediate, which causes the NTE domain to be imported. Therefore, the NTE domain is not available for interactions with the CTE domain and the TOM complex, which would stabilize and activate PINK1. Second, a possibility is that while HSP90/CDC37 is needed to protect PINK1 from premature cytosolic degradation, its removal is equally necessary to ensure full PINK1 kinase activity upon stabilization at the OMM (Meissner et al., 2015). A key in the removal of HSP90/CDC37, and thus PINK1 activation, may be a prolonged stable interaction of PINK1 with the TOM-TIM23 supercomplex, such as after mitochondrial depolarization. There, PINK1's
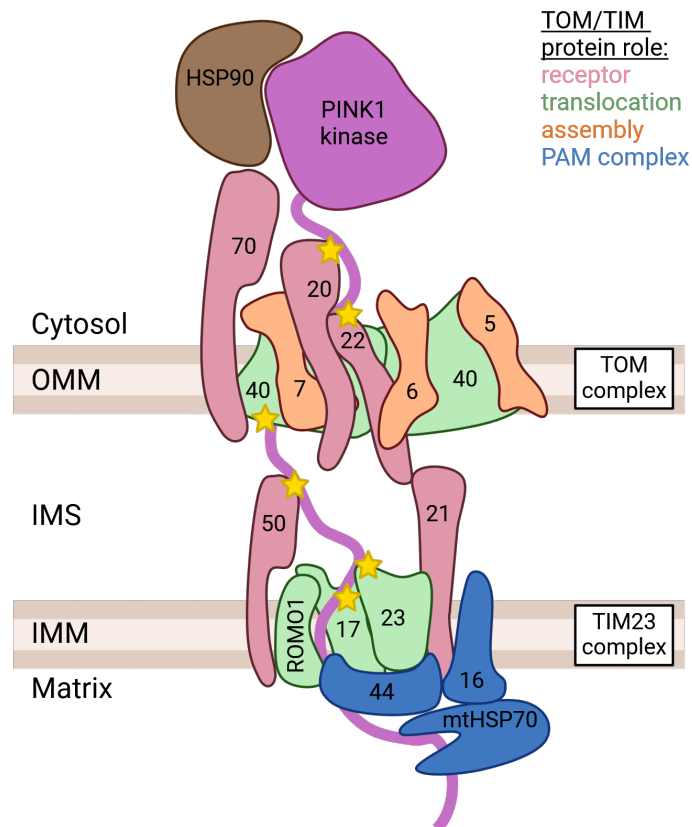
Figure 19: ***Model of PINK1 import intermediate interactions with TOM and TIM23 complex proteins under PARL inhibition.*** Yellow stars indicate interactions between PINK1 and the respective protein found via the co-immunoprecipitations in this work. TOM and TIM proteins, abbreviated to their numeration, were modeled after the available proteins from PDB entry 8W3J (TOM5/6/7/22/40) and PDB entry 8E1M (TIM17/23/44), and supplemented with information from Sim et al. (2023) and Busch et al. (2023). For clarity, the pairwise proteins around the TOM40 dimer were omitted. Additional PINK1 interactions that have been published, e.g. with TOM7 (Hasson et al., 2013; Sekine et al., 2019; Raimi et al., 2024) or TOM70 (Lazarou et al., 2012; Raimi et al., 2024), are likely also present under PARL inhibition, but have not been evaluated in this work and are therefore not highlighted. Created using BioRender.

MTS is not being continuously pulled into the matrix by the PAM machinery, but simply remains stuck in the TIM23 complex due to the dissipated $\Delta\Psi_m$, as evidenced by a lack of MPP cleavage. On the other hand, PINK1's interaction with the TOM-TIM23 supercomplex is more transient in PARL inhibitor-treated cells, as PINK1 is still being imported. Since, again, the NTE domain cannot stabilize PINK1 at the TOM complex when it is being imported, the less stable PINK1-TOM-TIM23 supercomplex may then result in inadequate removal of HSP90/CDC37. This fits to the likewise lower levels of Parkin recruitment as compared to depolarizing treatments. This suggests that a more stable PINK1-TOM-TIM23 supercomplex formation is likely necessary to allow equally high amounts of stabilized PINK1 dimer formation, subsequent PINK1 autophosphorylation and Parkin recruitment.

Regarding PINK1 import, the recent advancements on the mechanisms of TIM23-complex-mediated import pronounces a role of TIM17 rather than TIM23, and identified Mgr2/ROMO1 as a regulator of lateral protein release into the IMM (Fielden et al., 2023; Sim et al., 2023; Zhou et al., 2023; Maruszczak et al., 2024). The role of Mgr2/ROMO1 is especially interesting in the context of PINK1 cleavage by PARL. A lateral release of the TMD of an import-intermediate PINK1 in mitochondria with an intact $\Delta\Psi_m$ would allow access of PARL to the TMD and permit cleavage, fitting to my proposed model in **Section 3.2**. A current preprint by Lorriman et al. (2024) even finds that PINK1 in combination with TIM17 associates with either ROMO1 or PARL to form the translocation channel, with the former resulting in further PINK1 import and the latter resulting in PINK1 cleavage. How this exclusive association with either ROMO1 or PARL may be regulated is currently unclear; however, the prospect of this interaction is exciting news as a further pointer towards PARL as a dynamic regulator of PINK1-Parkin-mediated mitophagy.

3.5 PINK1 proteolysis by PARL as the common denominator of PINK1-mediated mitophagy regulation

For much of the time in PINK1 research, it has been mostly viewed as a simple $\Delta\Psi_m$ sensor, with depolarizing agents such as CCCP used as the primary model conditions for investigating PINK1 processing and PINK1-Parkin-mediated mitophagy (Vives-Bauza et al., 2010; Geisler et al., 2010a; Matsuda et al., 2010; Narendra et al., 2010b). However, as mentioned throughout this work, there are by now various stressors, genetic manipulations like KOs/KDs and specific protein mutations that have all been found to influence the ability of PINK1 to, on the one hand, accumulate at the OMM and induce mitophagy, or on the other hand, to be partially imported into mitochondria where it is cleaved by PARL at the IMM, priming it for retrotranslocation into the cytosol and proteasomal degradation. As PARL is the primary mitochondrial protease that

acts on PINK1 under physiological conditions, the question arises whether PARL could be seen as the major regulator for integrating various types of mitochondrial defects, rather than just $\Delta\Psi_m$ issues, by determining PINK1 fate and thus mediating mitophagy.

One of those alternative defects is the deactivation of mitochondrial protein import, independent of any mitochondrial depolarization. Michaelis et al. (2022) showed that a general inhibition of mitochondrial protein import is the underlying cause for PINK1 stabilization and mitophagy in reaction to proteotoxic matrix stress promoted by e.g. KD of LONP1, the matrix protease involved in mitochondrial protein import and UPRmt regulation (Matsushima et al., 2010, 2021). Yet another trigger for proteotoxic matrix stress that causes PINK1-Parkin-mediated mitophagy likely by affecting mitochondrial protein import is the accumulation of unfolded proteins via ΔOTC expression (Jin and Youle, 2013).

A second example are certain PINK1 mutations that have been found to exhibit no cleavage by PARL, yet are still imported into the mitochondria where they also interact with PARL, and which can cause Parkin recruitment even in polarized mitochondria (e.g. R98W, a PD-related mutation, Meissner et al., 2011, 2015).

Last but not least, I have demonstrated in this work that a simple lack of PARL-mediated cleavage by PARL inhibition can result in stabilized PINK1 and Parkin recruitment already in polarized mitochondria, and the same holds true for PARL KD (Meissner et al., 2015).

All of these defects or stressors ultimately have in common that PINK1 is not cleaved by PARL, causing mitophagy. I showed that even when mitochondrial import is permitted as usual and PARL thus has access to PINK1, PARL inhibition is sufficient to initiate the first steps of mitophagy. This would position the lack of PINK1 cleavage by PARL as the most upstream trigger for mitophagy. PARL's access to PINK1 may thus place it in a key role as the common denominator to various PINK1 fates. In this position, PARL and PINK1 may delegate the appropriate reaction to different stressors, including but not limited to a disruption of $\Delta\Psi_m$, via differences in PINK1 proteolysis and trafficking, thus integrating inner mitochondrial "status reports" into the cellular network by regulating mitochondrial health.

4   Future perspectives

Within this study, I successfully established the novel PARL inhibitors and employed them to find: inhibition of PARL stabilizes the substrates PGAM5 (under CCCP treatment) and PINK1 (resulting in Parkin recruitment); PINK1 exists as an import-intermediate form in polarized mitochondria upon PARL inhibition and is readily cleaved by other proteases; PARL inhibition results in an additional inner mitochondrial localized PINK1-62 pool; PARL inhibition is a novel condition for causing OMA1-mediated PINK1 cleavage; transient interactions of PINK1 with the TOM-TIM23 supercomplex are present under PARL inhibition. Building upon those findings, several interesting questions remain to be investigated.

In **Section 2.1.3**, I briefly discussed a PINK1 cleavage fragment stabilized upon PARL inhibition, with a molecular weight just above the usual PINK1-55 form. Though I suggest that this fragment may be a phosphorylated form of PINK1-53, its origin has not yet been identified. In a similar vein, the cleavage site of PINK1 recognized by OMA1 is not known. Determining this site would specifically be interesting in regards to deciphering the nature of the PINK1 import intermediate, as it would allow further deductions on how far PINK1 is reaching into the IMS under PARL inhibition and where its domains are localized.

This ties into the need for further investigation into the precise submitochondrial localizations of specifically PINK1-62; it is currently not known if the proteinase K protected pool resides in the IMS, IMM or even the matrix. A more sophisticated separation of the crude isolated mitochondria into their subcompartments would answer this question and give further hints on if this PINK1 form may be localized fittingly to phosphorylate postulated inner mitochondrial PINK1 substrates as mentioned in **Section 3.1**. Those substrates could then be investigated for changes in their phosphorylation status upon PARL inhibition.

Following stabilization of PINK1 at the TOM-TIM23 supercomplex, I observed Parkin recruitment under PARL inhibition. Parkin recruitment is a necessity for PINK1-caused mitophagy, but determining the actual quantity and rate of mitophagy caused by the PARL inhibitors would be even more enticing. Therefore, additional mitophagy tools should be employed such as recruitment of autophagy adapters or measurements via sensors like mito-Keima. This could then be further used to examine whether PARL inhibition, via priming of the PINK1 threshold needed to activate mitophagy, has a beneficial effect on mitochondrial health in organisms that suffer from PD-related PINK1 mutations that present with a reduced kinase activity. In addition, a first foray into exploration of other downstream effects upon PARL inhibition was performed via proteomics as detailed in **Section 2.3.4** and yielded the kinase RAF1 as a potential target

of PINK1 phosphorylation activity. However, the sample analysis suffered from contamination with non-mitochondrial proteins and non-ideal variances; therefore, technical improvements are in order to repeat this assay. This includes a higher overall protein load, a better purification of mitochondria, and larger replicate numbers.

A topic that is currently gaining renewed traction in the PINK1 research community is that of PARL/PINK1 interactors and PINK1 mitochondrial import. As I have discussed in **Section 3.2**, the role of HSP90/CDC37 is not fully elucidated and has not been thoroughly investigated after few initial studies when the PINK1 field was still rather young. It would be of special interest to see which PINK1 forms under PARL inhibition show interaction with HSP90/CDC37. Additionally, as discussed in **Section 3.4**, further investigation on which PINK1 forms interact with which TOM or TIM23 complex proteins under PARL inhibition is needed. Furthermore, the role of ROMO1 in PINK1 import and cleavage deserves a brighter spotlight, as the regulation of PINK1's lateral release into the IMM is important for delineating how PARL recognizes and cleaves PINK1. Related to this, it may be interesting to also be on the lookout for changes in association of the SPY complex as a possible regulatory response due to PARL inhibition. I detected OMA1 activity towards PINK1, and OMA1 as well as PARL can be regulated by SLP2 of the SPY complex (Wai et al., 2016); additionally, YME1L1 of the SPY complex can degrade ROMO1 (Richter et al., 2019) and may thus be involved in PINK1's lateral IMM release regulation.

Last but not least, I validated the PARL inhibitors using two known PARL substrates, PGAM5 and PINK1. How PARL inhibition affects the processing of its other substrates Smac/Diablo, TTC19, STARD7 and CLPB remains to be seen, and could contribute to the growing knowledge surrounding PARL as an important mitochondrial protease with diverse, critical functions.

5 Materials

5.1 Equipment

Table 1: Equipment / software and their manufacturer

Equipment / software	Manufacturer
Amersham ImageQuant 800	Cytiva
BD FACS Canto II	BD Biosciences
ImageQuant LAS 4000	GE Healthcare
Incubator HERA Cell Vios 160i	Thermo Scientific
Incucyte S3 live cell imaging system	Sartorius
Microscope LSM 780	Zeiss
Microscope Leica TCS SP5	Leica
Microscope Primovert	Zeiss
Mini gel chamber	BioRad
Multiple gel caster	Amersham Biosciences
NanoDrop One	Thermo Scientific
Omni live cell imaging system	Axion BioSystems
pH meter	Mettler Toledo
photometer TriStar2 Multimode Reader LB 942	Berthold Technologies
Pipettes (2/10/20/100/200/1000 µl)	Gilson
Sterile bench HERA SAFE 2025	Thermo Scientific
Tabletop centrifuges 5417R, 5415R	Eppendorf
Tabletop centrifuge Universal320	Hettich Zentrifugen
Thermomixer compact, comfort	Eppendorf
Ultracentrifuge Sorvall Discovery M120SE	Thermo Scientific
Ultracentrigue rotors S120AT2, S100AT3	Beckman Coulter
Ultrasonic processor VibraCell 75115	Bioblock Scientific
XCell SureLock MiniCell gel running tank	Invitrogen
BioRender	BioRender
ChemDoodle 2D Sketcher Demo	iChemLabs
Excel 2016	Microsoft
FlowJo	BD Biosciences

ImageJ	Schneider et al. (2012)
LAS AF3	Leica
Prism 6, 10	GraphPad
ZEN 2010	Zeiss

5.2   Consumables

Table 2: Consumables and their manufacturer

Consumable	Manufacturer
1 ml syringes	BD Plastipak
5 ml polystyrene round bottom tube	Corning
27-gauge needle	Henke Sass Wolf
Cell culture plates (6-/12-/24-/96-well)	Corning / Sarstedt
Cell culture dishes (10 cm)	Corning
Cell culture dishes (15 cm)	Sarstedt
Cell scraper	Sarstedt
Cover slips #1.5	Avantor
Cryotubes	Thermo Scientific
Falcon tubes (15/50 ml)	Cellstar
GE alumina plates	Cytiva
Glass plates	Glas Hlawatsch
ibiTreat µ-Slide 8 well	Ibidi
Microscope slides	Heinz Herenz Hamburg
Micro tubes (0.5/1.5/2/5 ml)	Sarstedt
NativePAGE 4-16 % Bis-Tris gel	Invitrogen
Pipet tips (10/20 µl)	Starlab
Pipet tips (200/1000 µl)	Sarstedt
Pipet tips filtered (10/20/200/1000 µl)	Starlab
Polycarbonate ultracentrifuge tubes	Beckman Instruments
PVDF membrane Immobilon-P	Sigma-Aldrich
Whatman 3MM CHR	Cytiva

5.3 Chemicals

Table 3: Reagents and their manufacturer

Reagent	Manufacturer
Acetic acid	VWR
Acetone	VWR
Acrylamide Rotiphorese Gel 30	Roth
6-Aminohexanoic acid	Sigma-Aldrich
Antimycin A	Sigma-Aldrich
Ammonium Peroxodisulfate (APS)	AppliChem
β-Mercaptoethanol	Sigma-Aldrich
Bis-Tris	AppliChem
Blasticidin	Gibco
Bromophenol blue	Chroma Waldeck
Bovine serum albumin (BSA)	Roth
Chloroacetamide (CAA)	Proteomics Core Facility Cologne
Carbonyl cyanide 3-chlorophenylhydrazone (CCCP)	Sigma-Aldrich
Coomassie G-250	Serva
4′,6-diamidino-2-phenylindole (DAPI)	Sigma-Aldrich
D-Glucose	Merck
D-Sucrose	AppliChem
Digitonin	Merck
Dulbecco's Modified Eagle Medium (DMEM)	Gibco
Dimethyl sulfoxide (DMSO)	Sigma-Aldrich / AppliChem
Doxycyline	AppliChem
Dithiobis[succinimidylpropionate] (DSP)	Thermo Scientific
Dithiothreitol (DTT)	Proteomics Core Facility Cologne
Ethylenediaminetetraacetic acid (EDTA)	Sigma-Aldrich
Ethylene glycol-bis (β-aminoethyl ether) - N,N,N′,N′-tetraacetic acid (EGTA)	AppliChem
Fetal bovine serum (FBS)	Thermo Fisher / Gibco
anti-FLAG M2 affinity gel	Sigma-Aldrich
FLAG peptide	Sigma-Aldrich
FluoroBrite DMEM	Gibco

Fluoromount-G	Southern Biotech
16 % Formaldehyde	Thermo Scientific
GlutaMax	Gibco
Glycerol	Promega
Glycine	AppliChem
4-(2-Hydroxyethyl)-1-piperazineethanesulfonic acid (HEPES)	AppliChem
Hoechst-33342	Sigma-Aldrich
Hygromycin B	Invitrogen
Inhibitor compounds 5, 6, 1258, 1343, 1866, 1868	Stříšovský group, Institute of Organic Chemistry and Biochemistry, Prague
KCl	Merck
KH_2PO_4	AppliChem
KOAc	AppliChem
KOH	Grüssing
Lipofectamine RNAiMAX	Thermo Fisher
Oligomycin	Cayman Chemical
OptiMEM	Gibco
$Mg(OAc)_2$	AppliChem
$MgCl_2$	AppliChem
NaCl	Fisher Chemical
Na_2CO_3	AppliChem
NaH_2PO_4	AppliChem
NaN_3	Sigma-Aldrich
NativeMark unstained Protein Standard	Invitrogen (LC0725)
NHS-activated Sepharose 4 Fast Flow	Cytiva
Nonfat dried milk powder	AppliChem
Opti-MEM	Gibco
PageRules Plus Prestained Protein ladder	Thermo Scientific (26619)
25-kDa linear polyethylenimine (PEI)	Polysciences
Pen Strep	Gibco
PhosSTOP	Roche

c0mplete, EDTA-free protease inhibitor cocktail (PI), 50x	Roche
Phenylmethylsulfonyl fluoride (PMSF)	AppliChem
Poly-l-lysine solution	Sigma-Aldrich
Proteinase K	Merck
Sodium dodecyl sulfate (SDS)	Sigma-Aldrich
Sodium pyruvate	Gibco
Tetraethylammonium bromide (TEAB)	Proteomics Core Facility Cologne
Tetramethylethylenediamine (TEMED)	AppliChem
Trichloracetic acid (TCA)	VWR
Tris	Sigma-Aldrich
Trypsin	Proteomics Core Facility Cologne
Trypsin-EDTA, 0.05 %	Gibco
Tween 20	AppliChem

5.4 Commercial kits

Table 4: Kits and their manufacturer

Kit	Manufacturer
NucleoBond Xtra Midi Kit	Macherey-Nagel (740410.100)
JC-1 mitochondrial staining kit	Sigma-Aldrich (CS0390)
NativePAGE Running Buffer kit	invitrogen (BN2007)
Pierce BCA protein assay kit	Thermo Scientific (23227)
TMRE mitochondrial membrane potential assay kit	abcam (ab113852)
WesternBright enhanced chemiluminescence (ECL)	Advansta (K-12045)

5.5 Buffers and media

Table 5: Compositions of buffer and medium

Buffer / medium	Content
2D-PAGE sample buffer	125 mM Tris pH 6.8
	20 % (v/v) Glycerol
	4 % (w/v) SDS
	0.01 % (w/v) Bromophenol blue
	2 % (v/v) β-mercaptoethanol
Blocking solution	5 % (w/v) nonfat dried milk powder
	TBS-T
BN sample buffer (40x)	500 mM 6-Aminohexanoic acid
	100 mM Bis-Tris pH 7.0
	5 % (w/v) Coomassie G-250
BN fixation solution	40 % (v/v) Methanol
	10 % Acetic acid
4 % Formaldehyde	16 % Formaldehyde
	PBS pH 7.4
Harsh stripping buffer	62.5 mM Tris pH 7.4
	2 % (v/v) SDS
	0.7 % (v/v) β-Mercaptoethanol
HEK293T medium	DMEM
	10 % (v/v) FBS
HeLa medium	DMEM
	10 % (v/v) FBS
	2 % (v/v) GlutaMax

HEK293 T-REx medium	DMEM
	10 % (v/v) FBS
	1 % (v/v) GlutaMax
	1 % (v/v) Sodium pyruvate
	125 µg/ml Hygromycin
	10 µg/ml Blasticidin
Hypotonic buffer	10 mM HEPES pH 7.4
	1.5 mM MgCl$_2$
	10 mM KOAc
	0.5 mM DTT
	2.5 mM PMSF
	1x PI
Isolation buffer	250 mM D-Sucrose
	10 mM Tris pH 7.4
	10 mM HEPES pH 7.4
	0.1 mM EGTA
	1x PI
Laemmli SDS-PAGE running buffer	25 mM Tris-Base
	192 mM Glycine
	0.1 % (v/v) SDS
Laemmli SDS-PAGE sample buffer	50 mM Tris pH 6.8
	10 mM EDTA
	4 % (v/v) Glycerol
	2 % (w/v) SDS
	0.01 % (w/v) Bromophenol blue
	5 % (v/v) β-Mercaptoethanol
Live cell imaging medium	FluoroBrite DMEM
	10 % (v/v) FBS

Mild glycine stripping buffer pH 2.2	100 mM Glycine
	30 mM $Mg(OAc)_2$
	50 mM KCl
	1 % (v/v) Tween-20
	0.1 % (v/v) SDS
Phosphate-buffered saline (PBS) pH 7.4	10 mM NaH_2PO_4
	1.4 mM KH_2PO_4
	2.7 mM KCl
	140 mM NaCl
PBS-EDTA	PBS pH 7.4
	1 mM EDTA
	0.2 g/l D-Glucose
Pulse-chase solution buffer	50 mM HEPES pH 7.4
	150 mM NaCl
	2 mM $Mg(OAc)_2$
	10 % (v/v) Glycerol
	1 mM EGTA
	1 mM PMSF
	1x PI
Semi-dry blotting buffer	48 mM Tris pH 7.5
	39 mM Glycine
	20 % (v/v) Methanol
Sucrose cushion	100 mM Na_2CO_3
	250 mM D-Sucrose
Tris-buffered saline (TBS)	10 mM Tris pH 7.4
	150 mM NaCl
TBS-T	TBS

	0.1 % (v/v) Tween-20
(+) Transfection medium	DMEM
	1 % (v/v) PS
(++) Transfection medium	DMEM
	10 % (v/v) FBS
	1 % (v/v) PS
Urea buffer	8 M Urea
	50 mM TEAB
	1x PI
	1x PhosSTOP
Wet blotting buffer	25 mM Tris
	192 mM Glycine
	20 % (v/v) Methanol

5.6   Plasmids and siRNA

Empty plasmid (pcDNA3.1+) was aquired from Invitrogen. The used plasmid constructs have been described previously: pcDNA3.1/PGAM5-FLAG (Sekine et al., 2012), pCDH/HA-Parkin-IRES-GFP (Weihofen et al., 2008), pEGFP-C1/Parkin-mEGFP (Meissner et al., 2015) and mito-mCherry (Lorenz et al., 2006). siRNA-oligonucleotides for OMA1 (4392420, ID s41776 in the main text or additionally s41777 in the uncropped blot section) and nontargeting control siRNA (4390843) were purchased from Ambion.

5.7 Antibodies

Table 6: Used antibodies

Antibody	Dilution	Source	Identifier
Anti-AIF Mouse mAb	1:500	Santa Cruz Biotechnology	sc-13116
Anti-β-Actin Mouse mAb	1:2000	Sigma-Aldrich	A1978
Anti-FLAG M2 Mouse mAb	1:1000-1:2000	Sigma-Aldrich	F1804
Anti-HA.11 Mouse mAb	1:1000	BioLegend	901502
Anti-mtHSP70 Mouse mAb	1:2000	Abcam	ab2799
Anti-OPA1 Mouse mAb	1:1000	BD Biosciences	612606
Anti-PINK1 Rabbit pAb	1:1000	Novus biologicals	BC100-494
Anti-PINK1 Rabbit mAb	1:1000	Cell Signaling Technology	6946
Anti-TOM20 Mouse mAb	1:1000	Santa Cruz Biotechnology	sc-17764
Anti-TOM22 Rabbit mAb	1:1000	Abcam	ab179826
Anti-TOM40 Rabbit pAb	1:2000	Proteintech	18409-1-AP
Anti-TIM17A Rabbit pAb	1:2000	Proteintech	11189-1-AP
Anti-TIM23 Rabbit pAb	1:1000	Proteintech	11123-1-AP
Anti-TIM50 Rabbit pAb	1:1000	Proteintech	22229-1-AP
Anti-VDAC Rabbit pAb	1:1000	Invitrogen	PA1-954A
Anti-Mouse IgG (H+L) Donkey-HRP	1:20,000	Dianova	715-035-150
Anti-Rabbit IgG (H+L) Donkey-HRP	1:20,000	Dianova	711-035-152

6 Methods

6.1 Cell Biology Methods

6.1.1 Used cell lines

HEK293T and Flp-In HEK293 T-REx cells were grown in their respective medium at 37 °C in 5 % (v/v) CO_2. Inducible stable Flp-In HEK293 T-REx cells expressing PINK1 were described previously (Meissner et al., 2015). Inducible stable Flp-In HEK293 T-REx cells expressing PINK1-FLAG were generated by previous lab member Cathrin Meissner; the PINK1-FLAG segment was generated from PINK1 subcloned into pFLAG-N1 (Meissner et al., 2011, 2015). Flp-In HEK293 T-REx cells were induced with 0.3 µg/ml doxycycline for 24 hours before further processing. HeLa wildtype and HeLa PARL-KO cells were a gift from Thomas Langer (MPI AGE, Cologne).

6.1.2 Transient transfection

Transient plasmid transfections were performed using PEI. 100 ng plasmid encoding HA-Parkin-IRES-GFP, mito-mCherry or Parkin-mEGFP, or 500 ng plasmid encoding PGAM5-FLAG were used per 6-well, total transfected DNA was 2 µg/6-well, held constant via addition of empty plasmid. Plasmid DNA was mixed with 250 µl (+) transfection medium and incubated for 5 min. 5 µl of PEI were added, the mixture was vortexed and incubated for another 10 min, before adding 375 µl each of (+) and (++) transfection medium. After vortexing, the cell medium was replaced with the transfection mixture. After 4 h, the transfection mixture was removed and fresh (++) transfection medium added. Amounts were scaled down accordingly for use in smaller well formats. Cells were analysed 27 hours post-transfection.

6.1.3 siRNA knockdown

For siRNA transfection, 2×10^5 cells were seeded per 6-well and transfected on the next day. 20 nM siRNA-oligonucleotide were mixed with 250 µl Opti-MEM and incubated for 5 min. Another 250 µl Opti-MEM were mixed with 3 µl lipofectamine RNAiMAX and also incubated for 5 min. Both mixtures were combined, incubated for 15 min and added onto the cells within their medium. On the next day, the medium was replaced with (++) transfection medium. Cells were analysed five days post-siRNA-transfection.

6.2 Biochemical Methods

6.2.1 Preparation of total cell lysates

Cells were washed with PBS and directly lysed with Laemmli SDS-PAGE sample buffer and heated for 15 min at 65 °C.

6.2.2 Subcellular fractionation

Unless mentioned otherwise, all steps were performed at 4 °C. For subcellular fractionation to separate cellular content into cytosolic and mitochondrial fractions, cells were washed with PBS, harvested in PBS-EDTA and centrifuged at 500×g for 5 min. The pellet was reconstituted in isolation buffer and incubated for 10 min. Cells were lysed by passing through a 27-gauge needle six times, then centrifuged at 200×g for 5 min. The supernatant was centrifuged at 10,000×g for 10 min. The resulting supernatant (cytosolic fraction) was subjected to a 10 % TCA precipitation, then an acetone wash at room temperature and was finally resuspended in Laemmli SDS-PAGE sample buffer. The resulting pellet (mitochondrial fraction) was washed twice with isolation buffer via centrifugation at 10,000×g for 10 min. The pellet was resuspended in Laemmli SDS-PAGE sample buffer. All samples were heated for 15 min at 65 °C.

6.2.3 Proteinase K protection assay

Unless mentioned otherwise, all steps were performed at 4 °C. For protease protection assay, cells were washed with PBS, harvested in PBS-EDTA and centrifuged at 500×g for 5 min. The pellet was reconstituted in EGTA-less isolation buffer and incubated for 10 min. Cells were lysed by passing through a 27-gauge needle six times, then centrifuged at 200×g for 5 min. The supernatant was centrifuged at 10,000×g for 10 min. The resulting pellet (mitochondrial fraction) was resuspended in EGTA-less isolation buffer without PI, then proteinase K was added and the suspension was incubated for 30 min or 1 h. To stop the reaction, 2.5 mM PMSF was added and incubated for 15 min. Samples were mixed with 4× Laemmli SDS-PAGE sample buffer and heated for 15 min at 65 °C.

6.2.4 Sodium carbonate extraction

Unless mentioned otherwise, all steps were performed at 4 °C. For sodium carbonate fractionation to detect endogenous PINK1 signals at enriched mitochondrial membranes, cells were washed and harvested with PBS and centrifuged at 500×g for 5 min. The pellet was reconsti-

tuted in hypotonic buffer and incubated for 10 min. The suspension was centrifuged at 500×g for 10 min and the pellet was resuspended in hypotonic buffer. Cells were lysed by passing through a 27-gauge needle six times, then centrifuged at 1,000×g for 10 min. The supernatant was centrifuged at 100,000×g for 15 min. The resulting pellet (mitochondrial membrane fraction) was resuspended in hypotonic buffer, then an equal amount of 200 mM Na_2CO_3 (pH 11.3) was added and resuspended. The suspension was incubated for 30 min and then overlaid on a sucrose cushion and centrifuged at 130,000×g for 15 min. The pellet (membrane fraction) was resuspended in Laemmli SDS-PAGE sample buffer. The supernatant (membrane-contained soluble proteins and peripheral membrane proteins) was subjected to a 10 % TCA precipitation, then an acetone wash at room temperature and was finally resuspended in Laemmli SDS-PAGE sample buffer. All samples were heated for 15 min at 65 °C.

6.2.5   Crosslinking

For crosslinking, cells were washed with PBS and then incubated with 1 mM DSP in PBS, including relevant treatments, for 30 min with gentle agitation. 1 M Tris pH 7.4 was added to a final concentration of 12 mM and incubated for 15 min to quench the reaction. Cells were further processed by co-immunoprecipitation.

6.2.6   Co-immunoprecipitation

Unless mentioned otherwise, all steps were performed at 4 °C. For co-immunoprecipitation of FLAG-tagged PINK1, cells were washed with PBS, harvested in PBS-EDTA and centrifuged at 500×g for 5 min. The pellet was reconstituted in pulse-chase solution buffer + 1 % digitonin and incubated for 1 h. The lysate was centrifuged at 20,000×g for 5 min. An input sample was taken from the supernatant. The supernatant was added to 30 µl BSA-coupled agarose beads (made by coworker Martina Costa from NHS-activated Sepharose 4 Fast Flow beads and BSA) and incubated rotating for 1 h to remove unspecific binding. The lysate-BSA-bead mix was centrifuged at 1,500×g for 2 min, the supernatant was added to 60 µl anti-FLAG M2 affinity gel and incubated rotating over night. The lysate-FLAG gel mix was centrifuged at 1,500×g for 2 min. An unbound sample was taken from the supernatant. The pellet was washed twice with pulse-chase solution buffer + 0.1 % digitonin via 5 min rotating and centrifugation at 500×g for 2 min. The bound proteins were eluted by shaking incubation for 30 min with pulse-chase solution buffer + 0.1 % digitonin + 0.5 mg/ml FLAG peptides. Following a last centrifugation at 1,500×g for 2 min, the supernatant (bound/immunoprecipitated sample) was collected. Only if

samples were further resolved via SDS-PAGE were they mixed with 4× Laemmli SDS-PAGE sample buffer and heated for 15 min at 65 °C.

6.2.7   SDS-PAGE

Proteins were resolved by tris-glycine SDS-PAGE according to Laemmli (1970). Gels were run first at a constant 60 V for 30 min, followed by constant 20 mA/gel until the bromophenol blue front had run past the bottom of the gel, followed by western blotting procedure (**Section 6.2.10**).

6.2.8   BN-PAGE

For resolving of protein complexes, a BN-PAGE approach was used (Schägger and von Jagow, 1991). Protein samples resulting from a co-immunoprecipitation were mixed with 1/40th BN sample buffer and resolved via a NativePAGE 4-16 % Bis-Tris gel and the NativePAGE Running Buffer kit at a constant 150 V for 2.5 h at 4 °C. The gel was incubated for 15 min in wet blotting buffer prior to wet blotting onto a PVDF membrane at constant 85 mA for 70 min at 4 °C. The membrane was incubated in BN fixation solution in order to mark the unstained protein ladder bands, destained in methanol and washed in water before continuing with the blocking step of the western blotting procedure (**Section 6.2.10**).

6.2.9   2D-PAGE

To resolve protein complexes captured via BN-PAGE, the according sample lane was cut from the BN-PAGE gel and incubated for 10 min in 2D-PAGE sample buffer before a brief boiling step. The cooled down gel lane was loaded horizontally onto a SDS-PAGE gel and overlayed with 2D-PAGE sample buffer. The SDS-PAGE was run as described above.

6.2.10   Western Blotting and protein detection

SDS-PAGE gels were blotted onto a PVDF membrane via semi-dry blotting, incubated with blocking solution and then incubated with primary antibody in blocking solution over night at 4 °C. Membranes were washed with TBS-T, and incubated with the respective secondary HRP-coupled antibody. Membranes were washed again with TBS-T before imaging via ECL. For stripping and reprobing, membranes were incubated for 30 min in either harsh stripping buffer at 50 °C, or in mild glycine stripping buffer at room temperature. Stripped membranes were washed in TBS-T before continuing with the blocking step as above.

6.2.11   Parkin recruitment via fluorescence microscopy

Cells were seeded on poly-l-lysine coated cover slips. Hoechst staining (1 µg/ml) was done immediately before adding treatment to the cells. For fixation, cells were incubated for 15 min with 4 % formaldehyde and washed in PBS. The cover slips were mounted with Fluoromount-G on microscope slides.

6.2.12   JC-1 assay

Cells were seeded on poly-l-lysine coated µ-slides. Hoechst staining (1 µg/ml) was done immediately before adding treatment to the cells. Staining of cells for determination of mitochondrial membrane potential was carried out with the JC-1 mitochondrial staining kit according to the kit's instructions and in live cell imaging medium; stained cells were immediately taken to live cell imaging.

6.2.13   TMRE assay

For microscopy, cells were seeded on poly-l-lysine coated µ-slides. Hoechst staining (1 µg/ml) was done together with the TMRE staining according to the TMRE mitochondrial membrane potential assay kit's instructions and in live cell imaging medium. Stained cells were immediately taken to live cell imaging.

For FACS analysis, cells were stained with TMRE according to the TMRE mitochondrial membrane potential assay kit's instructions, then handled at 4 °C. Cells were washed twice with PBS, then harvested in PBS-EDTA. The cells were centrifuged at 300×g for 3 mins and resuspended in PBS + 5 % FBS. Cells were then stained with DAPI (0.1 µg/ml) to label dead cells for later exclusion from analysis. Cells were again centrifuged at 300×g for 3 mins, washed twice with PBS and again resuspended in PBS + 5 % FBS and subjected to a cell strainer. Cells were immediately taken for FACS analysis according to the TMRE mitochondrial membrane potential assay kit's instructions.

6.2.14   Sample preparation for proteomics

Unless mentioned otherwise, all steps were performed at 4 °C. For proteomics, samples were collected from 15 cm dishes and subjected to a subcellular fractionation with the addition of PhosSTOP to the buffer. Only the mitochondrial fraction was kept. Instead of adding Laemmli SDS-PAGE sample buffer to the pellet, it was resuspended in 8 M urea buffer and sonicated twice for five seconds at 30 % amplitude. The sample was centrifuged at 20,000×g for 15 min,

the supernatant was kept and frozen until all biological replicates were collected. All samples' protein concentrations were measured according to the Pierce BCA protein assay kit's instructions. Then, technical replicates were pooled such that in the end there were a total of four technical replicates of 650 µg protein each distributed among two biological replicates. In order to reduce disulfide bonds, DTT was added to the samples to a final concentration of 5 mM and incubated shaking at 25 °C for 1 h. To alkylate thiol groups, CAA was added to a final concentration of 40 mM and incubated for 30 min in the dark at room temperature. The samples were diluted with 50 mM TEAB to achieve a final urea concentration < 2 M. Trypsin was added at an enzyme:substrate ratio of 1:75 and incubated shaking at 25 °C over night. Further sample processing, including Stage-Tip purification and enrichment of phosphopeptides with titanium dioxide beads, mass spectrometry measurements as well as data preparation were performed by the Proteomics Core Facility Cologne.

6.3   Data processing and analysis

Image processing and analysis was performed using ImageJ (Schneider et al., 2012). Quantifications and data presentations were performed with Excel and Prism. FACS data was analyzed with FlowJo.

Parkin recruitment event analysis was carried out in a blinded fashion using the ImageJ plug-in "Blind Analysis Tools", developed by Jaiswal and Lorenz. Parkin recruitment events to mitochondria were counted by hand throughout each z-stack and cell. The percentage of cells that displayed more than three recruitment events was calculated.

JC-1 images were handled as summed intensity z-stack projections, subjected to flatfield correction and subtraction of background before measuring the fluorescence levels normalized to the number of cell nuclei. The fluorescence intensity ratio between red and green signal was calculated and compared to DMSO as a ratio of 1.

7   References

Adebayo, M., Singh, S., Singh, A. P., and Dasgupta, S. (2021). Mitochondrial fusion and fission: The fine-tune balance for cellular homeostasis. *The FASEB Journal*, 35(6):e21620.

Adrain, C., Strisovsky, K., Zettl, M., Hu, L., Lemberg, M. K., and Freeman, M. (2011). Mammalian EGF receptor activation by the rhomboid protease RHBDL2. *EMBO Reports*, 12(5):421–427.

Akabane, S., Watanabe, K., Kosako, H., Yamashita, S.-i., Nishino, K., Kato, M., Sekine, S., Kanki, T., Matsuda, N., Endo, T., and Oka, T. (2023). TIM23 facilitates PINK1 activation by safeguarding against OMA1-mediated degradation in damaged mitochondria. *Cell Reports*, page 112454.

Anand, R., Wai, T., Baker, M. J., Kladt, N., Schauss, A. C., Rugarli, E., and Langer, T. (2014). The i-AAA protease YME1L and OMA1 cleave OPA1 to balance mitochondrial fusion and fission. *The Journal of Cell Biology*, 204(6):919–929.

Anderson, S., Bankier, A. T., Barrell, B. G., de Bruijn, M. H. L., Coulson, A. R., Drouin, J., Eperon, I. C., Nierlich, D. P., Roe, B. A., Sanger, F., Schreier, P. H., Smith, A. J. H., Staden, R., and Young, I. G. (1981). Sequence and organization of the human mitochondrial genome. *Nature*, 290(5806):457–465.

Ando, M., Fiesel, F. C., Hudec, R., Caulfield, T. R., Ogaki, K., Górka-Skoczylas, P., Koziorowski, D., Friedman, A., Chen, L., Dawson, V. L., Dawson, T. M., Bu, G., Ross, O. A., Wszolek, Z. K., and Springer, W. (2017). The PINK1 p.I368N mutation affects protein stability and ubiquitin kinase activity. *Molecular Neurodegeneration*, 12(1):32.

Arretz, M., Schneider, H., Guiard, B., Brunner, M., and Neupert, W. (1994). Characterization of the mitochondrial processing peptidase of Neurospora crassa. *Journal of Biological Chemistry*, 269(7):4959–4967.

Bach, K., Dohnálek, J., Škerlová, J., Kuzmík, J., Poláchová, E., Stanchev, S., Majer, P., Fanfrlík, J., Pecina, A., Řezáč, J., Lepšík, M., Borshchevskiy, V., Polovinkin, V., and Strisovsky, K. (2024). Extensive targeting of chemical space at the prime side of ketoamide inhibitors of rhomboid proteases by branched substituents empowers their selectivity and potency. *European Journal of Medicinal Chemistry*, 275:116606.

Baker, M. J., Blau, K. U., Anderson, A. J., Palmer, C. S., Fielden, L. F., Crameri, J. J., Milenkovic, D., Thorburn, D. R., Frazier, A. E., Langer, T., and Stojanovski, D. (2024). CLPB disaggregase

dysfunction impacts the functional integrity of the proteolytic SPY complex. *Journal of Cell Biology*, 223(3):e202305087.

Baker, M. J., Lampe, P. A., Stojanovski, D., Korwitz, A., Anand, R., Tatsuta, T., and Langer, T. (2014). Stress-induced OMA1 activation and autocatalytic turnover regulate OPA1-dependent mitochondrial dynamics. *The EMBO journal*, 33(6):578–593.

Baker, R. P., Young, K., Feng, L., Shi, Y., and Urban, S. (2007). Enzymatic analysis of a rhomboid intramembrane protease implicates transmembrane helix 5 as the lateral substrate gate. *Proceedings of the National Academy of Sciences*, 104(20):8257–8262.

Ban, T., Ishihara, T., Kohno, H., Saita, S., Ichimura, A., Maenaka, K., Oka, T., Mihara, K., and Ishihara, N. (2017). Molecular basis of selective mitochondrial fusion by heterotypic action between OPA1 and cardiolipin. *Nature Cell Biology*, 19(7):856–863.

Baughman, J. M., Perocchi, F., Girgis, H. S., Plovanich, M., Belcher-Timme, C. A., Sancak, Y., Bao, X. R., Strittmatter, L., Goldberger, O., Bogorad, R. L., Koteliansky, V., and Mootha, V. K. (2011). Integrative genomics identifies MCU as an essential component of the mitochondrial calcium uniporter. *Nature*, 476(7360):341–345.

Bayne, A. N., Dong, J., Amiri, S., Farhan, S. M. K., and Trempe, J.-F. (2023). MTSviewer: A database to visualize mitochondrial targeting sequences, cleavage sites, and mutations on protein structures. *PLOS ONE*, 18(4):e0284541.

Becker, D., Richter, J., Tocilescu, M. A., Przedborski, S., and Voos, W. (2012). Pink1 Kinase and Its Membrane Potential ($\Delta\psi$)-dependent Cleavage Product Both Localize to Outer Mitochondrial Membrane by Unique Targeting Mode*. *Journal of Biological Chemistry*, 287(27):22969–22987.

Becker, T., Wenz, L.-S., Krüger, V., Lehmann, W., Müller, J. M., Goroncy, L., Zufall, N., Lithgow, T., Guiard, B., Chacinska, A., Wagner, R., Meisinger, C., and Pfanner, N. (2011). The mitochondrial import protein Mim1 promotes biogenesis of multispanning outer membrane proteins. *The Journal of Cell Biology*, 194(3):387–395.

Beilina, A., Van Der Brug, M., Ahmad, R., Kesavapany, S., Miller, D. W., Petsko, G. A., and Cookson, M. R. (2005). Mutations in PTEN-induced putative kinase 1 associated with recessive parkinsonism have differential effects on protein stability. *Proceedings of the National Academy of Sciences of the United States of America*, 102(16):5703–5708.

Bernardi, P., Gerle, C., Halestrap, A. P., Jonas, E. A., Karch, J., Mnatsakanyan, N., Pavlov, E., Sheu, S.-S., and Soukas, A. A. (2023). Identity, structure, and function of the mitochondrial permeability transition pore: Controversies, consensus, recent advances, and future directions. *Cell Death & Differentiation*, 30(8):1869–1885.

Bezawork-Geleta, A., Brodie, E. J., Dougan, D. A., and Truscott, K. N. (2015). LON is the master protease that protects against protein aggregation in human mitochondria through direct degradation of misfolded proteins. *Scientific Reports*, 5(1):17397.

Bhujabal, Z., Birgisdottir, Å. B., Sjøttem, E., Brenne, H. B., Øvervatn, A., Habisov, S., Kirkin, V., Lamark, T., and Johansen, T. (2017). FKBP8 recruits LC3A to mediate Parkin-independent mitophagy. *EMBO reports*, 18(6):947–961.

Bi, P. Y., Killackey, S. A., Schweizer, L., Arnoult, D., Philpott, D. J., and Girardin, S. E. (2024). Cytosolic retention of HtrA2 during mitochondrial protein import stress triggers the DELE1-HRI pathway. *Communications Biology*, 7(1):391.

Bock, J., Kühnle, N., Knopf, J. D., Landscheidt, N., Lee, J.-G., Ye, Y., and Lemberg, M. K. (2022). Rhomboid protease RHBDL4 promotes retrotranslocation of aggregation-prone proteins for degradation. *Cell Reports*, 40(6):111175.

Bohg, C., Öster, C., Türkaydin, B., Lisurek, M., Sanchez-Carranza, P., Lange, S., Utesch, T., Sun, H., and Lange, A. (2023). The opening dynamics of the lateral gate regulates the activity of rhomboid proteases. *Science Advances*, 9(29):eadh3858.

Bohnert, M., Rehling, P., Guiard, B., Herrmann, J. M., Pfanner, N., and van der Laan, M. (2010). Cooperation of Stop-Transfer and Conservative Sorting Mechanisms in Mitochondrial Protein Transport. *Current Biology*, 20(13):1227–1232.

Bolliger, L., Junne, T., Schatz, G., and Lithgow, T. (1995). Acidic receptor domains on both sides of the outer membrane mediate translocation of precursor proteins into yeast mitochondria. *The EMBO Journal*, 14(24):6318–6326.

Bonen, L., Cunningham, R., Gray, M., and Doolittle, W. (1977). Wheat embryo mitochondrial 18S ribosomal RNA: Evidence for its prokaryotic nature. *Nucleic Acids Research*, 4(3):663–671.

Brandt, U. (1996). Bifurcated ubihydroquinone oxidation in the cytochrome bc 1 complex by proton-gated charge transfer. *FEBS Letters*, 387(1):1–6.

Brix, J., Dietmeier, K., and Pfanner, N. (1997). Differential Recognition of Preproteins by the Purified Cytosolic Domains of the Mitochondrial Import Receptors Tom20, Tom22, and Tom70 *. *Journal of Biological Chemistry*, 272(33):20730–20735.

Burman, J. L., Pickles, S., Wang, C., Sekine, S., Vargas, J. N. S., Zhang, Z., Youle, A. M., Nezich, C. L., Wu, X., Hammer, J. A., and Youle, R. J. (2017). Mitochondrial fission facilitates the selective mitophagy of protein aggregates. *The Journal of Cell Biology*, 216(10):3231–3247.

Burri, L., Strahm, Y., Hawkins, C. J., Gentle, I. E., Puryer, M. A., Verhagen, A., Callus, B., Vaux, D., and Lithgow, T. (2005). Mature DIABLO/Smac Is Produced by the IMP Protease Complex on the Mitochondrial Inner Membrane. *Molecular Biology of the Cell*, 16(6):2926–2933.

Busch, J. D., Fielden, L. F., Pfanner, N., and Wiedemann, N. (2023). Mitochondrial protein transport: Versatility of translocases and mechanisms. *Molecular Cell*, 83(6):890–910.

Bustillo-Zabalbeitia, I., Montessuit, S., Raemy, E., Basañez, G., Terrones, O., and Martinou, J.-C. (2014). Specific Interaction with Cardiolipin Triggers Functional Activation of Dynamin-Related Protein 1. *PLoS ONE*, 9(7):e102738.

Cadenas, E. and Davies, K. J. A. (2000). Mitochondrial free radical generation, oxidative stress, and aging1. *Free Radical Biology and Medicine*, 29(3):222–230.

Carroll, M. P. and May, W. S. (1994). Protein kinase C-mediated serine phosphorylation directly activates Raf-1 in murine hematopoietic cells. *The Journal of Biological Chemistry*, 269(2):1249–1256.

Chacinska, A., Lind, M., Frazier, A. E., Dudek, J., Meisinger, C., Geissler, A., Sickmann, A., Meyer, H. E., Truscott, K. N., Guiard, B., Pfanner, N., and Rehling, P. (2005). Mitochondrial Presequence Translocase: Switching between TOM Tethering and Motor Recruitment Involves Tim21 and Tim17. *Cell*, 120(6):817–829.

Chacinska, A., Pfannschmidt, S., Wiedemann, N., Kozjak, V., Sanjuán Szklarz, L. K., Schulze-Specking, A., Truscott, K. N., Guiard, B., Meisinger, C., and Pfanner, N. (2004). Essential role of Mia40 in import and assembly of mitochondrial intermembrane space proteins. *The EMBO Journal*, 23(19):3735–3746.

Chakrabarti, R., Ji, W.-K., Stan, R. V., Sanz, J. d. J., Ryan, T. A., and Higgs, H. N. (2018). INF2-mediated actin polymerization at the ER stimulates mitochondrial calcium uptake, inner membrane constriction, and division. *The Journal of Cell Biology*, 217(1):251.

Chan, N. C., Salazar, A. M., Pham, A. H., Sweredoski, M. J., Kolawa, N. J., Graham, R. L., Hess, S., and Chan, D. C. (2011). Broad activation of the ubiquitin–proteasome system by Parkin is critical for mitophagy. *Human Molecular Genetics*, 20(9):1726–1737.

Chen, G., Han, Z., Feng, D., Chen, Y., Chen, L., Wu, H., Huang, L., Zhou, C., Cai, X., Fu, C., Duan, L., Wang, X., Liu, L., Liu, X., Shen, Y., Zhu, Y., and Chen, Q. (2014). A regulatory signaling loop comprising the PGAM5 phosphatase and CK2 controls receptor-mediated mitophagy. *Molecular Cell*, 54(3):362–377.

Chen, H., Chomyn, A., and Chan, D. C. (2005). Disruption of fusion results in mitochondrial heterogeneity and dysfunction. *The Journal of Biological Chemistry*, 280(28):26185–26192.

Chen, Y. and Dorn, G. W. (2013). PINK1-Phosphorylated Mitofusin 2 Is a Parkin Receptor for Culling Damaged Mitochondria. *Science*, 340(6131):471–475.

Chomyn, A., Cleeter, M. W., Ragan, C. I., Riley, M., Doolittle, R. F., and Attardi, G. (1986). URF6, last unidentified reading frame of human mtDNA, codes for an NADH dehydrogenase subunit. *Science (New York, N.Y.)*, 234(4776):614–618.

Chomyn, A., Mariottini, P., Cleeter, M. W. J., Ragan, C. I., Matsuno-Yagi, A., Hatefi, Y., Doolittle, R. F., and Attardi, G. (1985). Six unidentified reading frames of human mitochondrial DNA encode components of the respiratory-chain NADH dehydrogenase. *Nature*, 314(6012):592–597.

Cipolat, S., Rudka, T., Hartmann, D., Costa, V., Serneels, L., Craessaerts, K., Metzger, K., Frezza, C., Annaert, W., D'Adamio, L., Derks, C., Dejaegere, T., Pellegrini, L., D'Hooge, R., Scorrano, L., and De Strooper, B. (2006). Mitochondrial Rhomboid PARL Regulates Cytochrome c Release during Apoptosis via OPA1-Dependent Cristae Remodeling. *Cell*, 126(1):163–175.

Clark, I. E., Dodson, M. W., Jiang, C., Cao, J. H., Huh, J. R., Seol, J. H., Yoo, S. J., Hay, B. A., and Guo, M. (2006). Drosophila pink1 is required for mitochondrial function and interacts genetically with parkin. *Nature*, 441(7097):1162–1166.

Cupo, R. R. and Shorter, J. (2020). Skd3 (human ClpB) is a potent mitochondrial protein disaggregase that is inactivated by 3-methylglutaconic aciduria-linked mutations. *eLife*, 9:e55279.

De Los Rios, P., Ben-Zvi, A., Slutsky, O., Azem, A., and Goloubinoff, P. (2006). Hsp70 chaperones accelerate protein translocation and the unfolding of stable protein aggregates by entropic pulling. *Proceedings of the National Academy of Sciences*, 103(16):6166–6171.

De Stefani, D., Raffaello, A., Teardo, E., Szabò, I., and Rizzuto, R. (2011). A forty-kilodalton protein of the inner membrane is the mitochondrial calcium uniporter. *Nature*, 476(7360):336–340.

Deas, E., Plun-Favreau, H., Gandhi, S., Desmond, H., Kjaer, S., Loh, S. H., Renton, A. E., Harvey, R. J., Whitworth, A. J., Martins, L. M., Abramov, A. Y., and Wood, N. W. (2011). PINK1 cleavage at position A103 by the mitochondrial protease PARL. *Human Molecular Genetics*, 20(5):867–879.

Denton, R. M. (2009). Regulation of mitochondrial dehydrogenases by calcium ions. *Biochimica Et Biophysica Acta*, 1787(11):1309–1316.

Deshwal, S., Fiedler, K. U., and Langer, T. (2020). Mitochondrial Proteases: Multifaceted Regulators of Mitochondrial Plasticity. *Annual Review of Biochemistry*, 89(1):501–528.

Deshwal, S., Onishi, M., Tatsuta, T., Bartsch, T., Cors, E., Ried, K., Lemke, K., Nolte, H., Giavalisco, P., and Langer, T. (2023). Mitochondria regulate intracellular coenzyme Q transport and ferroptotic resistance via STARD7. *Nature Cell Biology*, pages 1–12.

Devenish, R. J., Prescott, M., Boyle, G. M., and Nagley, P. (2000). The Oligomycin Axis of Mitochondrial ATP Synthase: OSCP and the Proton Channel. *Journal of Bioenergetics and Biomembranes*, 32(5):507–515.

Dickey, S. W., Baker, R. P., Cho, S., and Urban, S. (2013). Proteolysis inside the Membrane Is a Rate-Governed Reaction Not Driven by Substrate Affinity. *Cell*, 155(6):1270–1281.

Doan, K. N., Grevel, A., Mårtensson, C. U., Ellenrieder, L., Thornton, N., Wenz, L.-S., Opaliński, Ł., Guiard, B., Pfanner, N., and Becker, T. (2020). The Mitochondrial Import Complex MIM Functions as Main Translocase for α-Helical Outer Membrane Proteins. *Cell Reports*, 31(4).

Dudek, J., Rehling, P., and van der Laan, M. (2013). Mitochondrial protein import: Common principles and physiological networks. *Biochimica et Biophysica Acta (BBA) - Molecular Cell Research*, 1833(2):274–285.

Ehses, S., Raschke, I., Mancuso, G., Bernacchia, A., Geimer, S., Tondera, D., Martinou, J.-C., Westermann, B., Rugarli, E. I., and Langer, T. (2009). Regulation of OPA1 processing and mitochondrial fusion by m-AAA protease isoenzymes and OMA1. *The Journal of Cell Biology*, 187(7):1023–1036.

Eldeeb, M. A., Bayne, A. N., Fallahi, A., Goiran, T., MacDougall, E. J., Soumbasis, A., Zorca, C. E., Tabah, J.-J., Thomas, R. A., Karpilovsky, N., Mathur, M., Durcan, T. M., Trempe, J.-F., and Fon, E. A. (2024). Tom20 gates PINK1 activity and mediates its tethering of the TOM and TIM23 translocases upon mitochondrial stress. *Proceedings of the National Academy of Sciences of the United States of America*, 121(10):e2313540121.

Elgass, K., Pakay, J., Ryan, M. T., and Palmer, C. S. (2013). Recent advances into the understanding of mitochondrial fission. *Biochimica et Biophysica Acta (BBA) - Molecular Cell Research*, 1833(1):150–161.

Endres, M., Neupert, W., and Brunner, M. (1999). Transport of the ADP/ATP carrier of mitochondria from the TOM complex to the TIM22·54 complex. *The EMBO Journal*, 18(12):3214–3221.

Falabella, M., Vernon, H. J., Hanna, M. G., Claypool, S. M., and Pitceathly, R. D. S. (2021). Cardiolipin, Mitochondria, and Neurological Disease. *Trends in Endocrinology & Metabolism*, 32(4):224–237.

Fallaize, D., Chin, L.-S., and Li, L. (2015). Differential submitochondrial localization of PINK1 as a molecular switch for mediating distinct mitochondrial signaling pathways. *Cellular Signalling*, 27(12):2543–2554.

Fedorenko, A., Lishko, P. V., and Kirichok, Y. (2012). Mechanism of Fatty-Acid-Dependent UCP1 Uncoupling in Brown Fat Mitochondria. *Cell*, 151(2):400–413.

Fessler, E., Eckl, E.-M., Schmitt, S., Mancilla, I. A., Meyer-Bender, M. F., Hanf, M., Philippou-Massier, J., Krebs, S., Zischka, H., and Jae, L. T. (2020). A pathway coordinated by DELE1 relays mitochondrial stress to the cytosol. *Nature*, 579(7799):433–437.

Fielden, L. F., Busch, J. D., Merkt, S. G., Ganesan, I., Steiert, C., Hasselblatt, H. B., Busto, J. V., Wirth, C., Zufall, N., Jungbluth, S., Noll, K., Dung, J. M., Butenko, L., von der Malsburg, K., Koch, H.-G., Hunte, C., van der Laan, M., and Wiedemann, N. (2023). Central role of Tim17 in mitochondrial presequence protein translocation. *Nature*, 621(7979):627–634.

Filipuzzi, I., Steffen, J., Germain, M., Goepfert, L., Conti, M. A., Potting, C., Cerino, R., Pfeifer, M., Krastel, P., Hoepfner, D., Bastien, J., Koehler, C. M., and Helliwell, S. B. (2017). Stendomycin selectively inhibits TIM23-dependent mitochondrial protein import. *Nature Chemical Biology*, 13(12):1239–1244.

Fiorese, C. J., Schulz, A. M., Lin, Y.-F., Rosin, N., Pellegrino, M. W., and Haynes, C. M. (2016).

The Transcription Factor ATF5 Mediates a Mammalian Mitochondrial UPR. *Current Biology*, 26(15):2037–2043.

Fleig, L., Bergbold, N., Sahasrabudhe, P., Geiger, B., Kaltak, L., and Lemberg, M. K. (2012). Ubiquitin-dependent intramembrane rhomboid protease promotes ERAD of membrane proteins. *Molecular Cell*, 47(4):558–569.

Fleury, C., Mignotte, B., and Vayssière, J.-L. (2002). Mitochondrial reactive oxygen species in cell death signaling. *Biochimie*, 84(2):131–141.

Friedman, J. R., Lackner, L. L., West, M., DiBenedetto, J. R., Nunnari, J., and Voeltz, G. K. (2011). ER Tubules Mark Sites of Mitochondrial Division. *Science*, 334(6054):358–362.

Gan, Z. Y., Callegari, S., Cobbold, S. A., Cotton, T. R., Mlodzianoski, M. J., Schubert, A. F., Geoghegan, N. D., Rogers, K. L., Leis, A., Dewson, G., Glukhova, A., and Komander, D. (2022). Activation mechanism of PINK1. *Nature*, 602(7896):328–335.

Gandre-Babbe, S. and van der Bliek, A. M. (2008). The Novel Tail-anchored Membrane Protein Mff Controls Mitochondrial and Peroxisomal Fission in Mammalian Cells. *Molecular Biology of the Cell*, 19(6):2402–2412.

Gaume, B., Klaus, C., Ungermann, C., Guiard, B., Neupert, W., and Brunner, M. (1998). Unfolding of preproteins upon import into mitochondria. *The EMBO Journal*, 17(22):6497–6507.

Ge, P., Dawson, V. L., and Dawson, T. M. (2020). PINK1 and Parkin mitochondrial quality control: A source of regional vulnerability in Parkinson's disease. *Molecular Neurodegeneration*, 15(1):20.

Geisler, S., Holmström, K. M., Skujat, D., Fiesel, F. C., Rothfuss, O. C., Kahle, P. J., and Springer, W. (2010a). PINK1/Parkin-mediated mitophagy is dependent on VDAC1 and p62/SQSTM1. *Nature Cell Biology*, 12(2):119–131.

Geisler, S., Holmström, K. M., Treis, A., Skujat, D., Weber, S. S., Fiesel, F. C., Kahle, P. J., and Springer, W. (2010b). The PINK1/Parkin-mediated mitophagy is compromised by PD-associated mutations. *Autophagy*, 6(7):871–878.

Ghezzi, D., Arzuffi, P., Zordan, M., Da Re, C., Lamperti, C., Benna, C., D'Adamo, P., Diodato, D., Costa, R., Mariotti, C., Uziel, G., Smiderle, C., and Zeviani, M. (2011). Mutations in TTC19 cause mitochondrial complex III deficiency and neurological impairment in humans and flies. *Nature Genetics*, 43(3):259–263.

Ghosh, P., Vidal, C., Dey, S., and Zhang, L. (2020). Mitochondria Targeting as an Effective Strategy for Cancer Therapy. *International Journal of Molecular Sciences*, 21(9):3363.

Gomes, F., Palma, F. R., Barros, M. H., Tsuchida, E. T., Turano, H. G., Alegria, T. G. P., Demasi, M., and Netto, L. E. S. (2017). Proteolytic cleavage by the inner membrane peptidase (IMP) complex or Oct1 peptidase controls the localization of the yeast peroxiredoxin Prx1 to distinct mitochondrial compartments. *Journal of Biological Chemistry*, 292(41):17011–17024.

Gornicka, A., Bragoszewski, P., Chroscicki, P., Wenz, L.-S., Schulz, C., Rehling, P., and Chacinska, A. (2014). A discrete pathway for the transfer of intermembrane space proteins across the outer membrane of mitochondria. *Molecular Biology of the Cell*, 25(25):3999–4009.

Greene, A. W., Grenier, K., Aguileta, M. A., Muise, S., Farazifard, R., Haque, M. E., McBride, H. M., Park, D. S., and Fon, E. A. (2012). Mitochondrial processing peptidase regulates PINK1 processing, import and Parkin recruitment. *EMBO reports*, 13(4):378–385.

Greene, J. C., Whitworth, A. J., Kuo, I., Andrews, L. A., Feany, M. B., and Pallanck, L. J. (2003). Mitochondrial pathology and apoptotic muscle degeneration in Drosophila parkin mutants. *Proceedings of the National Academy of Sciences of the United States of America*, 100(7):4078–4083.

Griparic, L., Kanazawa, T., and van der Bliek, A. M. (2007). Regulation of the mitochondrial dynamin-like protein Opa1 by proteolytic cleavage. *The Journal of Cell Biology*, 178(5):757–764.

Guo, X., Aviles, G., Liu, Y., Tian, R., Unger, B. A., Lin, Y.-H. T., Wiita, A. P., Xu, K., Correia, M. A., and Kampmann, M. (2020). Mitochondrial stress is relayed to the cytosol by an OMA1–DELE1–HRI pathway. *Nature*, 579(7799):427–432.

Han, D., Williams, E., and Cadenas, E. (2001). Mitochondrial respiratory chain-dependent generation of superoxide anion and its release into the intermembrane space. *Biochemical Journal*, 353(2):411–416.

Hanna, R. A., Quinsay, M. N., Orogo, A. M., Giang, K., Rikka, S., and Gustafsson, Å. B. (2012). Microtubule-associated Protein 1 Light Chain 3 (LC3) Interacts with Bnip3 Protein to Selectively Remove Endoplasmic Reticulum and Mitochondria via Autophagy*. *Journal of Biological Chemistry*, 287(23):19094–19104.

Hasson, S. A., Kane, L. A., Yamano, K., Huang, C.-H., Sliter, D. A., Buehler, E., Wang, C., Heman-Ackah, S. M., Hessa, T., Guha, R., Martin, S. E., and Youle, R. J. (2013). High-content

genome-wide RNAi screens identify regulators of parkin upstream of mitophagy. *Nature*, 504(7479):291–295.

Hawlitschek, G., Schneider, H., Schmidt, B., Tropschug, M., Hartl, F. U., and Neupert, W. (1988). Mitochondrial protein import: Identification of processing peptidase and of PEP, a processing enhancing protein. *Cell*, 53(5):795–806.

Haynes, C. M., Petrova, K., Benedetti, C., Yang, Y., and Ron, D. (2007). ClpP Mediates Activation of a Mitochondrial Unfolded Protein Response in *C. elegans*. *Developmental Cell*, 13(4):467–480.

Haynes, C. M., Yang, Y., Blais, S. P., Neubert, T. A., and Ron, D. (2010). The Matrix Peptide Exporter HAF-1 Signals a Mitochondrial UPR by Activating the Transcription Factor ZC376.7 in *C. elegans*. *Molecular Cell*, 37(4):529–540.

Head, B., Griparic, L., Amiri, M., Gandre-Babbe, S., and van der Bliek, A. M. (2009). Inducible proteolytic inactivation of OPA1 mediated by the OMA1 protease in mammalian cells. *The Journal of Cell Biology*, 187(7):959–966.

Hearne, A., Chen, H., Monarchino, A., and Wiseman, J. S. (2020). Oligomycin-induced proton uncoupling. *Toxicology in Vitro*, 67:104907.

Heinitz, S., Klein, C., and Djarmati, A. (2011). The p.S77N presenilin-associated rhomboid-like protein mutation is not a frequent cause of early-onset Parkinson's disease. *Movement Disorders*, 26(13):2441–2442.

Hopfer, U., Lehninger, A. L., and Thompson, T. E. (1968). Protonic conductance across phospholipid bilayer membranes induced by uncoupling agents for oxidative phosphorylation. *Proceedings of the National Academy of Sciences*, 59(2):484–490.

Hoshino, A., Wang, W.-j., Wada, S., McDermott-Roe, C., Evans, C. S., Gosis, B., Morley, M. P., Rathi, K. S., Li, J., Li, K., Yang, S., McMannus, M. J., Bowman, C., Potluri, P., Levin, M., Damrauer, S., Wallace, D. C., Holzbaur, E. L. F., and Arany, Z. (2019). The ATP/ADP translocase drives mitophagy independent of nucleotide exchange. *Nature*, 575(7782):375–379.

Huang, E., Qu, D., Huang, T., Rizzi, N., Boonying, W., Krolak, D., Ciana, P., Woulfe, J., Klein, C., Slack, R. S., Figeys, D., and Park, D. S. (2017). PINK1-mediated phosphorylation of LETM1 regulates mitochondrial calcium transport and protects neurons against mitochondrial stress. *Nature Communications*, 8:1399.

Huang, K. C., Mukhopadhyay, R., and Wingreen, N. S. (2006). A Curvature-Mediated Mechanism for Localization of Lipids to Bacterial Poles. *PLOS Computational Biology*, 2(11):e151.

Hytti, M., Korhonen, E., Hyttinen, J. M. T., Roehrich, H., Kaarniranta, K., Ferrington, D. A., and Kauppinen, A. (2019). Antimycin A-Induced Mitochondrial Damage Causes Human RPE Cell Death despite Activation of Autophagy. *Oxidative Medicine and Cellular Longevity*, 2019:1583656.

Ieva, R., Schrempp, S. G., Opaliński, Ł., Wollweber, F., Höß, P., Heißwolf, A. K., Gebert, M., Zhang, Y., Guiard, B., Rospert, S., Becker, T., Chacinska, A., Pfanner, N., and van der Laan, M. (2014). Mgr2 Functions as Lateral Gatekeeper for Preprotein Sorting in the Mitochondrial Inner Membrane. *Molecular Cell*, 56(5):641–652.

Ishihara, N., Fujita, Y., Oka, T., and Mihara, K. (2006). Regulation of mitochondrial morphology through proteolytic cleavage of OPA1. *The EMBO journal*, 25(13):2966–2977.

Itakura, E., Kishi-Itakura, C., Koyama-Honda, I., and Mizushima, N. (2012). Structures containing Atg9A and the ULK1 complex independently target depolarized mitochondria at initial stages of Parkin-mediated mitophagy. *Journal of Cell Science*, 125(6):1488–1499.

Ito, A. (1999). Mitochondrial Processing Peptidase: Multiple-Site Recognition of Precursor Proteins. *Biochemical and Biophysical Research Communications*, 265(3):611–616.

Jeyaraju, D. V., McBride, H. M., Hill, R. B., and Pellegrini, L. (2011). Structural and mechanistic basis of Parl activity and regulation. *Cell Death and Differentiation*, 18(9):1531–1539.

Jeyaraju, D. V., Xu, L., Letellier, M.-C., Bandaru, S., Zunino, R., Berg, E. A., McBride, H. M., and Pellegrini, L. (2006). Phosphorylation and cleavage of presenilin-associated rhomboid-like protein (PARL) promotes changes in mitochondrial morphology. *Proceedings of the National Academy of Sciences of the United States of America*, 103(49):18562–18567.

Jin, S., Zhuo, Y., Guo, W., and Field, J. (2005). P21-activated Kinase 1 (Pak1)-dependent Phosphorylation of Raf-1 Regulates Its Mitochondrial Localization, Phosphorylation of BAD, and Bcl-2 Association*. *Journal of Biological Chemistry*, 280(26):24698–24705.

Jin, S. M., Lazarou, M., Wang, C., Kane, L. A., Narendra, D. P., and Youle, R. J. (2010). Mitochondrial membrane potential regulates PINK1 import and proteolytic destabilization by PARL. *Journal of Cell Biology*, 191(5):933–942.

Jin, S. M. and Youle, R. J. (2013). The accumulation of misfolded proteins in the mitochondrial matrix is sensed by PINK1 to induce PARK2/Parkin-mediated mitophagy of polarized mitochondria. *Autophagy*, 9(11):1750–1757.

Johnson, N., Březinová, J., Stephens, E., Burbridge, E., Freeman, M., Adrain, C., and Strisovsky, K. (2017). Quantitative proteomics screen identifies a substrate repertoire of rhomboid protease RHBDL2 in human cells and implicates it in epithelial homeostasis. *Scientific Reports*, 7:7283.

Kalbáčová, M., Vrbacký, M., Drahota, Z., and Mělková, Z. (2003). Comparison of the effect of mitochondrial inhibitors on mitochondrial membrane potential in two different cell lines using flow cytometry and spectrofluorometry. *Cytometry Part A*, 52A(2):110–116.

Káldi, K., Bauer, M. F., Sirrenberg, C., Neupert, W., and Brunner, M. (1998). Biogenesis of Tim23 and Tim17, integral components of the TIM machinery for matrix-targeted preproteins. *The EMBO Journal*, 17(6):1569–1576.

Kane, L. A., Lazarou, M., Fogel, A. I., Li, Y., Yamano, K., Sarraf, S. A., Banerjee, S., and Youle, R. J. (2014). PINK1 phosphorylates ubiquitin to activate Parkin E3 ubiquitin ligase activity. *The Journal of Cell Biology*, 205(2):143–153.

Kazlauskaite, A., Kondapalli, C., Gourlay, R., Campbell, D. G., Ritorto, M. S., Hofmann, K., Alessi, D. R., Knebel, A., Trost, M., and Muqit, M. M. K. (2014). Parkin is activated by PINK1-dependent phosphorylation of ubiquitin at Ser65. *The Biochemical Journal*, 460(1):127–139.

Khalifat, N., Puff, N., Bonneau, S., Fournier, J.-B., and Angelova, M. I. (2008). Membrane Deformation under Local pH Gradient: Mimicking Mitochondrial Cristae Dynamics. *Biophysical Journal*, 95(10):4924–4933.

Kirkin, V., Lamark, T., Sou, Y.-S., Bjørkøy, G., Nunn, J. L., Bruun, J.-A., Shvets, E., McEwan, D. G., Clausen, T. H., Wild, P., Bilusic, I., Theurillat, J.-P., Øvervatn, A., Ishii, T., Elazar, Z., Komatsu, M., Dikic, I., and Johansen, T. (2009). A Role for NBR1 in Autophagosomal Degradation of Ubiquitinated Substrates. *Molecular Cell*, 33(4):505–516.

Kitada, T., Asakawa, S., Hattori, N., Matsumine, H., Yamamura, Y., Minoshima, S., Yokochi, M., Mizuno, Y., and Shimizu, N. (1998). Mutations in the parkin gene cause autosomal recessive juvenile parkinsonism. *Nature*, 392(6676):605–608.

Knopf, J. D., Landscheidt, N., Pegg, C. L., Schulz, B. L., Kühnle, N., Chao, C.-W., Huck, S., and Lemberg, M. K. (2020). Intramembrane protease RHBDL4 cleaves oligosaccharyl-

transferase subunits to target them for ER-associated degradation. *Journal of Cell Science*, 133(6):jcs243790.

Knopf, J. D., Steigleder, S. S., Korn, F., Kühnle, N., Badenes, M., Tauber, M., Theobald, S. J., Rybniker, J., Adrain, C., and Lemberg, M. K. (2024). RHBDL4-triggered downregulation of COPII adaptor protein TMED7 suppresses TLR4-mediated inflammatory signaling. *Nature Communications*, 15(1):1528.

Koehler, C. M., Merchant, S., Oppliger, W., Schmid, K., Jarosch, E., Dolfini, L., Junne, T., Schatz, G., and Tokatlidis, K. (1998). Tim9p, an essential partner subunit of Tim10p for the import of mitochondrial carrier proteins. *The EMBO Journal*, 17(22):6477–6486.

Kondapalli, C., Kazlauskaite, A., Zhang, N., Woodroof, H. I., Campbell, D. G., Gourlay, R., Burchell, L., Walden, H., Macartney, T. J., Deak, M., Knebel, A., Alessi, D. R., and Muqit, M. M. K. (2012). PINK1 is activated by mitochondrial membrane potential depolarization and stimulates Parkin E3 ligase activity by phosphorylating Serine 65. *Open Biology*, 2(5):120080.

König, T., Nolte, H., Aaltonen, M. J., Tatsuta, T., Krols, M., Stroh, T., Langer, T., and McBride, H. M. (2021). MIROs and DRP1 drive mitochondrial-derived vesicle biogenesis and promote quality control. *Nature Cell Biology*, 23(12):1271–1286.

König, T., Tröder, S. E., Bakka, K., Korwitz, A., Richter-Dennerlein, R., Lampe, P. A., Patron, M., Mühlmeister, M., Guerrero-Castillo, S., Brandt, U., Decker, T., Lauria, I., Paggio, A., Rizzuto, R., Rugarli, E. I., De Stefani, D., and Langer, T. (2016). The m-AAA Protease Associated with Neurodegeneration Limits MCU Activity in Mitochondria. *Molecular Cell*, 64(1):148–162.

Koyano, F., Okatsu, K., Kosako, H., Tamura, Y., Go, E., Kimura, M., Kimura, Y., Tsuchiya, H., Yoshihara, H., Hirokawa, T., Endo, T., Fon, E. A., Trempe, J.-F., Saeki, Y., Tanaka, K., and Matsuda, N. (2014). Ubiquitin is phosphorylated by PINK1 to activate parkin. *Nature*, 510(7503):162–166.

Krimmer, T., Rapaport, D., Ryan, M. T., Meisinger, C., Kassenbrock, C. K., Blachly-Dyson, E., Forte, M., Douglas, M. G., Neupert, W., Nargang, F. E., and Pfanner, N. (2001). Biogenesis of Porin of the Outer Mitochondrial Membrane Involves an Import Pathway via Receptors and the General Import Pore of the Tom Complex. *Journal of Cell Biology*, 152(2):289–300.

Kühnle, N., Dederer, V., and Lemberg, M. K. (2019). Intramembrane proteolysis at a glance: From signalling to protein degradation. *Journal of Cell Science*, 132(16):jcs217745.

Laemmli, U. K. (1970). Cleavage of Structural Proteins during the Assembly of the Head of Bacteriophage T4. *Nature*, 227(5259):680–685.

Lampert, M. A., Orogo, A. M., Najor, R. H., Hammerling, B. C., Leon, L. J., Wang, B. J., Kim, T., Sussman, M. A., and Gustafsson, Å. B. (2019). BNIP3L/NIX and FUNDC1-mediated mitophagy is required for mitochondrial network remodeling during cardiac progenitor cell differentiation. *Autophagy*, 15(7):1182–1198.

Lazarou, M., Jin, S. M., Kane, L. A., and Youle, R. J. (2012). Role of PINK1 Binding to the TOM Complex and Alternate Intracellular Membranes in Recruitment and Activation of the E3 Ligase Parkin. *Developmental Cell*, 22(2):320–333.

Lazarou, M., Sliter, D. A., Kane, L. A., Sarraf, S. A., Wang, C., Burman, J. L., Sideris, D. P., Fogel, A. I., and Youle, R. J. (2015). The ubiquitin kinase PINK1 recruits autophagy receptors to induce mitophagy. *Nature*, 524(7565):309–314.

LeBlanc Jr., O. (1971). The effect of uncouplers of oxidative phosphorylation on lipid bilayer membranes: Carbonylcyanide m-chlorophenylhydrazone. *The Journal of Membrane Biology*, 4(1):227–251.

Lee, S., Lee, H., Yoo, S., Ieva, R., van der Laan, M., von Heijne, G., and Kim, H. (2020). The Mgr2 subunit of the TIM23 complex regulates membrane insertion of marginal stop-transfer signals in the mitochondrial inner membrane. *FEBS Letters*, 594(6):1081–1087.

Leonhard, K., Stiegler, A., Neupert, W., and Langer, T. (1999). Chaperone-like activity of the AAA domain of the yeast Yme1 AAA protease. *Nature*, 398(6725):348–351.

Lin, W. and Kang, U. J. (2008). Characterization of PINK1 processing, stability, and subcellular localization. *Journal of Neurochemistry*, 106(1):464–474.

Lin, W. and Kang, U. J. (2010). Structural determinants of PINK1 topology and dual subcellular distribution. *BMC Cell Biology*, 11(1):90.

Liu, L., Feng, D., Chen, G., Chen, M., Zheng, Q., Song, P., Ma, Q., Zhu, C., Wang, R., Qi, W., Huang, L., Xue, P., Li, B., Wang, X., Jin, H., Wang, J., Yang, F., Liu, P., Zhu, Y., Sui, S., and Chen, Q. (2012). Mitochondrial outer-membrane protein FUNDC1 mediates hypoxia-induced mitophagy in mammalian cells. *Nature Cell Biology*, 14(2):177–185.

Lohi, O., Urban, S., and Freeman, M. (2004). Diverse substrate recognition mechanisms for rhomboids; thrombomodulin is cleaved by Mammalian rhomboids. *Current biology: CB*, 14(3):236–241.

Lorenz, H., Hailey, D. W., Wunder, C., and Lippincott-Schwartz, J. (2006). The fluorescence protease protection (FPP) assay to determine protein localization and membrane topology. *Nature Protocols*, 1(1):276–279.

Lorriman, J. S., Grieve, A. G., Corey, R. A., and Collinson, I. (2024). Alternative Import-Channels And Destinations Of Mitochondrial PINK1 Controlled By Trans-Membrane-Domain Structural Plasticity.

Lu, W., Karuppagounder, S. S., Springer, D. A., Allen, M. D., Zheng, L., Chao, B., Zhang, Y., Dawson, V. L., Dawson, T. M., and Lenardo, M. (2014). Genetic deficiency of the mitochondrial protein PGAM5 causes a Parkinson's-like movement disorder. *Nature Communications*, 5(1):1–11.

Lysyk, L., Brassard, R., Arutyunova, E., Siebert, V., Jiang, Z., Takyi, E., Morrison, M., Young, H. S., Lemberg, M. K., O'Donoghue, A. J., and Lemieux, M. J. (2020a). Insights into the catalytic properties of the mitochondrial rhomboid protease PARL. Preprint, Biochemistry.

Lysyk, L., Brassard, R., Touret, N., and Lemieux, M. J. (2020b). PARL Protease: A Glimpse at Intramembrane Proteolysis in the Inner Mitochondrial Membrane. *Journal of Molecular Biology*, 432(18):5052–5062.

Macdonald, P. J., Stepanyants, N., Mehrotra, N., Mears, J. A., Qi, X., Sesaki, H., and Ramachandran, R. (2014). A dimeric equilibrium intermediate nucleates Drp1 reassembly on mitochondrial membranes for fission. *Molecular Biology of the Cell*, 25(12):1905.

Macreadie, I. G., Novitski, C. E., Maxwell, R. J., John, U., Ooi, B. G., McMullen, G. L., Lukins, H. B., Linnane, A. W., and Nagley, P. (1983). Biogenesis of mitochondria: The mitochondrial gene (aap1) coding for mitochondrial ATPase subunit 8 in Saccharomyces cerevisiae. *Nucleic Acids Research*, 11(13):4435–4451.

Martin, J., Mahlke, K., and Pfanner, N. (1991). Role of an energized inner membrane in mitochondrial protein import. Delta psi drives the movement of presequences. *Journal of Biological Chemistry*, 266(27):18051–18057.

Maruszczak, K. K., Draczkowski, P., Wnorowski, A., and Chacinska, A. (2024). Structure prediction analysis of human core TIM23 complex reveals conservation of the protein translocation mechanism. *FEBS Open Bio*, 14(10):1656–1667.

Maruszczak, K. K., Jung, M., Rasool, S., Trempe, J.-F., and Rapaport, D. (2022). The role of the

individual TOM subunits in the association of PINK1 with depolarized mitochondria. *Journal of Molecular Medicine*, 100(5):747–762.

Matsuda, N., Sato, S., Shiba, K., Okatsu, K., Saisho, K., Gautier, C. A., Sou, Y.-S., Saiki, S., Kawajiri, S., Sato, F., Kimura, M., Komatsu, M., Hattori, N., and Tanaka, K. (2010). PINK1 stabilized by mitochondrial depolarization recruits Parkin to damaged mitochondria and activates latent Parkin for mitophagy. *The Journal of Cell Biology*, 189(2):211–221.

Matsushima, Y., Goto, Y.-i., and Kaguni, L. S. (2010). Mitochondrial Lon protease regulates mitochondrial DNA copy number and transcription by selective degradation of mitochondrial transcription factor A (TFAM). *Proceedings of the National Academy of Sciences of the United States of America*, 107(43):18410–18415.

Matsushima, Y., Takahashi, K., Yue, S., Fujiyoshi, Y., Yoshioka, H., Aihara, M., Setoyama, D., Uchiumi, T., Fukuchi, S., and Kang, D. (2021). Mitochondrial Lon protease is a gatekeeper for proteins newly imported into the matrix. *Communications Biology*, 4(1):1–13.

McLelland, G.-L., Soubannier, V., Chen, C. X., McBride, H. M., and Fon, E. A. (2014). Parkin and PINK1 function in a vesicular trafficking pathway regulating mitochondrial quality control. *The EMBO Journal*, 33(4):282–295.

Meeusen, S., DeVay, R., Block, J., Cassidy-Stone, A., Wayson, S., McCaffery, J. M., and Nunnari, J. (2006). Mitochondrial inner-membrane fusion and crista maintenance requires the dynamin-related GTPase Mgm1. *Cell*, 127(2):383–395.

Meissner, C., Lorenz, H., Hehn, B., and Lemberg, M. K. (2015). Intramembrane protease PARL defines a negative regulator of PINK1- and PARK2/Parkin-dependent mitophagy. *Autophagy*, 11(9):1484–1498.

Meissner, C., Lorenz, H., Weihofen, A., Selkoe, D. J., and Lemberg, M. K. (2011). The mitochondrial intramembrane protease PARL cleaves human Pink1 to regulate Pink1 trafficking. *Journal of Neurochemistry*, 117(5):856–867.

Michaelis, J. B., Brunstein, M. E., Bozkurt, S., Alves, L., Wegner, M., Kaulich, M., Pohl, C., and Münch, C. (2022). Protein import motor complex reacts to mitochondrial misfolding by reducing protein import and activating mitophagy. *Nature Communications*, 13(1):5164.

Milenkovic, D., Ramming, T., Müller, J. M., Wenz, L.-S., Gebert, N., Schulze-Specking, A., Stojanovski, D., Rospert, S., and Chacinska, A. (2009). Identification of the Signal Directing

Tim9 and Tim10 into the Intermembrane Space of Mitochondria. *Molecular Biology of the Cell*, 20(10):2530–2539.

Mizushima, N. and Komatsu, M. (2011). Autophagy: Renovation of Cells and Tissues. *Cell*, 147(4):728–741.

Morais, V. A., Haddad, D., Craessaerts, K., Bock, P.-J. D., Swerts, J., Vilain, S., Aerts, L., Overbergh, L., Grünewald, A., Seibler, P., Klein, C., Gevaert, K., Verstreken, P., and Strooper, B. D. (2014). PINK1 Loss-of-Function Mutations Affect Mitochondrial Complex I Activity via NdufA10 Ubiquinone Uncoupling. *Science*, 344(6180):203–207.

Moriwaki, Y., Kim, Y.-J., Ido, Y., Misawa, H., Kawashima, K., Endo, S., and Takahashi, R. (2008). L347P PINK1 mutant that fails to bind to Hsp90/Cdc37 chaperones is rapidly degraded in a proteasome-dependent manner. *Neuroscience Research*, 61(1):43–48.

Müller, J. M., Milenkovic, D., Guiard, B., Pfanner, N., and Chacinska, A. (2008). Precursor Oxidation by Mia40 and Erv1 Promotes Vectorial Transport of Proteins into the Mitochondrial Intermembrane Space. *Molecular Biology of the Cell*, 19(1):226–236.

Nag, S., Szederkenyi, K., Gorbenko, O., Tyrrell, H., Yip, C. M., and McQuibban, G. A. (2023). PGAM5 is an MFN2 phosphatase that plays an essential role in the regulation of mitochondrial dynamics. *Cell Reports*, 42(8):112895.

Narendra, D., Kane, L. A., Hauser, D. N., Fearnley, I. M., and Youle, R. J. (2010a). P62/SQSTM1 is required for Parkin-induced mitochondrial clustering but not mitophagy; VDAC1 is dispensable for both. *Autophagy*, 6(8):1090–1106.

Narendra, D., Tanaka, A., Suen, D.-F., and Youle, R. J. (2008). Parkin is recruited selectively to impaired mitochondria and promotes their autophagy. *The Journal of Cell Biology*, 183(5):795–803.

Narendra, D. P., Jin, S. M., Tanaka, A., Suen, D.-F., Gautier, C. A., Shen, J., Cookson, M. R., and Youle, R. J. (2010b). PINK1 is selectively stabilized on impaired mitochondria to activate Parkin. *PLoS biology*, 8(1):e1000298.

Narendra, D. P. and Youle, R. J. (2024). The role of PINK1–Parkin in mitochondrial quality control. *Nature Cell Biology*, 26(10):1639–1651.

Nargund, A. M., Pellegrino, M. W., Fiorese, C. J., Baker, B. M., and Haynes, C. M. (2012). Mitochondrial Import Efficiency of ATFS-1 Regulates Mitochondrial UPR Activation. *Science*, 337(6094):587–590.

Ng, M. Y. W., Wai, T., and Simonsen, A. (2021). Quality control of the mitochondrion. *Developmental Cell*, 56(7):881–905.

Nguyen, T. N., Padman, B. S., Usher, J., Oorschot, V., Ramm, G., and Lazarou, M. (2016). Atg8 family LC3/GABARAP proteins are crucial for autophagosome–lysosome fusion but not autophagosome formation during PINK1/Parkin mitophagy and starvation. *Journal of Cell Biology*, 215(6):857–874.

Nguyen, T. N., Sawa-Makarska, J., Khuu, G., Lam, W. K., Adriaenssens, E., Fracchiolla, D., Shoebridge, S., Bernklau, D., Padman, B. S., Skulsuppaisarn, M., Lindblom, R. S. J., Martens, S., and Lazarou, M. (2023). Unconventional initiation of PINK1/Parkin mitophagy by Optineurin. *Molecular Cell*, 83(10):1693–1709.e9.

Novak, I., Kirkin, V., McEwan, D. G., Zhang, J., Wild, P., Rozenknop, A., Rogov, V., Löhr, F., Popovic, D., Occhipinti, A., Reichert, A. S., Terzic, J., Dötsch, V., Ney, P. A., and Dikic, I. (2010). Nix is a selective autophagy receptor for mitochondrial clearance. *EMBO reports*, 11(1):45–51.

Noy, P. J., Swain, R. K., Khan, K., Lodhia, P., and Bicknell, R. (2016). Sprouting angiogenesis is regulated by shedding of the C-type lectin family 14, member A (CLEC14A) ectodomain, catalyzed by rhomboid-like 2 protein (RHBDL2). *FASEB journal: official publication of the Federation of American Societies for Experimental Biology*, 30(6):2311–2323.

Okatsu, K., Kimura, M., Oka, T., Tanaka, K., and Matsuda, N. (2015). Unconventional PINK1 localization to the outer membrane of depolarized mitochondria drives Parkin recruitment. *Journal of Cell Science*, 128(5):964–978.

Okatsu, K., Oka, T., Iguchi, M., Imamura, K., Kosako, H., Tani, N., Kimura, M., Go, E., Koyano, F., Funayama, M., Shiba-Fukushima, K., Sato, S., Shimizu, H., Fukunaga, Y., Taniguchi, H., Komatsu, M., Hattori, N., Mihara, K., Tanaka, K., and Matsuda, N. (2012). PINK1 autophosphorylation upon membrane potential dissipation is essential for Parkin recruitment to damaged mitochondria. *Nature Communications*, 3:1016.

Okatsu, K., Uno, M., Koyano, F., Go, E., Kimura, M., Oka, T., Tanaka, K., and Matsuda, N. (2013). A dimeric PINK1-containing complex on depolarized mitochondria stimulates Parkin recruitment. *The Journal of Biological Chemistry*, 288(51):36372–36384.

Orrenius, S., Gogvadze, V., and Zhivotovsky, B. (2015). Calcium and mitochondria in the regulation of cell death. *Biochemical and Biophysical Research Communications*, 460(1):72–81.

Otera, H., Wang, C., Cleland, M. M., Setoguchi, K., Yokota, S., Youle, R. J., and Mihara, K. (2010). Mff is an essential factor for mitochondrial recruitment of Drp1 during mitochondrial fission in mammalian cells. *Journal of Cell Biology*, 191(6):1141–1158.

Padman, B. S., Nguyen, T. N., Uoselis, L., Skulsuppaisarn, M., Nguyen, L. K., and Lazarou, M. (2019). LC3/GABARAPs drive ubiquitin-independent recruitment of Optineurin and NDP52 to amplify mitophagy. *Nature Communications*, 10(1):408.

Palmer, C. S., Osellame, L. D., Laine, D., Koutsopoulos, O. S., Frazier, A. E., and Ryan, M. T. (2011). MiD49 and MiD51, new components of the mitochondrial fission machinery. *EMBO reports*, 12(6):565–573.

Papić, D., Krumpe, K., Dukanovic, J., Dimmer, K. S., and Rapaport, D. (2011). Multispan mitochondrial outer membrane protein Ugo1 follows a unique Mim1-dependent import pathway. *The Journal of Cell Biology*, 194(3):397–405.

Park, J., Lee, S. B., Lee, S., Kim, Y., Song, S., Kim, S., Bae, E., Kim, J., Shong, M., Kim, J.-M., and Chung, J. (2006). Mitochondrial dysfunction in Drosophila PINK1 mutants is complemented by parkin. *Nature*, 441(7097):1157–1161.

Park, Y. S., Choi, S. E., and Koh, H. C. (2018). PGAM5 regulates PINK1/Parkin-mediated mitophagy via DRP1 in CCCP-induced mitochondrial dysfunction. *Toxicology Letters*, 284:120–128.

Pascall, J. C. and Brown, K. D. (2004). Intramembrane cleavage of ephrinB3 by the human rhomboid family protease, RHBDL2. *Biochemical and Biophysical Research Communications*, 317(1):244–252.

Paschkowsky, S., Hamzé, M., Oestereich, F., and Munter, L. M. (2016). Alternative Processing of the Amyloid Precursor Protein Family by Rhomboid Protease RHBDL4. *The Journal of Biological Chemistry*, 291(42):21903–21912.

Peleh, V., Cordat, E., and Herrmann, J. M. (2016). Mia40 is a trans-site receptor that drives protein import into the mitochondrial intermembrane space by hydrophobic substrate binding. *eLife*, 5:e16177.

Pellegrini, L., Passer, B. J., Canelles, M., Lefterov, I., Ganjei, J. K., Fowlkes, B. J., Koonin, E. V., and D'Adamio, L. (2001). PAMP and PARL, two novel putative metalloproteases interacting with the COOH-terminus of Presenilin-1 and -2. *Journal of Alzheimer's disease: JAD*, 3(2):181–190.

Penefsky, H. S. (1985). Mechanism of inhibition of mitochondrial adenosine triphosphatase by dicyclohexylcarbodiimide and oligomycin: Relationship to ATP synthesis. *Proceedings of the National Academy of Sciences*, 82(6):1589–1593.

Plun-Favreau, H., Klupsch, K., Moisoi, N., Gandhi, S., Kjaer, S., Frith, D., Harvey, K., Deas, E., Harvey, R. J., McDonald, N., Wood, N. W., Martins, L. M., and Downward, J. (2007). The mitochondrial protease HtrA2 is regulated by Parkinson's disease-associated kinase PINK1. *Nature Cell Biology*, 9(11):1243–1252.

Poláchová, E., Bach, K., Heuten, E., Stanchev, S., Tichá, A., Lampe, P., Majer, P., Langer, T., Lemberg, M. K., and Stříšovský, K. (2022). Chemical Blockage of the Mitochondrial Rhomboid Protease PARL by Novel Ketoamide Inhibitors Reveals Its Role in PINK1/Parkin-Dependent Mitophagy. *Journal of Medicinal Chemistry*.

Pridgeon, J. W., Olzmann, J. A., Chin, L.-S., and Li, L. (2007). PINK1 Protects against Oxidative Stress by Phosphorylating Mitochondrial Chaperone TRAP1. *PLoS Biology*, 5(7):e172.

Qiu, J., Wenz, L.-S., Zerbes, R. M., Oeljeklaus, S., Bohnert, M., Stroud, D. A., Wirth, C., Ellenrieder, L., Thornton, N., Kutik, S., Wiese, S., Schulze-Specking, A., Zufall, N., Chacinska, A., Guiard, B., Hunte, C., Warscheid, B., van der Laan, M., Pfanner, N., Wiedemann, N., and Becker, T. (2013). Coupling of mitochondrial import and export translocases by receptor-mediated supercomplex formation. *Cell*, 154(3):596–608.

Radaelli, E., Assenmacher, C.-A., Verrelle, J., Banerjee, E., Manero, F., Khiati, S., Girona, A., Lopez-Lluch, G., Navas, P., and Spinazzi, M. (2023). Mitochondrial defects leading to arrested spermatogenesis and ferroptosis in the PARL deficient mouse model of Leigh Syndrome. *eLife*, 12:e84710.

Raimi, O. G., Ojha, H., Ehses, K., Dederer, V., Lange, S. M., Rivera, C. P., Deegan, T. D., Chen, Y., Wightman, M., Toth, R., Labib, K. P. M., Mathea, S., Ranson, N., Fernández-Busnadiego, R., and Muqit, M. M. K. (2024). Mechanism of human PINK1 activation at the TOM complex in a reconstituted system. *Science Advances*, 10(23):eadn7191.

Rainbolt, T. K., Lebeau, J., Puchades, C., and Wiseman, R. L. (2016). Reciprocal Degradation of YME1L and OMA1 Adapts Mitochondrial Proteolytic Activity during Stress. *Cell Reports*, 14(9):2041–2049.

Ramage, L., Junne, T., Hahne, K., Lithgow, T., and Schatz, G. (1993). Functional cooperation of mitochondrial protein import receptors in yeast. *The EMBO Journal*, 12(11):4115–4123.

Rapizzi, E., Pinton, P., Szabadkai, G., Wieckowski, M. R., Vandecasteele, G., Baird, G., Tuft, R. A., Fogarty, K. E., and Rizzuto, R. (2002). Recombinant expression of the voltage-dependent anion channel enhances the transfer of Ca2+ microdomains to mitochondria. *The Journal of Cell Biology*, 159(4):613.

Rasola, A. and Bernardi, P. (2011). Mitochondrial permeability transition in Ca2+-dependent apoptosis and necrosis. *Cell Calcium*, 50(3):222–233.

Rasool, S., Veyron, S., Soya, N., Eldeeb, M. A., Lukacs, G. L., Fon, E. A., and Trempe, J.-F. (2022). Mechanism of PINK1 activation by autophosphorylation and insights into assembly on the TOM complex. *Molecular Cell*, 82(1):44–59.e6.

Redza-Dutordoir, M. and Averill-Bates, D. A. (2016). Activation of apoptosis signalling pathways by reactive oxygen species. *Biochimica et Biophysica Acta (BBA) - Molecular Cell Research*, 1863(12):2977–2992.

Reers, M., Smith, T. W., and Chen, L. B. (1991). J-aggregate formation of a carbocyanine as a quantitative fluorescent indicator of membrane potential. *Biochemistry*, 30(18):4480–4486.

Ren, L., Meng, L., Gao, J., Lu, M., Guo, C., Li, Y., Rong, Z., and Ye, Y. (2023). PHB2 promotes colorectal cancer cell proliferation and tumorigenesis through NDUFS1-mediated oxidative phosphorylation. *Cell Death & Disease*, 14(1):1–11.

Richter, B., Sliter, D. A., Herhaus, L., Stolz, A., Wang, C., Beli, P., Zaffagnini, G., Wild, P., Martens, S., Wagner, S. A., Youle, R. J., and Dikic, I. (2016). Phosphorylation of OPTN by TBK1 enhances its binding to Ub chains and promotes selective autophagy of damaged mitochondria. *Proceedings of the National Academy of Sciences of the United States of America*, 113(15):4039–4044.

Richter, F., Dennerlein, S., Nikolov, M., Jans, D. C., Naumenko, N., Aich, A., MacVicar, T., Linden, A., Jakobs, S., Urlaub, H., Langer, T., and Rehling, P. (2019). ROMO1 is a constituent of the human presequence translocase required for YME1L protease import. *The Journal of Cell Biology*, 218(2):598–614.

Roberts, R. F., Bayne, A. N., Goiran, T., Lévesque, D., Boisvert, F.-M., Trempe, J.-F., and Fon, E. A. (2021). Proteomic Profiling of Mitochondrial-Derived Vesicles in Brain Reveals Enrichment of Respiratory Complex Sub-assemblies and Small TIM Chaperones. *Journal of Proteome Research*, 20(1):506–517.

Rojo, M., Legros, F., Chateau, D., and Lombès, A. (2002). Membrane topology and mitochondrial targeting of mitofusins, ubiquitous mammalian homologs of the transmembrane GTPase Fzo. *Journal of Cell Science*, 115(Pt 8):1663–1674.

Ryan, T. A., Phillips, E. O., Collier, C. L., JB Robinson, A., Routledge, D., Wood, R. E., Assar, E. A., and Tumbarello, D. A. (2020). Tollip coordinates Parkin-dependent trafficking of mitochondrial-derived vesicles. *The EMBO Journal*, n/a(n/a):e102539.

Sagan, L. (1967). On the origin of mitosing cells. *Journal of Theoretical Biology*, 14(3):225–IN6.

Saita, S., Nolte, H., Fiedler, K. U., Kashkar, H., Venne, A. S., Zahedi, R. P., Krüger, M., and Langer, T. (2017). PARL mediates Smac proteolytic maturation in mitochondria to promote apoptosis. *Nature Cell Biology*, 19(4):318–328.

Saita, S., Tatsuta, T., Lampe, P. A., König, T., Ohba, Y., and Langer, T. (2018). PARL partitions the lipid transfer protein STARD7 between the cytosol and mitochondria. *The EMBO journal*, 37(4).

Santel, A. and Fuller, M. T. (2001). Control of mitochondrial morphology by a human mitofusin. *Journal of Cell Science*, 114(Pt 5):867–874.

Schägger, H. and von Jagow, G. (1991). Blue native electrophoresis for isolation of membrane protein complexes in enzymatically active form. *Analytical Biochemistry*, 199(2):223–231.

Schneider, C. A., Rasband, W. S., and Eliceiri, K. W. (2012). NIH Image to ImageJ: 25 years of image analysis. *Nature Methods*, 9(7):671–675.

Schweers, R. L., Zhang, J., Randall, M. S., Loyd, M. R., Li, W., Dorsey, F. C., Kundu, M., Opferman, J. T., Cleveland, J. L., Miller, J. L., and Ney, P. A. (2007). NIX is required for programmed mitochondrial clearance during reticulocyte maturation. *Proceedings of the National Academy of Sciences of the United States of America*, 104(49):19500–19505.

Sekine, S., Kanamaru, Y., Koike, M., Nishihara, A., Okada, M., Kinoshita, H., Kamiyama, M., Maruyama, J., Uchiyama, Y., Ishihara, N., Takeda, K., and Ichijo, H. (2012). Rhomboid protease PARL mediates the mitochondrial membrane potential loss-induced cleavage of PGAM5. *The Journal of Biological Chemistry*, 287(41):34635–34645.

Sekine, S., Wang, C., Sideris, D. P., Bunker, E., Zhang, Z., and Youle, R. J. (2019). Reciprocal Roles of Tom7 and OMA1 during Mitochondrial Import and Activation of PINK1. *Molecular Cell*, 73(5):1028–1043.e5.

Sekine, Y., Houston, R., Eckl, E.-M., Fessler, E., Narendra, D. P., Jae, L. T., and Sekine, S. (2023). A mitochondrial iron-responsive pathway regulated by DELE1. *Molecular Cell*, 83(12):2059–2076.e6.

Shi, G., Lee, J. R., Grimes, D. A., Racacho, L., Ye, D., Yang, H., Ross, O. A., Farrer, M., McQuibban, G. A., and Bulman, D. E. (2011). Functional alteration of PARL contributes to mitochondrial dysregulation in Parkinson's disease. *Human Molecular Genetics*, 20(10):1966–1974.

Shi, G. and McQuibban, G. A. (2017). The Mitochondrial Rhomboid Protease PARL Is Regulated by PDK2 to Integrate Mitochondrial Quality Control and Metabolism. *Cell Reports*, 18(6):1458–1472.

Shiba-Fukushima, K., Arano, T., Matsumoto, G., Inoshita, T., Yoshida, S., Ishihama, Y., Ryu, K.-Y., Nukina, N., Hattori, N., and Imai, Y. (2014). Phosphorylation of Mitochondrial Polyubiquitin by PINK1 Promotes Parkin Mitochondrial Tethering. *PLOS Genetics*, 10(12):e1004861.

Shiba-Fukushima, K., Imai, Y., Yoshida, S., Ishihama, Y., Kanao, T., Sato, S., and Hattori, N. (2012). PINK1-mediated phosphorylation of the Parkin ubiquitin-like domain primes mitochondrial translocation of Parkin and regulates mitophagy. *Scientific Reports*, 2:1002.

Shoshan-Barmatz, V. and Gincel, D. (2003). The voltage-dependent anion channel. *Cell Biochemistry and Biophysics*, 39(3):279–292.

Siebert, V., Silber, M., Heuten, E., Muhle-Goll, C., and Lemberg, M. K. (2022). Cleavage of mitochondrial homeostasis regulator PGAM5 by the intramembrane protease PARL is governed by transmembrane helix dynamics and oligomeric state. *Journal of Biological Chemistry*, 0(0).

Sík, A., Passer, B. J., Koonin, E. V., and Pellegrini, L. (2004). Self-regulated cleavage of the mitochondrial intramembrane-cleaving protease PARL yields Pbeta, a nuclear-targeted peptide. *The Journal of Biological Chemistry*, 279(15):15323–15329.

Sim, S. I., Chen, Y., Lynch, D. L., Gumbart, J. C., and Park, E. (2023). Structural basis of mitochondrial protein import by the TIM23 complex. *Nature*, 621(7979):620–626.

Sirrenberg, C., Endres, M., Fölsch, H., Stuart, R. A., Neupert, W., and Brunner, M. (1998). Carrier protein import into mitochondria mediated by the intermembrane proteins Tim10/Mrs11 and Tim12/Mrs5. *Nature*, 391(6670):912–915.

Smirnova, E., Griparic, L., Shurland, D.-L., and van der Bliek, A. M. (2001). Dynamin-related Protein Drp1 Is Required for Mitochondrial Division in Mammalian Cells. *Molecular Biology of the Cell*, 12(8):2245–2256.

Söllner, T., Griffiths, G., Pfaller, R., Pfanner, N., and Neupert, W. (1989). MOM19, an import receptor for mitochondrial precursor proteins. *Cell*, 59(6):1061–1070.

Söllner, T., Pfaller, R., Griffiths, G., Pfanner, N., and Neupert, W. (1990). A mitochondrial import receptor for the ADP/ATP carrier. *Cell*, 62(1):107–115.

Song, Z., Chen, H., Fiket, M., Alexander, C., and Chan, D. C. (2007). OPA1 processing controls mitochondrial fusion and is regulated by mRNA splicing, membrane potential, and Yme1L. *The Journal of Cell Biology*, 178(5):749–755.

Soubannier, V., McLelland, G.-L., Zunino, R., Braschi, E., Rippstein, P., Fon, E. A., and McBride, H. M. (2012a). A Vesicular Transport Pathway Shuttles Cargo from Mitochondria to Lysosomes. *Current Biology*, 22(2):135–141.

Soubannier, V., Rippstein, P., Kaufman, B. A., Shoubridge, E. A., and McBride, H. M. (2012b). Reconstitution of Mitochondria Derived Vesicle Formation Demonstrates Selective Enrichment of Oxidized Cargo. *PLOS ONE*, 7(12):e52830.

Spinazzi, M., Radaelli, E., Horré, K., Arranz, A. M., Gounko, N. V., Agostinis, P., Maia, T. M., Impens, F., Morais, V. A., Lopez-Lluch, G., Serneels, L., Navas, P., and De Strooper, B. (2019). PARL deficiency in mouse causes Complex III defects, coenzyme Q depletion, and Leigh-like syndrome. *Proceedings of the National Academy of Sciences*, 116(1):277–286.

Steglich, G., Neupert, W., and Langer, T. (1999). Prohibitins Regulate Membrane Protein Degradation by the m-AAA Protease in Mitochondria. *Molecular and Cellular Biology*, 19(5):3435–3442.

Strisovsky, K. (2017). Chapter Eleven - Mechanism and Inhibition of Rhomboid Proteases. In Gelb, M. H., editor, *Methods in Enzymology*, volume 584 of *Enzymology at the Membrane Interface: Intramembrane Proteases*, pages 279–293. Academic Press.

Strisovsky, K., Sharpe, H. J., and Freeman, M. (2009). Sequence-Specific Intramembrane Proteolysis: Identification of a Recognition Motif in Rhomboid Substrates. *Molecular Cell*, 36(6):1048–1059.

Sugiura, A., McLelland, G.-L., Fon, E. A., and McBride, H. M. (2014). A new pathway for mitochondrial quality control: Mitochondrial-derived vesicles. *The EMBO journal*, 33(19):2142–2156.

Symersky, J., Osowski, D., Walters, D. E., and Mueller, D. M. (2012). Oligomycin frames a common drug-binding site in the ATP synthase. *Proceedings of the National Academy of Sciences*, 109(35):13961–13965.

Szabadkai, G., Bianchi, K., Várnai, P., De Stefani, D., Wieckowski, M. R., Cavagna, D., Nagy, A. I., Balla, T., and Rizzuto, R. (2006). Chaperone-mediated coupling of endoplasmic reticulum and mitochondrial Ca2+ channels. *The Journal of Cell Biology*, 175(6):901–911.

Tanaka, A., Cleland, M. M., Xu, S., Narendra, D. P., Suen, D.-F., Karbowski, M., and Youle, R. J. (2010). Proteasome and p97 mediate mitophagy and degradation of mitofusins induced by Parkin. *The Journal of Cell Biology*, 191(7):1367–1380.

Taylor, A. B., Smith, B. S., Kitada, S., Kojima, K., Miyaura, H., Otwinowski, Z., Ito, A., and Deisenhofer, J. (2001). Crystal Structures of Mitochondrial Processing Peptidase Reveal the Mode for Specific Cleavage of Import Signal Sequences. *Structure*, 9(7):615–625.

Tichá, A., Collis, B., and Strisovsky, K. (2018). The Rhomboid Superfamily: Structural Mechanisms and Chemical Biology Opportunities. *Trends in Biochemical Sciences*, 43(9):726–739.

Tichá, A., Stanchev, S., Vinothkumar, K. R., Mikles, D. C., Pachl, P., Began, J., Škerle, J., Švehlová, K., Nguyen, M. T. N., Verhelst, S. H. L., Johnson, D. C., Bachovchin, D. A., Lepšík, M., Majer, P., and Strisovsky, K. (2017). General and Modular Strategy for Designing Potent, Selective, and Pharmacologically Compliant Inhibitors of Rhomboid Proteases. *Cell Chemical Biology*, 24(12):1523–1536.e4.

Trempe, J.-F. and Gehring, K. (2023). Structural Mechanisms of Mitochondrial Quality Control Mediated by PINK1 and Parkin. *Journal of Molecular Biology*, 435(12):168090.

Tsai, P.-I., Lin, C.-H., Hsieh, C.-H., Papakyrikos, A. M., Kim, M. J., Napolioni, V., Schoor, C., Couthouis, J., Wu, R.-M., Wszolek, Z. K., Winter, D., Greicius, M. D., Ross, O. A., and Wang, X. (2018). PINK1 Phosphorylates MIC60/Mitofilin to Control Structural Plasticity of Mitochondrial Crista Junctions. *Molecular Cell*, 69(5):744–756.e6.

Uoselis, L., Nguyen, T. N., and Lazarou, M. (2023). Mitochondrial degradation: Mitophagy and beyond. *Molecular Cell*, pages S1097–2765(23)00656–1.

Valente, E. M., Abou-Sleiman, P. M., Caputo, V., Muqit, M. M. K., Harvey, K., Gispert, S., Ali, Z., Turco, D. D., Bentivoglio, A. R., Healy, D. G., Albanese, A., Nussbaum, R., González-Maldonado, R., Deller, T., Salvi, S., Cortelli, P., Gilks, W. P., Latchman, D. S., Harvey, R. J.,

Dallapiccola, B., Auburger, G., and Wood, N. W. (2004). Hereditary Early-Onset Parkinson's Disease Caused by Mutations in PINK1. *Science*, 304(5674):1158–1160.

Vande Walle, L., Lamkanfi, M., and Vandenabeele, P. (2008). The mitochondrial serine protease HtrA2/Omi: An overview. *Cell Death & Differentiation*, 15(3):453–460.

Vargas, J. N. S., Wang, C., Bunker, E., Hao, L., Maric, D., Schiavo, G., Randow, F., and Youle, R. J. (2019). Spatiotemporal Control of ULK1 Activation by NDP52 and TBK1 during Selective Autophagy. *Molecular Cell*, 74(2):347–362.e6.

Vives-Bauza, C., Zhou, C., Huang, Y., Cui, M., de Vries, R. L. A., Kim, J., May, J., Tocilescu, M. A., Liu, W., Ko, H. S., Magrané, J., Moore, D. J., Dawson, V. L., Grailhe, R., Dawson, T. M., Li, C., Tieu, K., and Przedborski, S. (2010). PINK1-dependent recruitment of Parkin to mitochondria in mitophagy. *Proceedings of the National Academy of Sciences*, 107(1):378–383.

Vizziello, M., Borellini, L., Franco, G., and Ardolino, G. (2021). Disruption of Mitochondrial Homeostasis: The Role of PINK1 in Parkinson's Disease. *Cells*, 10(11):3022.

Wai, T., Saita, S., Nolte, H., Müller, S., König, T., Richter-Dennerlein, R., Sprenger, H.-G., Madrenas, J., Mühlmeister, M., Brandt, U., Krüger, M., and Langer, T. (2016). The membrane scaffold SLP2 anchors a proteolytic hub in mitochondria containing PARL and the i-AAA protease YME1L. *EMBO reports*, 17(12):1844–1856.

Wang, H.-G., Rapp, U. R., and Reed, J. C. (1996). Bcl-2 Targets the Protein Kinase Raf-1 to Mitochondria. *Cell*, 87(4):629–638.

Wang, Y., Zhang, Y., and Ha, Y. (2006). Crystal structure of a rhomboid family intramembrane protease. *Nature*, 444(7116):179–180.

Waters, C. S., Angenent, S. B., Altschuler, S. J., and Wu, L. F. (2023). A PINK1 input threshold arises from positive feedback in the PINK1/Parkin mitophagy decision circuit. *Cell Reports*, 42(10):113260.

Weihofen, A., Ostaszewski, B., Minami, Y., and Selkoe, D. J. (2008). Pink1 Parkinson mutations, the Cdc37/Hsp90 chaperones and Parkin all influence the maturation or subcellular distribution of Pink1. *Human Molecular Genetics*, 17(4):602–616.

Wiedemann, N. and Pfanner, N. (2017). Mitochondrial Machineries for Protein Import and Assembly. *Annual Review of Biochemistry*, 86(Volume 86, 2017):685–714.

Wiedemann, N., Truscott, K. N., Pfannschmidt, S., Guiard, B., Meisinger, C., and Pfanner, N. (2004). Biogenesis of the Protein Import Channel Tom40 of the Mitochondrial Outer Membrane: INTERMEMBRANE SPACE COMPONENTS ARE INVOLVED IN AN EARLY STAGE OF THE ASSEMBLY PATHWAY*. *Journal of Biological Chemistry*, 279(18):18188–18194.

Wiedemann, N., van der Laan, M., and Pfanner, N. (2009). SnapShot: Import and Sortingof Mitochondrial Proteins. *Cell*, 138(4):808–808.e1.

Wolf, D. M., Segawa, M., Kondadi, A. K., Anand, R., Bailey, S. T., Reichert, A. S., van der Bliek, A. M., Shackelford, D. B., Liesa, M., and Shirihai, O. S. (2019). Individual cristae within the same mitochondrion display different membrane potentials and are functionally independent. *The EMBO Journal*, 38(22):e101056.

Wong, Y. C. and Holzbaur, E. L. F. (2014). Optineurin is an autophagy receptor for damaged mitochondria in parkin-mediated mitophagy that is disrupted by an ALS-linked mutation. *Proceedings of the National Academy of Sciences of the United States of America*, 111(42):E4439–4448.

Wu, Z., Yan, N., Feng, L., Oberstein, A., Yan, H., Baker, R. P., Gu, L., Jeffrey, P. D., Urban, S., and Shi, Y. (2006). Structural analysis of a rhomboid family intramembrane protease reveals a gating mechanism for substrate entry. *Nature Structural & Molecular Biology*, 13(12):1084–1091.

Wunderle, L., Knopf, J. D., Kühnle, N., Morlé, A., Hehn, B., Adrain, C., Strisovsky, K., Freeman, M., and Lemberg, M. K. (2016). Rhomboid intramembrane protease RHBDL4 triggers ER-export and non-canonical secretion of membrane-anchored TGFα. *Scientific Reports*, 6:27342.

Wüst, R., Maurer, B., Hauser, K., Woitalla, D., Sharma, M., and Krüger, R. (2016). Mutation analyses and association studies to assess the role of the presenilin-associated rhomboid-like gene in Parkinson's disease. *Neurobiology of Aging*, 39:217.e13–217.e15.

Yamano, K., Kikuchi, R., Kojima, W., Hayashida, R., Koyano, F., Kawawaki, J., Shoda, T., Demizu, Y., Naito, M., Tanaka, K., and Matsuda, N. (2020). Critical role of mitochondrial ubiquitination and the OPTN-ATG9A axis in mitophagy. *The Journal of Cell Biology*, 219(9).

Yamano, K. and Youle, R. J. (2013). PINK1 is degraded through the N-end rule pathway. *Autophagy*, 9(11):1758–1769.

Yan, C., Gong, L., Chen, L., Xu, M., Abou-Hamdan, H., Tang, M., Désaubry, L., and Song, Z. (2019). PHB2 (prohibitin 2) promotes PINK1-PRKN/Parkin-dependent mitophagy by the PARL-PGAM5-PINK1 axis. *Autophagy*, 16(3):419–434.

Yang, D., Oyaizu, Y., Oyaizu, H., Olsen, G. J., and Woese, C. R. (1985). Mitochondrial origins. *Proceedings of the National Academy of Sciences*, 82(13):4443–4447.

Yao, C.-H., Wang, R., Wang, Y., Kung, C.-P., Weber, J. D., and Patti, G. J. (2019). Mitochondrial fusion supports increased oxidative phosphorylation during cell proliferation. *eLife*, 8:e41351.

Youle, R. J. and van der Bliek, A. M. (2012). Mitochondrial Fission, Fusion, and Stress. *Science*, 337(6098):1062–1065.

Young, J. C., Hoogenraad, N. J., and Hartl, F. U. (2003). Molecular Chaperones Hsp90 and Hsp70 Deliver Preproteins to the Mitochondrial Import Receptor Tom70. *Cell*, 112(1):41–50.

Yu, B., Ma, J., Li, J., Wang, D., Wang, Z., and Wang, S. (2020). Mitochondrial phosphatase PGAM5 modulates cellular senescence by regulating mitochondrial dynamics. *Nature Communications*, 11:2549.

Zacksenhaus, E., Shrestha, M., Liu, J. C., Vorobieva, I., Chung, P. E. D., Ju, Y., Nir, U., and Jiang, Z. (2017). Mitochondrial OXPHOS Induced by RB1 Deficiency in Breast Cancer: Implications for Anabolic Metabolism, Stemness, and Metastasis. *Trends in Cancer*, 3(11):768–779.

Žárský, V. and Doležal, P. (2016). Evolution of the Tim17 protein family. *Biology Direct*, 11:54.

Zhang, K., Li, H., and Song, Z. (2014). Membrane depolarization activates the mitochondrial protease OMA1 by stimulating self-cleavage. *EMBO reports*, 15(5):576–585.

Zhang, W., Ren, H., Xu, C., Zhu, C., Wu, H., Liu, D., Wang, J., Liu, L., Li, W., Ma, Q., Du, L., Zheng, M., Zhang, C., Liu, J., and Chen, Q. (2016). Hypoxic mitophagy regulates mitochondrial quality and platelet activation and determines severity of I/R heart injury. *eLife*, 5:e21407.

Zhao, J., Liu, T., Jin, S., Wang, X., Qu, M., Uhlén, P., Tomilin, N., Shupliakov, O., Lendahl, U., and Nistér, M. (2011). Human MIEF1 recruits Drp1 to mitochondrial outer membranes and promotes mitochondrial fusion rather than fission. *The EMBO Journal*, 30(14):2762–2778.

Zhou, X., Yang, Y., Wang, G., Wang, S., Sun, D., Ou, X., Lian, Y., and Li, L. (2023). Molecular pathway of mitochondrial preprotein import through the TOM–TIM23 supercomplex. *Nature Structural & Molecular Biology*, 30(12):1996–2008.

Zoll, S., Stanchev, S., Began, J., Škerle, J., Lepšík, M., Peclinovská, L., Majer, P., and Strisovsky, K. (2014). Substrate binding and specificity of rhomboid intramembrane protease revealed by substrate–peptide complex structures. *The EMBO Journal*, 33(20):2408–2421.

8   Supplemental material

8.1   Supplementary figures
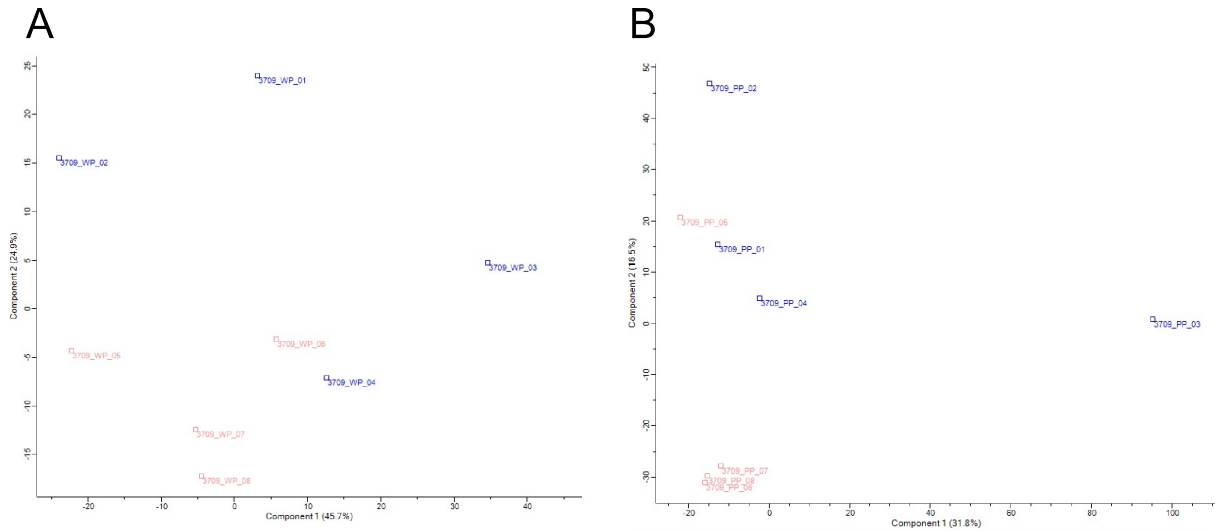
Figure S.1: *Principal component analyses of whole proteome and phosphoproteins following PARL inhibition.* **A)** Principal component analysis of samples in whole proteomics approach (DMSO samples in blue, inhibitor samples 1868 in orange). **B)** Principal component analysis of samples in phosphoproteomics approach (DMSO samples in blue, inhibitor samples 1868 in orange). Subfigures were generated by the CECAD Proteomics Facility.

8.2   Supplementary tables

Table S.1: Results of whole proteomics with a p-value equal or below -log(1.3) = 0.05

gene names	-Log Student's T-test p-value	Student's T-test q-value	Student's T-test Difference (inhibitor - control)	MitoCarta3.0 Localization
TIPIN	3.467	0.031	-1.940	
NBR1	2.521	0.021	-2.194	IMS
BROX	2.092	0.062	-9.443	
B3GNT2	1.856	0.016	-5.477	
CYCS	3.759	0.066	-0.995	IMS
RPL26	3.460	1.000	0.308	
NUDC	3.210	0.829	0.125	
UBA2	2.866	1.000	-0.339	
CMTM4	2.845	0.497	-0.565	
LETMD1	2.640	0.834	0.117	Membrane
ADO	2.638	1.000	-0.245	
EMILIN3	2.557	0.694	-0.478	
PARD6G	2.546	1.000	-0.317	
MYL6	2.479	0.906	0.177	
IMPDH1	2.434	0.540	-0.548	
CTSO	2.432	0.079	-1.536	
HERPUD1	2.424	1.000	-0.241	
TSN	2.396	0.836	-0.136	
PPP1R21	2.387	1.000	-0.221	
MYH10	2.385	0.840	0.156	
CTSA	2.314	0.847	0.103	
TNIK	2.294	0.829	0.130	
DCAF8	2.276	0.551	-0.650	
STARD7	2.254	0.785	0.484	IMS
TRUB2	2.243	1.000	0.247	Matrix
METAP2	2.243	1.000	-0.294	
RPS6KA3	2.228	0.828	-0.126	

RNF185	2.211	1.000	-0.247	
ATP6V1C1	2.200	0.846	0.162	
ERC1	2.196	1.000	-0.324	
SPECC1L	2.194	0.907	0.180	
CHMP1B	2.193	1.000	-0.360	
DIMT1	2.179	1.000	-0.302	
WDR13	2.177	0.933	-0.193	
SRPK2	2.164	1.000	-0.215	
ASAP1	2.144	1.000	-0.246	
BOLA2	2.117	0.953	-0.061	
LIG1	2.104	0.089	-1.606	
HAUS8	2.102	1.000	-0.367	
PXMP2	2.097	1.000	0.322	MIM
PLXNA2	2.075	0.984	0.208	
PPP1R13L	2.066	1.000	-0.300	
SLC44A1	2.057	0.831	0.136	
TPM3	2.045	0.833	0.155	
SLC20A2	2.023	1.000	-0.257	
MTHFD2	2.022	0.914	0.190	Matrix
PGP	2.001	0.832	-0.118	
MDFIC	1.996	0.569	-0.720	
RPS25	1.988	0.931	0.196	
ARFGAP1	1.971	0.866	-0.175	
PKN2	1.965	0.862	0.100	
XPO7	1.963	1.000	-0.321	
TMEM115	1.938	1.000	-0.402	
BANF1	1.922	0.877	-0.093	
ACTN1	1.922	0.991	0.215	
FKBP5	1.866	1.000	-0.265	
HCFC2	1.863	0.506	-0.736	
PEX10	1.852	0.828	-0.150	
TOR2A	1.830	1.000	-0.324	
PLCL2	1.828	0.832	0.157	

GLCE	1.802	0.900	0.080	
AAMP	1.797	0.922	-0.072	
DAXX	1.789	1.000	-0.456	
RPL10A	1.785	0.941	-0.067	
LRRFIP2	1.765	1.000	0.230	
PPP4R1	1.761	0.781	-0.541	
SPPL2A	1.756	1.000	0.263	
VTI1A	1.748	0.891	0.085	
TRMU	1.745	0.842	0.115	Matrix
DICER1	1.743	1.000	-0.316	
ZDHHC8	1.735	0.922	-0.198	
WDR20	1.733	0.828	-0.127	
ATL1	1.732	0.987	-0.219	
IST1	1.732	0.831	-0.135	
PRDX4	1.723	0.827	0.157	IMS
CDC42EP1	1.712	0.884	0.091	
NANS	1.711	0.848	-0.170	
TLE3	1.707	0.540	-0.717	
GOLGA5	1.706	0.859	0.102	
TCAF1	1.706	1.000	-0.361	
GOLGB1	1.705	0.843	0.116	
GEMIN2	1.702	1.000	-0.347	
KAT6A	1.698	0.614	-0.638	
ACTN4	1.696	0.903	0.188	
SNX12	1.686	0.925	0.071	
CMTM6	1.682	0.607	-0.638	
ATP9A	1.678	0.832	0.160	
PNP	1.673	0.829	0.139	
C3orf33	1.670	1.000	-0.256	Matrix
EIF4B	1.669	0.846	0.106	
LYAR	1.664	1.000	-0.283	
GLG1	1.659	0.831	0.121	
AP3M2	1.656	1.000	-0.368	

YTHDC2	1.646	0.904	-0.079	
CES2	1.645	0.551	-0.741	
TM9SF4	1.645	0.933	0.069	
GCC2	1.638	0.846	0.170	
PIAS2	1.637	0.099	-1.952	
IPO9	1.632	0.983	-0.222	
ENY2	1.632	0.856	-0.529	
RPS7	1.626	0.867	0.099	
ANKRD50	1.621	0.908	-0.192	
CTSD	1.614	0.826	0.157	
PDLIM1	1.598	1.000	0.247	
CSGALNACT2	1.598	1.000	-0.338	
ATP1B3	1.595	0.891	0.085	
ACSL1	1.587	0.835	0.120	MOM
ANKRD17	1.586	0.829	-0.135	
OTUD3	1.585	0.586	-0.657	
AARSD1	1.584	0.841	-0.167	
TBCA	1.582	0.915	0.075	
TM9SF3	1.582	0.847	0.172	
UBL4A	1.579	0.844	-0.108	
EIF4H	1.578	0.830	0.132	
EZR	1.575	0.925	0.072	
NDE1	1.574	0.834	-0.163	
MAD1L1	1.566	0.856	-0.540	
GNS	1.565	0.898	0.190	
MSN	1.559	0.830	0.137	
DUSP3	1.553	1.000	-0.282	
NPC2	1.548	0.828	0.134	
PITPNB	1.533	0.911	0.198	
PLBD2	1.533	1.000	0.298	
AP1B1	1.530	0.829	0.135	
DHX57	1.529	0.884	0.090	
TMF1	1.528	0.836	0.120	

HECTD4	1.527	1.000	-0.485	
WDR91	1.525	0.908	0.077	
ALDOA	1.520	1.000	0.272	
ATAD2B	1.519	0.497	-0.768	
ARRB2	1.517	0.830	-0.137	
HS2ST1	1.516	0.831	0.138	
KRT18	1.512	1.000	-0.318	
GOLGA4	1.506	0.826	0.129	
DMTN	1.506	1.000	-0.263	
ARFGAP3	1.500	0.836	-0.167	
PDE6D	1.499	0.832	-0.142	
NAP1L1	1.498	0.834	0.123	
VAC14	1.496	0.834	-0.124	
ARL6IP4	1.494	0.523	-0.831	
POC1A	1.492	0.923	-0.205	
QSOX2	1.491	0.912	0.200	
SFT2D3	1.488	0.841	-0.119	
MLF2	1.486	1.000	-0.249	
MAP1LC3B2; MAP1LC3B	1.486	1.000	-0.258	
GDPD1	1.486	0.890	-0.087	
INO80	1.484	0.555	-0.727	
DECR2	1.484	0.940	0.211	
GOLGA2	1.481	0.843	0.111	
EMC3	1.479	0.894	0.085	
MLLT1	1.479	1.000	-0.447	
CEP41	1.477	0.859	-0.180	
YBEY	1.474	1.000	-0.234	Matrix
H1FX	1.473	1.000	-0.394	
TANC1	1.470	0.833	-0.165	
DPY19L1	1.466	0.966	0.055	
YWHAH	1.465	0.888	0.089	
ASAP2	1.460	0.566	-0.823	

TTI1	1.460	0.843	-0.119	
CLN5	1.459	1.000	0.497	
CRABP2	1.458	0.857	-0.559	
TSNAX	1.454	0.855	-0.106	
TUBGCP6	1.453	1.000	-0.281	
GTPBP10	1.453	0.835	0.125	Matrix
INPP4A	1.452	1.000	-0.510	
HSPG2	1.452	0.865	-0.183	
CDK2AP1	1.451	0.092	-3.470	
SIPA1	1.450	0.928	0.071	
TUB	1.442	1.000	-0.306	
EFHD1	1.440	1.000	-0.401	MIM
PPME1	1.439	0.830	-0.141	
MRPL13	1.436	0.863	0.103	Matrix
ZEB1	1.435	0.494	-0.815	
PRDM2	1.435	0.695	-0.658	
EPHX1	1.434	1.000	0.288	
SPTBN4	1.434	1.000	-0.244	
COG3	1.430	1.000	-0.282	
ADCK2	1.430	1.000	-0.436	MIM
GSR	1.423	1.000	0.384	Matrix
CSNK1G3	1.422	0.939	0.069	
RYBP	1.421	0.235	-1.482	
HOXA5	1.421	0.595	-0.716	
HSP90AA1	1.418	0.956	0.060	
ZNF146	1.416	0.079	-3.056	
PI4K2A	1.416	0.872	0.097	
VPS54	1.412	1.000	0.248	
SLC29A2	1.409	0.848	-0.577	
GIGYF2	1.404	0.882	0.094	
CD81	1.403	0.832	0.146	
HMG20B	1.403	0.732	-0.652	
CCNT1	1.402	0.811	-0.614	

PDCD5	1.398	0.848	0.109	
ZRANB2	1.397	1.000	-0.334	
COPB1	1.396	0.952	0.062	
LGALS3BP	1.393	1.000	0.246	
FAM50A	1.390	1.000	-0.321	
SDF4	1.386	0.824	0.160	
AGAP1	1.386	0.844	-0.174	
SH3KBP1	1.384	0.950	-0.217	
CCNH	1.382	1.000	-0.481	
IGBP1	1.380	0.998	-0.233	
KIFC1	1.375	0.852	-0.592	
ANP32B	1.374	0.869	-0.187	
PEA15	1.374	1.000	-0.240	
SLC2A13	1.372	1.000	-0.423	
ACAA1	1.370	0.842	0.174	unknown
FSCN1	1.369	0.832	-0.167	
FLII	1.367	0.891	0.087	
MED23	1.366	1.000	-0.535	
PCDH7	1.365	0.898	0.084	
TIMM50	1.361	0.902	0.081	MIM
CAMSAP3	1.358	0.841	-0.172	
COMMD3	1.358	0.826	0.131	
MAPT	1.352	1.000	-0.314	
VPS35	1.352	0.858	0.184	
HOMEZ	1.351	1.000	-0.504	
BMP2K	1.348	0.881	0.095	
FAM8A1	1.345	0.964	-0.056	
ARIH2	1.337	0.857	-0.182	
TRMT5	1.335	0.832	0.128	Matrix
SAMD1	1.333	0.554	-0.834	
DNAJB1	1.332	0.965	-0.224	
DIP2C	1.330	0.863	-0.104	
NME4	1.329	0.872	0.099	MIM

PPP2R5C	1.325	1.000	-0.327	
FHOD1	1.325	0.840	0.118	
APOL2	1.321	0.829	-0.136	
MARK1	1.321	1.000	-0.527	
PRMT5	1.321	0.904	0.080	
CNOT7	1.319	0.833	-0.153	
RAD51AP1	1.318	0.545	-0.823	
EXOSC3	1.317	0.961	-0.562	
ANO5	1.316	1.000	-0.315	
GMDS	1.316	0.897	-0.083	
ELP3	1.315	0.830	-0.136	
ELMO1	1.315	1.000	-0.431	
VEZF1	1.312	0.082	-5.130	
ITFG1	1.312	0.865	0.187	
RPS19	1.307	0.832	0.124	
MRPL30	1.303	0.852	0.108	Matrix
TDP1	1.303	1.000	-0.320	
RIOK1	1.300	0.540	-0.849	

Table S.2: Results of phosphoproteomics with a p-value equal or below -log(1.3) = 0.05. None of the hits could be mapped to a mitochondrial localization according to MitoCarta3.0.

gene names	-Log Student's T-test p-value	Student's T-test q-value	Student's T-test Difference (inhibitor - control)	Whole Proteome Student's T-test q-value	Whole Proteome Student's T-test Difference (inhibitor - control)	PTM Site
TANC2	5.873	0	4.722	0.991	-0.043	S 404
CLASP1	5.212	0	6.092	0.869	-0.13	S 636
TADA3	5.128	0	-5.032	0.849	-0.238	S 298
PSD3	4.315	0.011	-6.08	0.86	-0.137	S 1009
RAF1	4.107	0.014	7.373	0.84	-0.132	S 619
GIGYF2	4.02	0.018	-4.537	0.882	0.094	S 199
GTF3C2	2.734	0.057	3.247	0.832	-0.241	Y 762
CHAMP1	2.464	0.396	-1	0.938	-0.366	S 416
OSBPL5	2.287	0.126	-2.877	0.983	0.047	S 82
NSUN5P2	2.205	0.18	-2.529	NaN	NaN	S 260
TUT4	2.096	0.208	2.384	NaN	NaN	S 104
SLC20A1	1.997	0.19	2.665	0.993	-0.041	Y 421
ZC3H13	1.962	0.667	-0.774	1	-0.533	S 643
KHDRBS1	1.93	0.296	-1.859	0.885	-0.357	S 20
SMO	1.902	1	0.443	NaN	NaN	S 771
FRMD4B	1.838	0.201	3.712	NaN	NaN	S 675
RPTOR	1.837	0.297	-2.539	0.951	-0.083	S 863
KIF14	1.832	1	0.308	0.998	0.009	S 272
LAMTOR1	1.801	0.943	0.506	0.942	0.075	S 56
AHNAK	1.748	1	0.314	0.98	0.039	S 5731
SRRM2	1.747	0.556	-1.051	1	-0.345	S 1124
LBR	1.745	0.655	-0.847	0.842	-0.191	S 3
PPHLN1	1.727	0.323	-1.698	0.908	-0.389	S 205
RNF19A	1.696	0.498	1.224	NaN	NaN	S 631

RALGAPB	1.654	0.306	2.192	0.902	-0.11	S 357
KIAA0754	1.652	0.287	-2.564	0.983	-0.047	S 668
APC	1.645	0.277	2.493	0.998	0.027	S 1362
NCOA6	1.642	0.245	-3.063	0.842	-0.306	S 2018
HNRNPM	1.635	0.986	-0.129	0.96	-0.376	S 575
HNRNPM	1.635	0.987	-0.129	0.96	-0.376	S 588
CHTF18	1.611	0.28	-3.423	0.983	-0.054	S 64
RAPH1	1.608	0.189	5.731	0.827	-0.143	S 965
SEC16A	1.607	0.24	3.213	0.899	-0.097	S 1368
TJP1	1.605	0.752	0.726	1	-0.018	T 1167
SPEN	1.587	0.321	2.227	0.837	-0.317	S 1206
NDRG1	1.58	0.291	3.842	0.838	-0.118	T 366
DOCK7	1.577	0.3	3.996	0.972	0.05	T 2124
DYNC1LI1	1.576	0.26	-3.635	0.955	-0.095	S 510
NUMA1	1.562	0.303	-2.47	1	-0.415	S 1757
LMNA	1.558	0.546	1.238	0.845	-0.316	S 458
NFX1	1.557	0.761	0.744	NaN	NaN	S 95
WWP2	1.557	0.286	-3.985	0.898	-0.091	S 211
XPC	1.547	0.673	0.98	1	-0.412	T 358
C7orf50	1.539	0.365	-1.965	0.987	-0.044	S 175
MAP3K1	1.512	0.614	1.063	NaN	NaN	S 275
GIGYF2	1.509	0.907	0.594	0.882	0.094	T 382
RBMX2	1.503	0.277	-3.206	0.956	-0.363	S 188
STX18	1.5	0.271	4.565	0.991	0.03	S 189
PALM3	1.493	0.372	2.061	0.825	-0.182	S 126
SRRM2	1.491	0.764	-0.773	1	-0.345	T 1492
CELSR1	1.48	0.744	-0.809	0.868	-0.136	S 2871
PIP5K1A	1.479	0.648	0.99	0.991	0.04	S 458
KHDRBS1	1.478	0.248	4.867	0.885	-0.357	S 18
DSN1	1.476	0.296	-3.787	1	-0.333	S 58
SPECC1	1.472	0.345	2.303	0.965	-0.062	T 65
SPAG9	1.466	0.307	-3.028	0.991	0.029	S 251
DCBLD1	1.455	0.312	2.648	0.99	-0.036	Y 652

AP1AR	1.453	0.464	1.761	NaN	NaN	T 228
NCL	1.448	0.532	-1.257	0.828	-0.172	T 99
SLC6A15	1.438	0.388	2.168	0.966	0.066	S 675
FBXO42	1.436	1	0.511	NaN	NaN	S 488
KLRG2	1.43	0.314	3.082	0.999	-0.014	S 177
FYN	1.415	0.722	0.878	0.999	-0.015	S 25
SRRM1	1.395	0.287	-4.611	1	-0.311	S 696
TJP1	1.389	0.4	-2.206	1	-0.018	Y 132
ABL1	1.387	0.313	3.012	NaN	NaN	S 718
PTPN2	1.384	0.495	1.772	0.911	-0.1	S 293
WDR6	1.383	0.697	0.934	0.847	0.13	T 555
JAG2	1.374	0.775	0.775	NaN	NaN	S 1208
NOC2L	1.368	0.595	1.24	0.833	-0.332	T 678
EPN2	1.363	0.316	3.465	1	-0.002	S 327
ZNF638	1.352	0.536	-1.4	0.835	-0.253	S 510
ZNF638	1.352	0.542	-1.4	0.835	-0.253	S 508
DMXL1	1.341	0.491	1.744	NaN	NaN	S 324
AGPS	1.341	0.999	0.548	0.843	0.14	S 65
CDC42EP1	1.333	1	0.356	0.884	0.091	S 350
EPB41L2	1.332	0.486	-1.919	0.999	0.013	S 683
SEPTIN9	1.33	1	0.384	0.992	0.035	S 85
ABI1	1.33	0.47	2.074	0.998	0.01	T 229
RBM23	1.326	1	-0.21	NaN	NaN	S 149
KIF23	1.321	1	0.308	0.969	-0.056	S 902
UBAP2L	1.312	0.315	4.555	0.984	0.042	S 454
APC	1.312	0.373	3.11	0.998	0.027	Y 986
SRGAP2	1.311	0.34	3.471	0.888	-0.106	S 908

8.3   Uncropped western blots
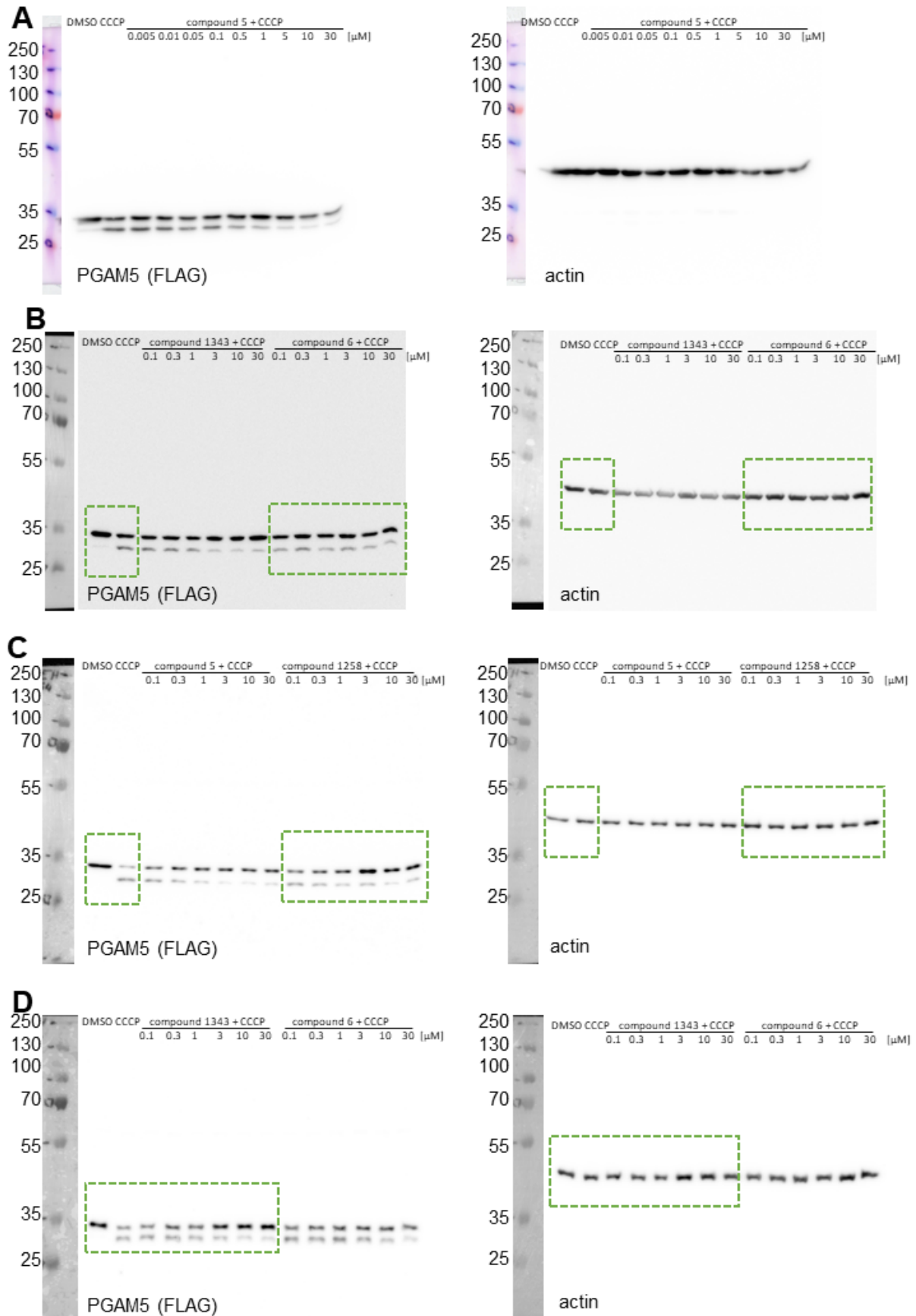
Figure S.2: *Uncropped blots of Figure 7*
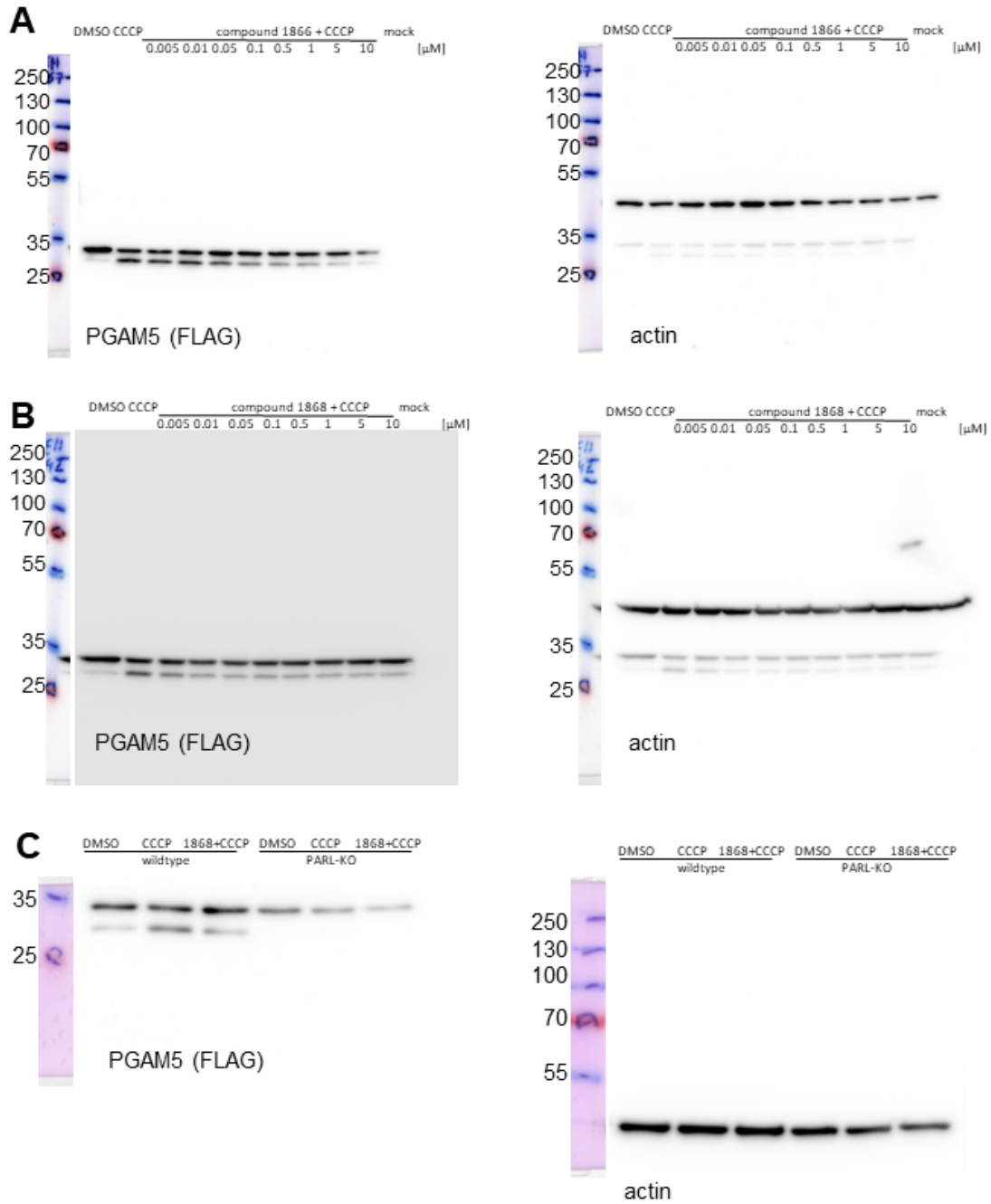
Figure S.3: *Uncropped blots of Figure 8*
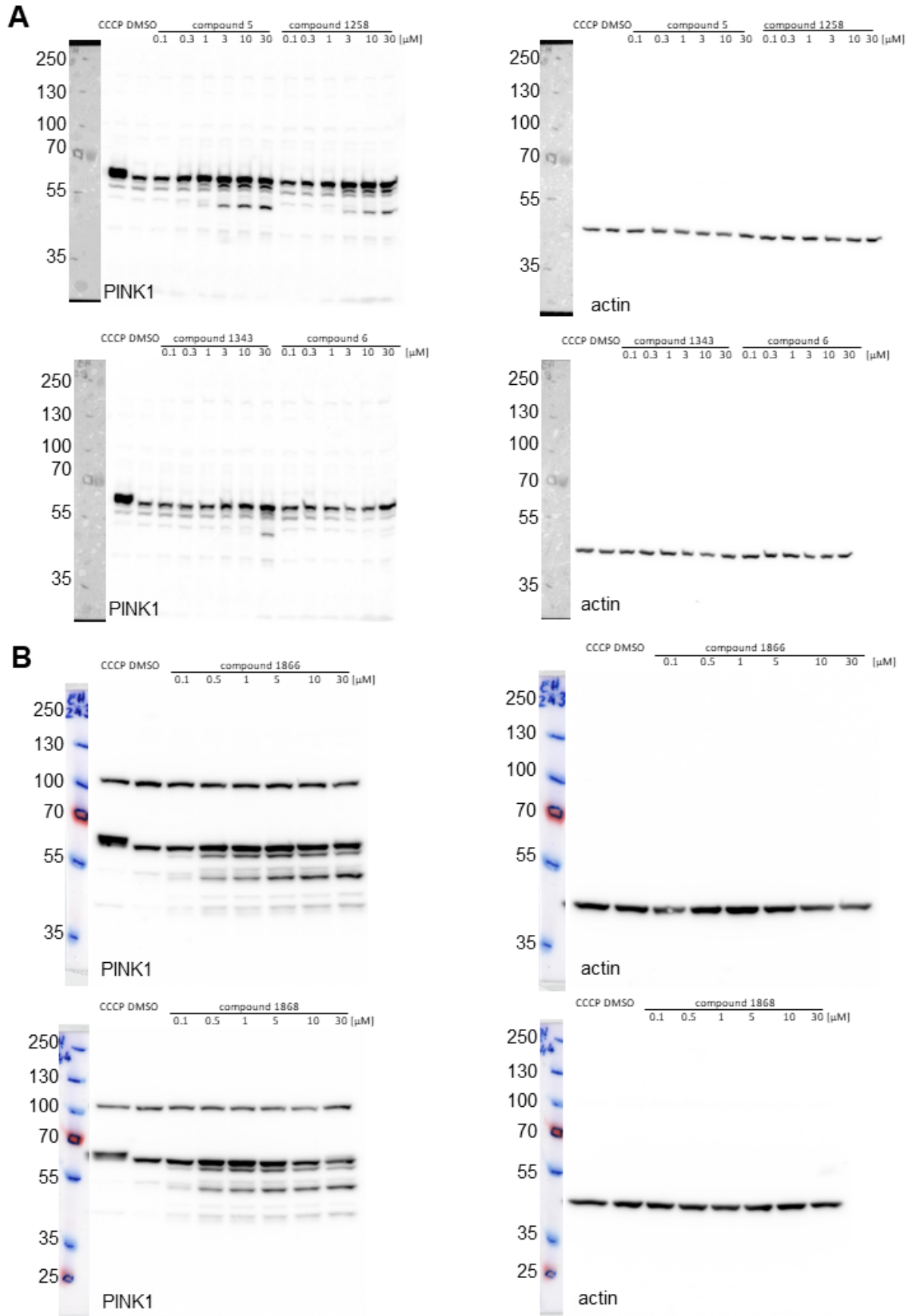
Figure S.4: *Uncropped blots of Figure 9*
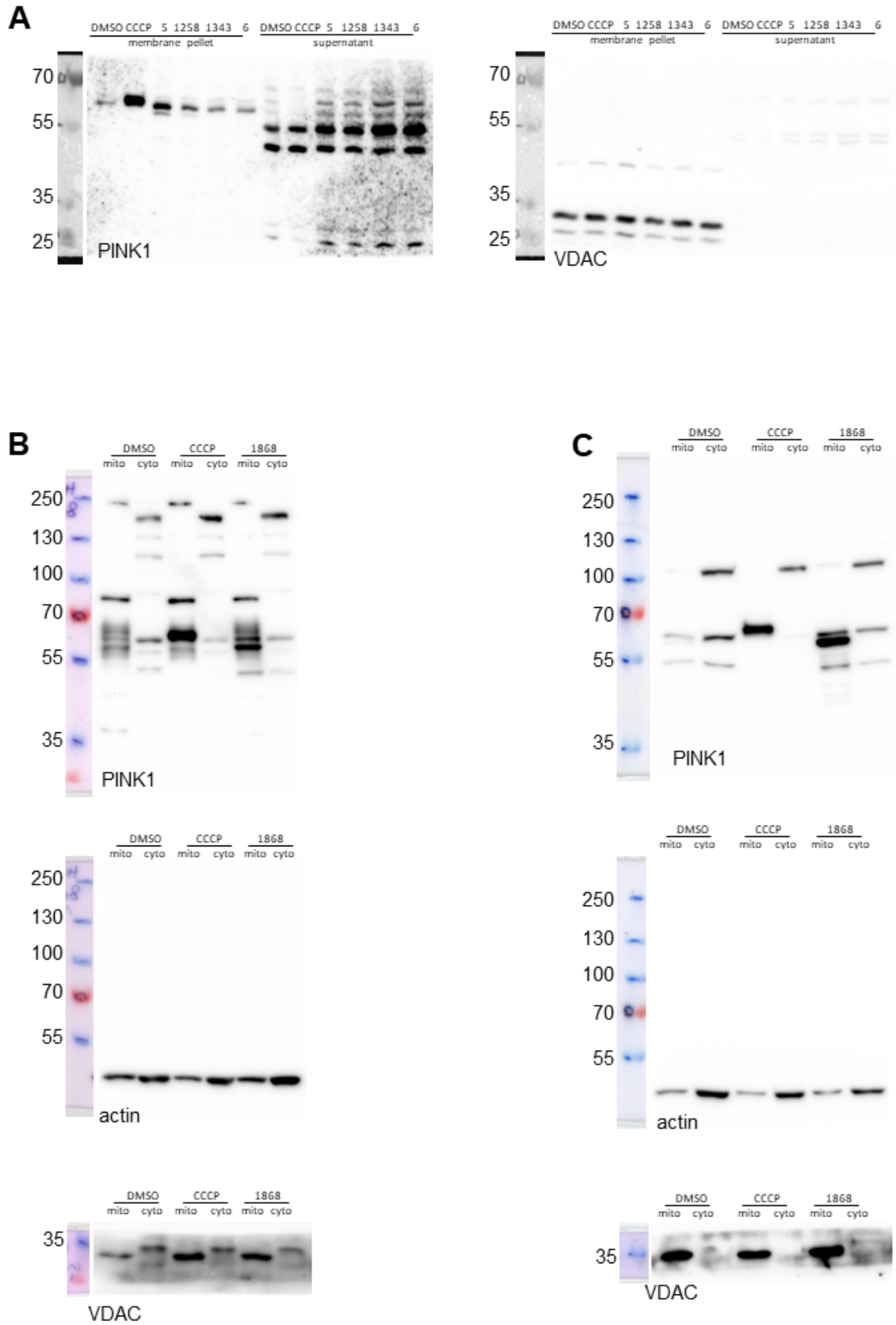
Figure S.5: *Uncropped blots of Figure 12 subfigures A, B and C*
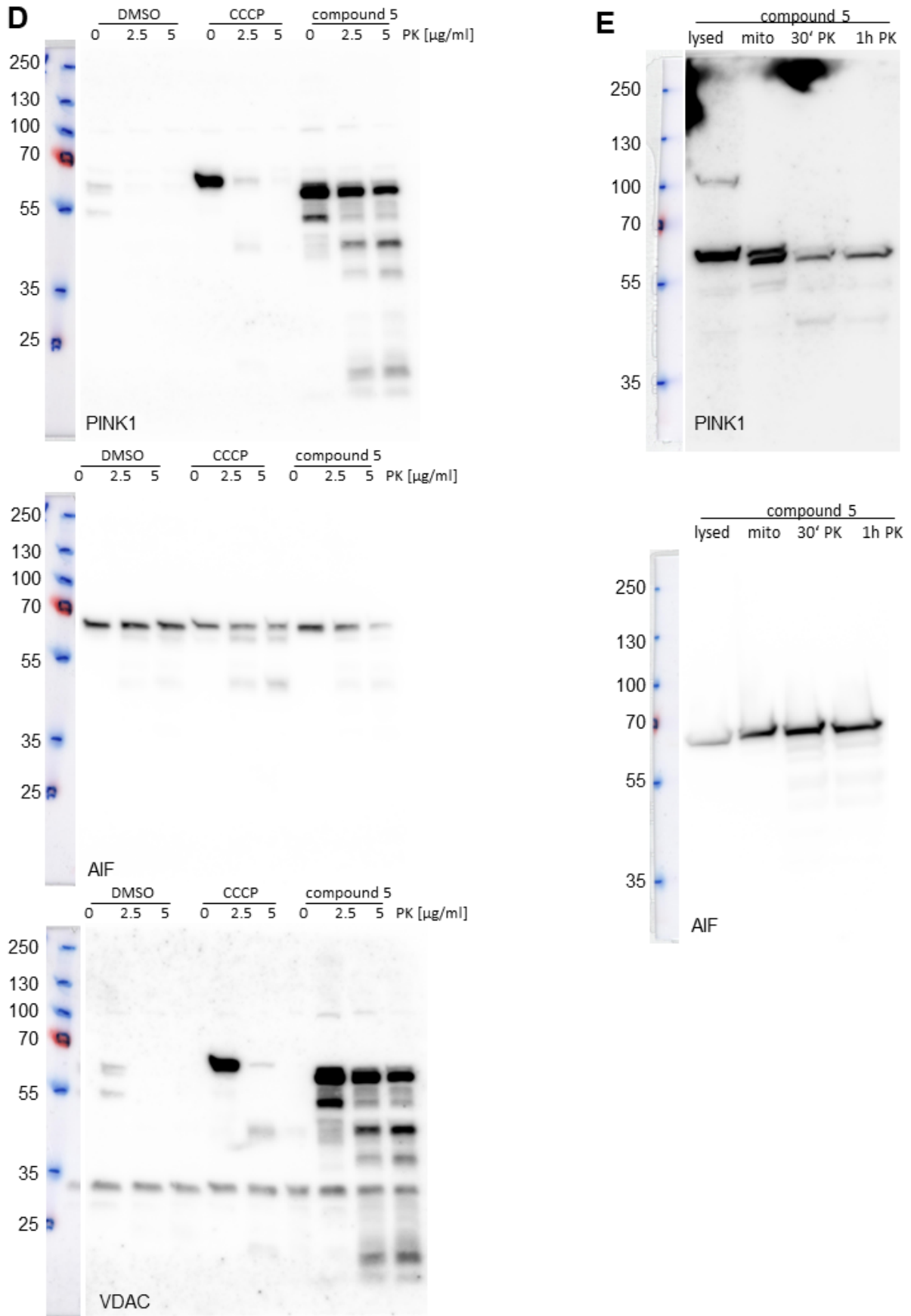
Figure S.6: *Uncropped blots of Figure 12 subfigures D and E*
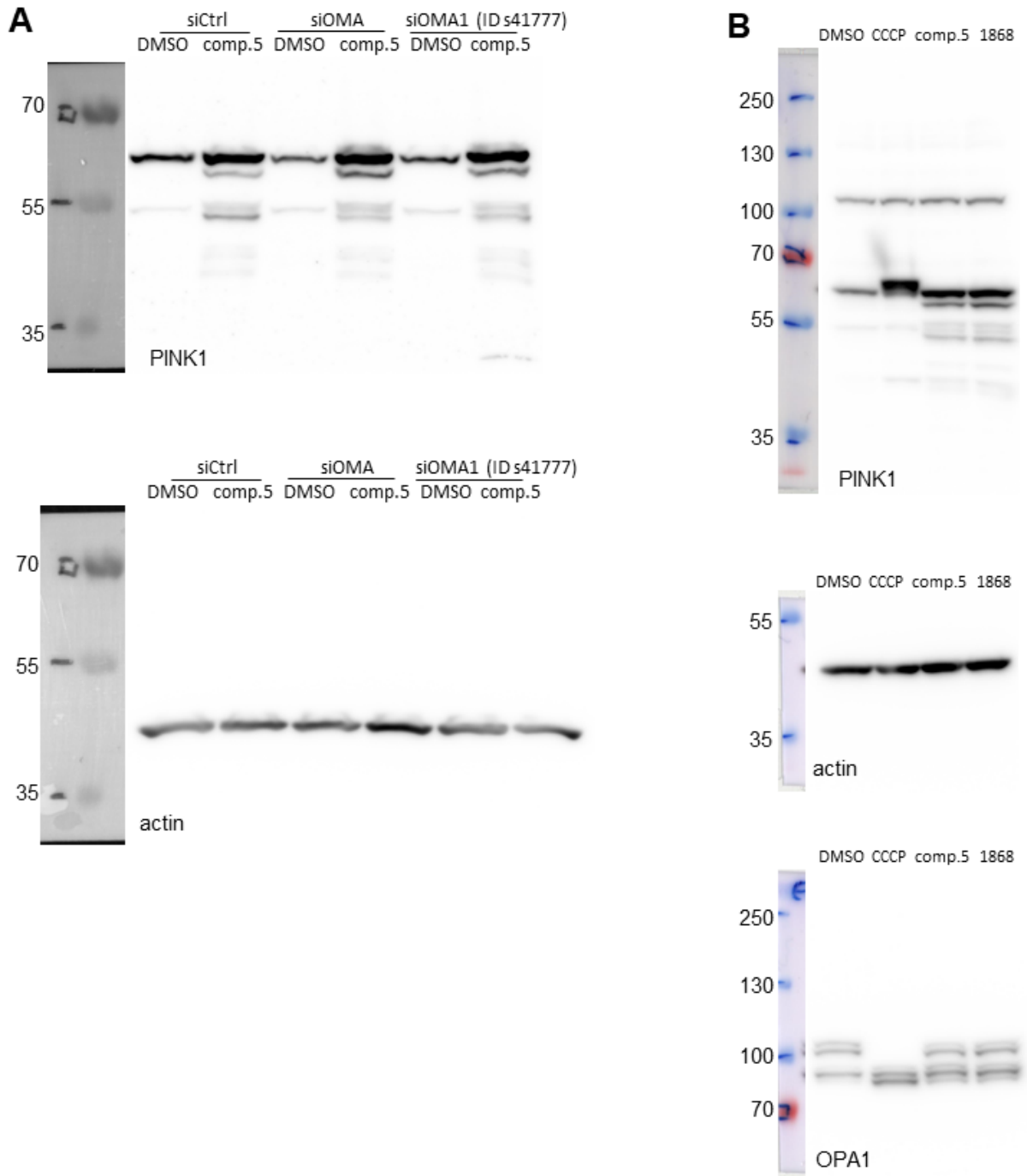
Figure S.7: *Uncropped blots of Figure 13*
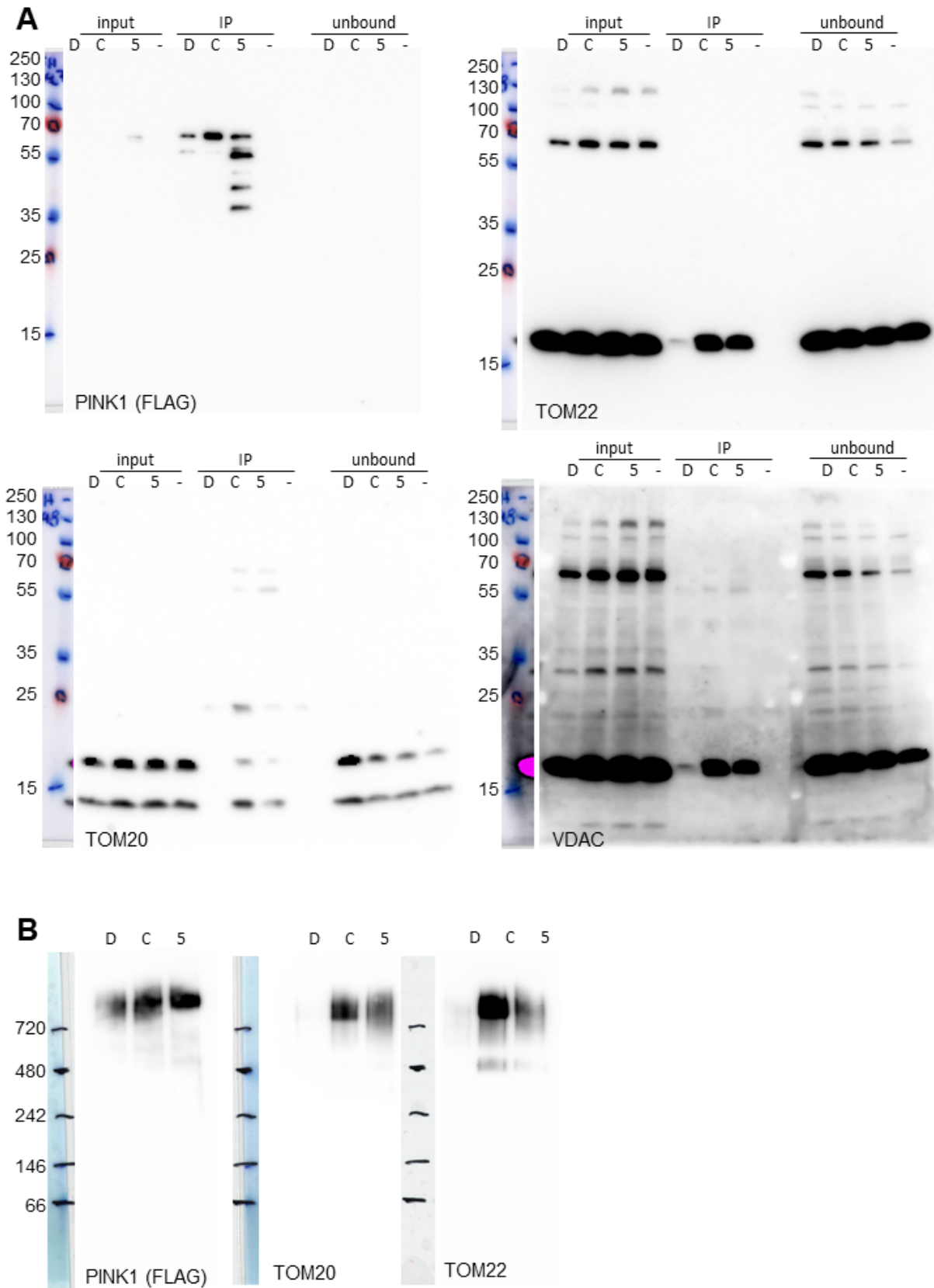
Figure S.8: *Uncropped blots of Figure 14 subfigures A and B*
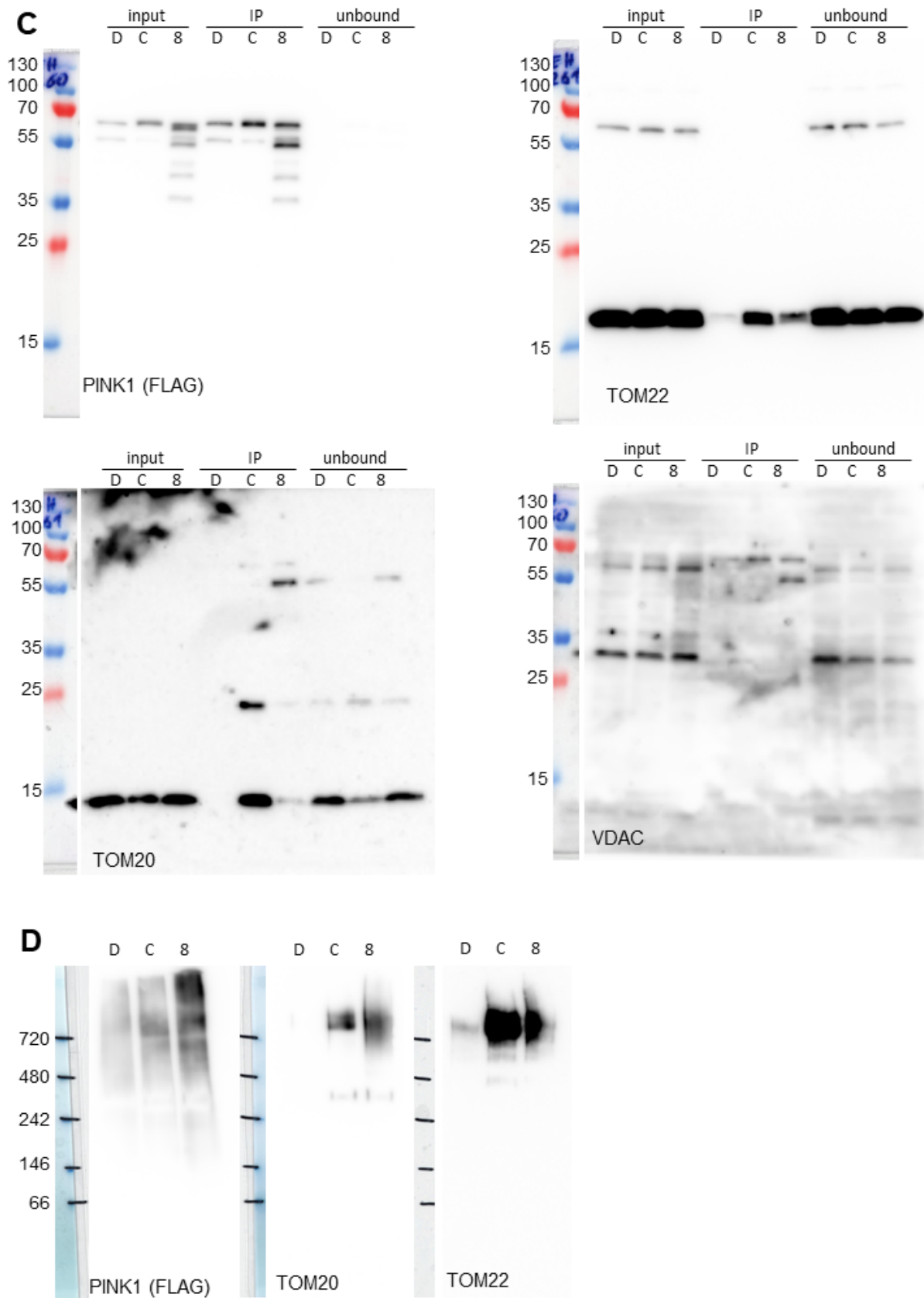
Figure S.9: *Uncropped blots of Figure 14 subfigures C and D*
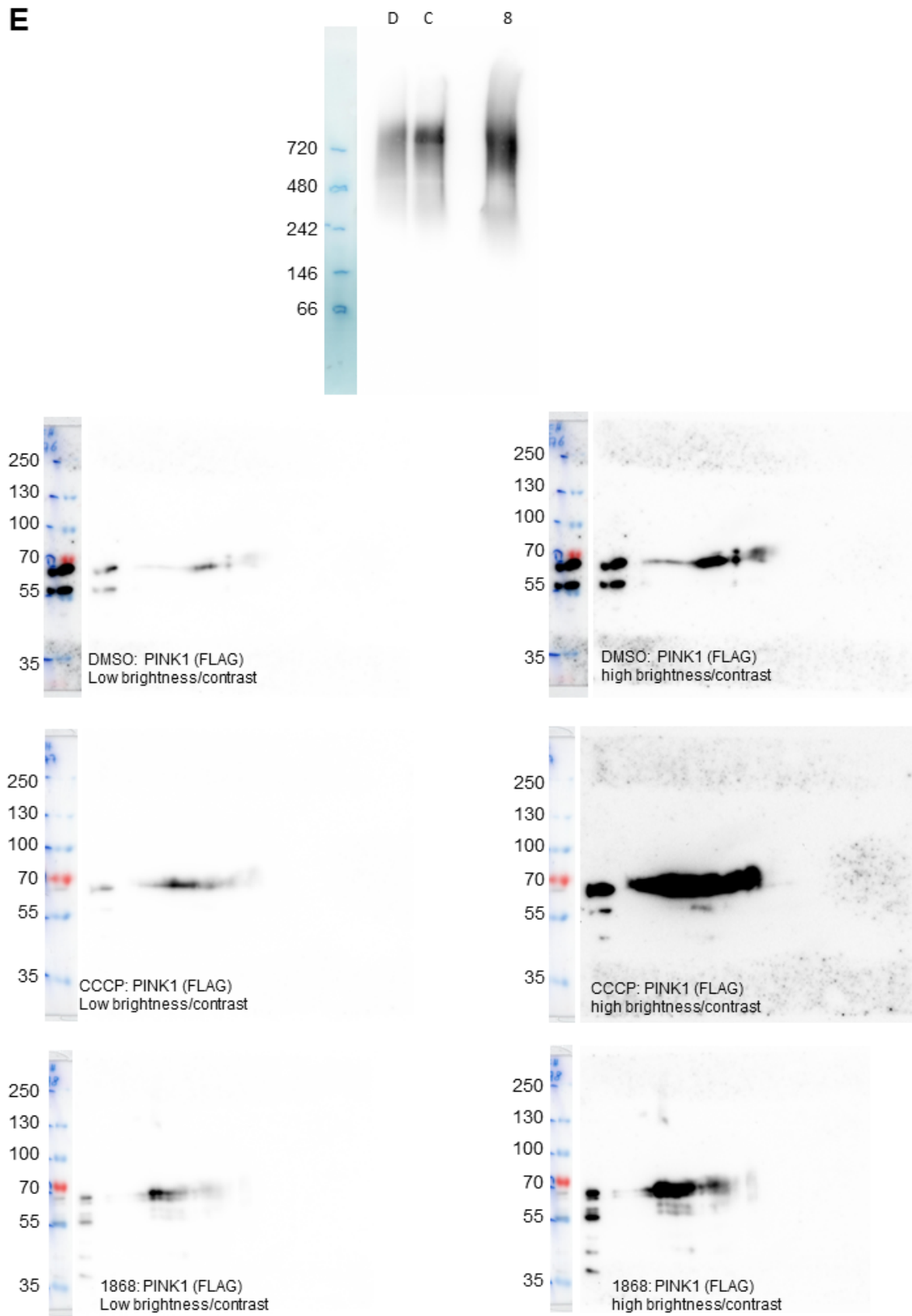
Figure S.10: *Uncropped blots of Figure 14 subfigure E*
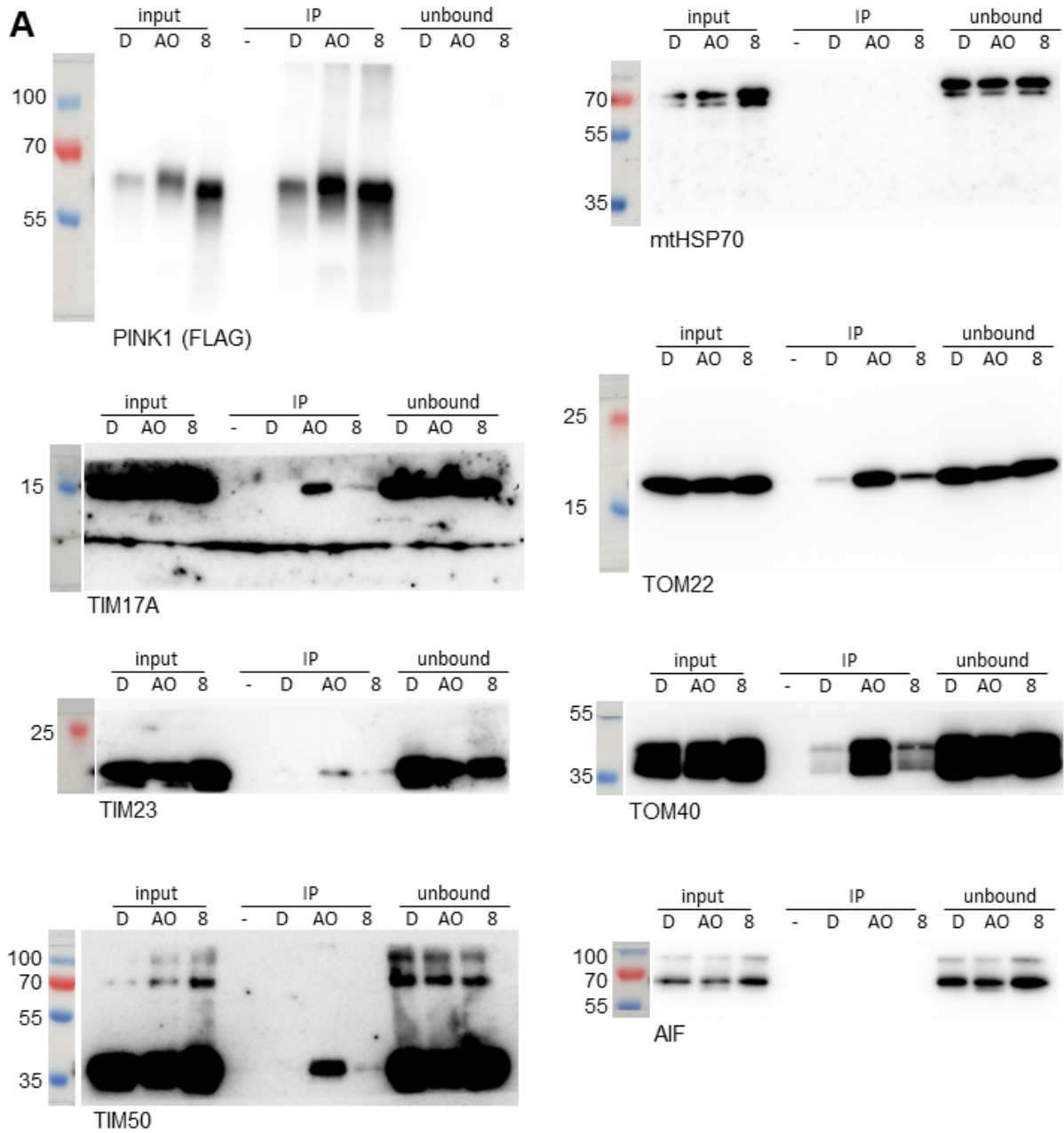
Figure S.11: *Uncropped blots of Figure 15 subfigure A*
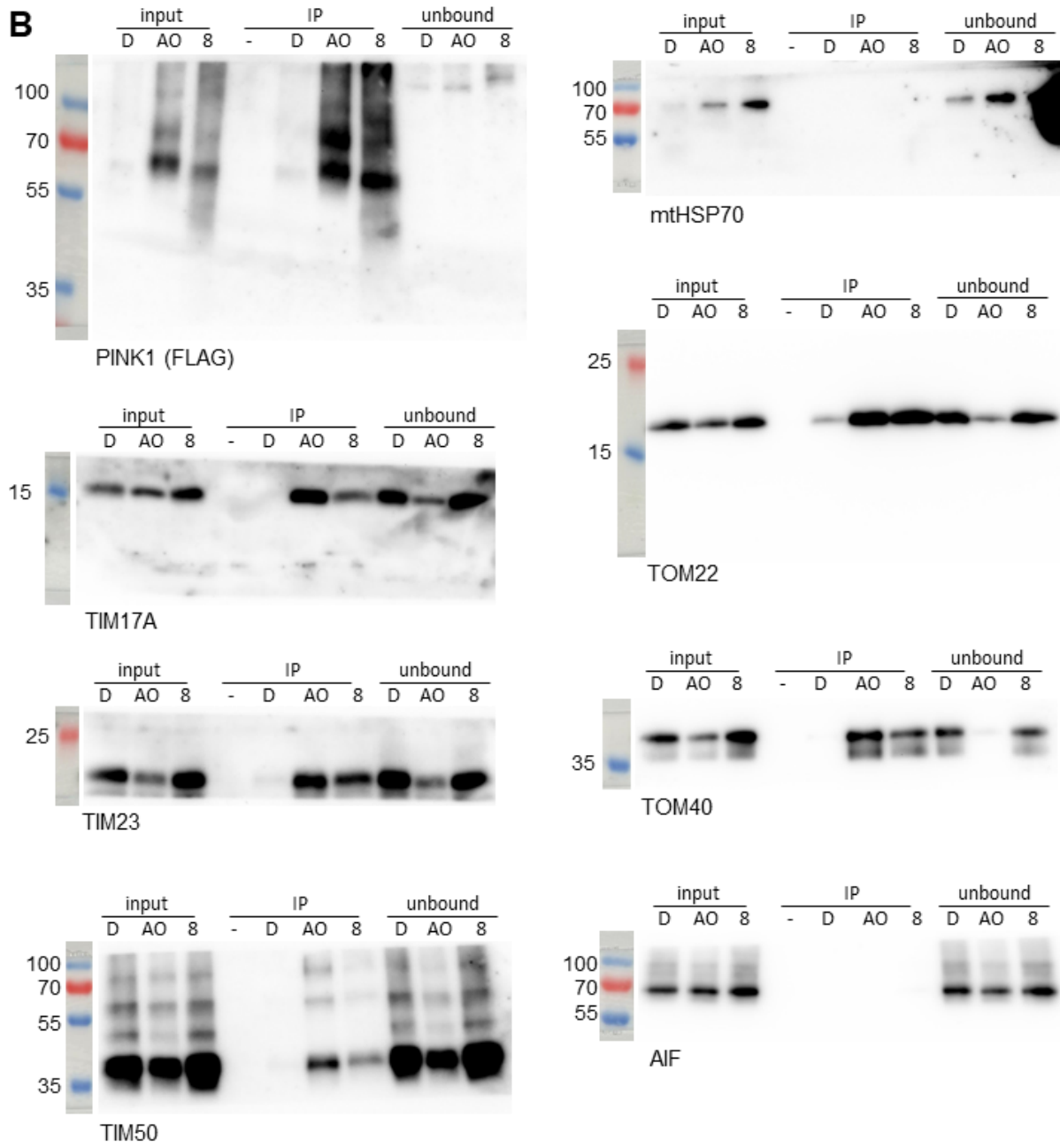
Figure S.12: *Uncropped blots of Figure 15 subfigure B*

A
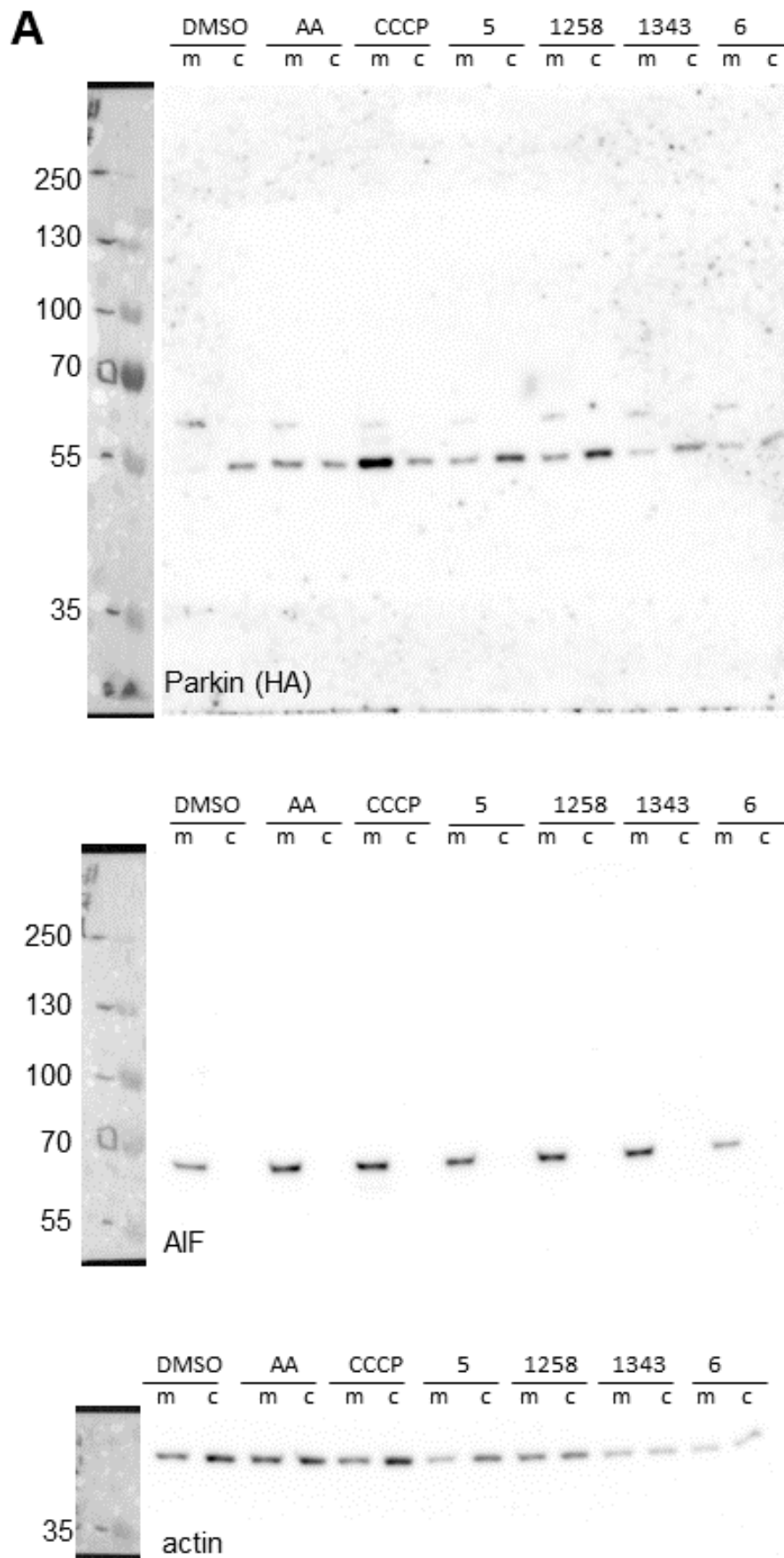
Figure S.13: *Uncropped blots of Figure 17*

9 Acknowledgements

First, I would like to express my gratitude to my thesis committee members, Prof. Dr. Natalia Kononenko and Prof. Dr. Elena Rugarli, for taking the time to evaluate my thesis. I am also deeply appreciative of Natalia and Prof. Dr. Thomas Langer for the engaging and insightful discussions during my two TAC meetings here in Cologne. My sincere recognition goes to Kvido Stříšovský and his group in Prague for the productive collaboration on the inhibitor establishment project and the resulting paper. Simon Feldkamp deserves special mention for all his work on this project during his Bachelor's, Master's, and as a student assistant - I wish you all the best wherever life takes you after completing your Master's! On campus, I am grateful to the proteomics and imaging facilities at CECAD, as well as the imaging facility at ZMBH in Heidelberg, for their support and readiness to assist me in establishing new protocols. A heartfelt acknowledgment goes to Marius for being an inspiring, supportive, and approachable group leader throughout my PhD journey. It's remarkable how you've maintained an open-door policy even amidst structural changes between Heidelberg and Cologne. (Also, the yearly chocolate Nikolaus tradition is highly appreciated!)

Next, of course, I want to say thanks to all my coworkers from Heidelberg and Cologne, past and present. To the Heidelberger: Corona, lab work in two shifts, institute-wide water leakage, spooky freezer and nitrogen tank checks in the abandoned ZMBH equipped with flashlights and our essential worker permission papers, communal trashing of almost an entire -80 °C freezer, lab and private moving on the Heidelberg campus, then to Cologne, and then again within the Biochemistry institute... We've really done it all. We could've done without it, but it sure was an experience! To all who joined us in Cologne: thank you for making the transition so, so much easier; I think we have become a great team. Thanks to those who joined me in my passion for pen-and-paper roleplaying games and board games, they were all really fun evenings. A special recognition goes to Friedi for encouraging me to finally join the btS (should've really done that sooner) and to Susi for helping me manage (survive) ENABLE!

Last but not least, I thank my family and friends who've been with me and supported me in this lengthy journey of almost 12 years (with some breaks) spanning my Bachelor, Master, PhD and so many planned and unplanned relocations around Germany. My biggest appreciation goes to Noé: you are my anchor and safe harbor through every storm, and I look so much forward to what the future now holds for us both (let's hope it doesn't include postponed couple weekends due to super urgent lab stuff)!